

Grounding Systems Analysis and Optimization

by

Xuan Wu

A Thesis Presented in Partial Fulfillment
of the Requirements for the Degree
Master of Science

Approved November 2013 by the
Graduate Supervisory Committee:

Daniel J. Tylavsky, Chair
John Undrill
Raja Ayyanar

ARIZONA STATE UNIVERSITY

December 2013

ABSTRACT

Today, more and more substations are created and reconstructed to satisfy the growing electricity demands for both industry and residence. It is always a big concern that the designed substation must guarantee the safety of persons who are in the area of the substation. As a result, the safety metrics (touch voltage, step voltage and grounding resistance), which should be considered at worst case, are supposed to be under the allowable values.

To improve the accuracy of calculating safety metrics, at first, it is necessary to have a relatively accurate soil model instead of uniform soil model. Hence, the two-layer soil model is employed in this thesis. The new approximate finite equations with soil parameters (upper-layer resistivity, lower-layer resistivity and upper-layer thickness) are used, which are developed based on traditional infinite expression. The weighted-least-squares regression with new bad data detection method (adaptive weighted function) is applied to fit the measurement data from the Wenner-method. At the end, a developed error analysis method is used to obtain the error (variance) of each parameter.

Once the soil parameters are obtained, it is possible to use a developed complex images method to calculate the mutual (self) resistance, which is the induced voltage of a conductor/rod by unit current from another conductor/rod. The basis of the calculation is Green's function between two point current sources, thus, it can be expanded to either the

functions between point and line current sources, or the functions between line and line current sources.

Finally, the grounding system optimization is implemented with developed three-step optimization strategy using MATLAB solvers. The first step is using “fmincon” solver to optimize the cost function with differentiable constraint equations from IEEE standard. The result of the first step is set as the initial values to the second step, which is using “patternsearch” solver, thus, the non-differentiable and more accurate constraint calculation can be employed. The final step is a backup step using “ga” solver, which is more robust but larger time cost.

ACKNOWLEDGMENTS

I would like to express my sincere appreciation and gratitude to my advisor, Dr. Tylavsky, for his patient guidance and insightful instructions. He used his valuable experience and brilliant wisdom to light my way forward to be a more skillful researcher and more professional engineer hopefully in the future.

I would also like to thank my committee members, Dr. John Undrill and Dr. Raja Ayyanar for their valuable time and suggestions.

I would like to thank the Salt River Project (SRP) for their financial support provided, especially, Mr. Tom LaRose who is the Executive Engineer as well as the supervisor for this project. I am so appreciated that Tom gave me a lot of advice and materials.

In addition, I am grateful to my parents for their endless love and support through all these years. Thanks to their encouragement and instruction, I can face and overcome all the challenges and difficulties.

Finally, I would like to thank all my friends I met here in Arizona State University. They would always be my most valuable asset though all my life.

CONTENTS

	Page
LIST OF TABLES	vii
LIST OF FIGURES	viii
NOMENCLATURE	xii
CHAPTER	
1 INTRODUCTION	1
1.1 Overview	1
1.2 Literature Review	2
1.3 Study Objective	6
1.4 Thesis Organization.....	7
2 SOIL RESISTIVITY MEASUREMENTS AND ANALYSIS	8
2.1 Soil Resistivity Measurements	8
2.2 Calculation of Apparent Soil Resistivity	12
2.3 Estimation of Two Layer Soil Parameters.....	14
2.4 Rejection of Bad Data	17
2.5 Estimation of Soil Parameter Errors.....	18
2.6 Description of Computer Program Modeling.....	21
2.7 Case Study and Comparison with WINIGS Results	27
3 ANALYSIS OF GROUNDING SYSTEM.....	34

CHAPTER	Page
3.1 The Equivalent Circuit of Body Shock	34
3.2 Grounding System Safety Assessment	37
3.3 Electromagnetic Analysis and Green's Functions	38
3.4 Complex Image Method	46
3.5 Comparison between Images Method and Complex Images Method	57
3.6 Voltage Produced by Horizontal Lines of Current	59
3.7 Calculation of Mutual and Self Resistance	63
3.8 Matrix Method	71
3.9 Results Compared with WINIGS	75
4 GROUNDING SYSTEM OPTIMIZATION	83
4.1 Step 1: Use of IEEE Standard Equations for Optimization	84
4.2 Step 2: Use of Pattern Search Method for Optimization	86
4.3 Step 3: Use of Genetic Algorithms for Optimization	91
4.4 Optimization Problem Based on SRP Design Rules	96
4.5 Program Structure	106
4.6 Case Study	111
5 CONCLUSIONS AND FUTRUE WORKS	120
5.1 Conclusions	120

CHAPTER	Page
5.2 Future Works	124
REFERENCE.....	126

LIST OF TABLES

Table	Page
2.1 The Comparison of Soil Parameters	29
2.2 Errors of Estimates at 80% Confidence Level	31
2.3 The Comparison of Case Acceptance	32
3.1 Parameters Used In Complex Image Equations.....	56
3.2 Complex Image Amplitudes and Locations	57
3.3 Potential at (r, 0) Produced by Unit Current Source	58
3.4 Comparison of Self-resistance and Surface Potential	76
3.5 Comparison of Mutual Resistance and Surface Potential	77
4.1 Relationship between Voltage Class and Fault duration	97
4.2 Rules for Selecting Segment Length.....	101
4.3 Description of m_r	105
4.4 Comparison of the Results Among All Optimization Methods	113

LIST OF FIGURES

Figure	Page
2.1 Two-layer soil model	8
2.2 Two different structures of soil model	9
2.3 Arrangement for driven rod measurements.....	10
2.4 Arrangement for Wenner measurements.....	11
2.5 Error of estimate versus confidence level.....	21
2.6 Flowchart of the program analyzing soil model	22
2.7 Soil model editor window.....	23
2.8 Soil model excel-formatted input example.....	23
2.9 Select file	24
2.10 Read data.....	24
2.11 Results and figures	25
2.12 Soil model results.....	26
2.13 Warning example	26
2.14 Linear-linear plot for apparent resistance vs. separation	27
2.15 Log-log plot for apparent resistance vs. separation	27
2.16 Input window of Wenner method field data.....	28
2.17 Output window of Wenner method soil parameters.....	28

Figure	Page
3.1 Description of touch voltage	35
3.2 Description of step voltage	35
3.3 Equivalent circuit of touch voltage	36
3.4 Cylindrical coordinate system for two-layer soil model	40
3.5 Modified Cylindrical coordinate system for two-layer soil model	44
3.6 Description of images in image method	45
3.7 $f(\lambda)$ versus λ curve from the original function ($k_{2I}=-0.9, h=100ft$)	50
3.8 Normalized absolute value of error between approximate and original $f(\lambda)$ versus λ curve ($k_{2I}=-0.9, h=100ft$)	51
3.9 $f(\lambda)$ versus λ curve from the original function ($k_{2I}=-0.9, h=5ft$)	51
3.10 Normalized absolute value of error between approximate and original $f(\lambda)$ versus λ curve ($k_{2I}=-0.9, h=5ft$)	52
3.11 $f(\lambda)$ versus λ curve from the original function ($k_{2I}=0.9, h=100ft$)	52
3.12 Normalized absolute value of error between approximate and original $f(\lambda)$ versus λ curve ($k_{2I}=0.9, h=100ft$)	53
3.13 $f(\lambda)$ versus λ curve from the original function ($k_{2I}=0.9, h=5ft$)	53
3.14 Normalized absolute value of error between approximate and original $f(\lambda)$ versus λ curve ($k_{2I}=0.9, h=5ft$)	54

Figure	Page
3.15 Rectangular coordinate system	59
3.16 Cylindrical x-directed conductor model for calculation of self-resistance	71
3.17 Two earth embedded conductor segments of length $2L_0$ and L_1	72
3.18 Horizontal conductor and field point	75
3.19 Square grid and field point.....	77
3.20 WINIGS single line fault diagram	78
3.21 WINIGS grounding system diagram.....	79
3.22 WINIGS touch voltage profile	79
3.23 WINIGS step voltage profile	80
3.24 Error of Emesh between two methods	81
3.25 Error of Estep between two methods	81
3.26 Error of Rg between two methods	82
4.1 Flowchart of pattern search method.....	90
4.2 General Flowchart of Genetic Algorithms	95
4.3 2-by-2 Grounding Grid with X-Y Coordinate System.....	102
4.4 Flowchart of the new grounding systems optimization strategy	110
4.5 Top view of Ealy substation with the old SRP design	111
4.6 WINIGS grounding system diagram of the designed case	117

Figure	Page
4.7 Touch voltage plot of the design case	118
4.8 Step voltage plot of the design case	118
4.9 Grounding system resistance report.....	119

NOMENCLATURE

a	Length of rectangular substation
b	Width of rectangular substation
ρ_1	Upper layer soil resistivity
ρ_2	Lower layer resistivity
h	Thickness of upper layer
V	Voltage measurement (volts) from the voltmeter
A	Current measurement (amps) from the ammeter
R	V/A
l_{dr}	Rod driven depth
dia_r	Rod diameter
sep	Separation between two probes
l_r	Rod length
ρ_a	Apparent resistivity
SRP	Salt River Project
k_{21}	Reflection factor between upper layer and lower layer
k_{32}	Reflection factor between upper layer and the air
R_i	Measured apparent resistance for i th measurement
R_{mi}	Computed apparent resistance for i th measurement
w_i	Weight for i th measurement

η_i	Difference between R_i and R_{mi}
σ_{Ri}	Expected standard deviation of i th measurement
\hat{R}_i	Expected value of i th measurement
σ_{ρ_1}	Standard deviation of estimate of ρ_1
σ_{ρ_2}	Standard deviation of estimate of ρ_2
σ_h	Standard deviation of estimate of h
P_1	Confidence level
R_{ft}	Equivalent feet resistance
R_b	Body resistance
R_f	Foot resistance
ρ	Homogeneous earth of resistivity
I_b	Electric body current
σ_1	Conductivity of lower layer soil
σ_2	Conductivity of upper layer soil
d	Depth of the point current source
J_0	Bessel function of first kind of order zero
G_{23}	Green's function for the field point in the air
G_{22}	Green's function for the field point in the upper-layer soil
G_{21}	Green's function for the field point in the lower-layer soil

r	Radius in cylindrical coordinate system
r_{nk}	Distance between the point current source and the k th complex image at the n th iteration
α_n	Complex coefficient of n th term
β_n	Another complex coefficient of n th term
I	Current injecting into the point source
L_1	Half of length of the line current source
L_0	Half of length of the field conductor
VX	Potential at a point caused by a x-directed line current source
VY	Potential at a point caused by a y-directed line current source
VZ	Potential at a point caused by a z-directed line current source
VXX	Average potential along a x-directed conductor caused by a x-directed line current source
VYY	Average potential along a y-directed conductor caused by a y-directed line current source
VZZ	Average potential along a z-directed conductor caused by a z-directed line current source
VXY	Average potential along a x-directed conductor caused by a y-directed line current source
VYZ	Average potential along a y-directed conductor caused by a z-directed line current source
VZX	Average potential along a z-directed conductor caused by a x-directed line current source

F, H, O	Sub-functions
(X_l, Y_l, Z_l)	Coordinate of the midpoint of a line current source in a rectangular-coordinate system
(x, y, z)	Coordinate of the midpoint of a field conductor in a rectangular-coordinate system
VDF	Voltage-distribution-factor matrix including self and mutual resistances
i_k	Leakage current of the k th segment
r_{jk}	Mutual resistance between segment j and segment k
GPR	Grounding potential rise to remote earth
E_{mesh}	Worst touch potential of a grounding system
E_{step}	Worst step potential of a grounding system
R_g	Grounding resistance to remote earth
dia_c	Diameter of a horizontal grounding conductor
dia_r	Diameter of a vertical grounding rod
Dep	Depth of a grounding grid
I_f	Maximum fault current
I_g	Maximum current flowing through a grounding system
D_f	Current division factor
t_f	Fault current duration
n_r	Number of rods
D	Spacing between two parallel conductors
m_r	Method of rod placement

$E_{touch_allowable}$	Allowable touch voltage
$E_{step_allowable}$	Allowable step voltage
n_r	Number of rods
D	Spacing between two parallel conductors

1 INTRODUCTION

1.1 Overview

According to the IEEE Guide for Safety in AC Substation Grounding, the two main design goals to be achieved by any substation ground system under both normal and fault conditions are:

1. To provide means to dissipate electric currents into the earth without exceeding any operating and equipment limits
2. To assure that a person in the vicinity of grounded facilities is not exposed to the danger of critical electric shock [1].

In order to ensure the safety and well-being of personnel who may come close to conductive media, it is significant to do proper and practical analysis and calculations of substation grounding systems parameters. In other words, the primary purpose of creating ground systems is to avoid the injury of human beings during unbalanced fault conditions. However, the design metrics used in assessing the adequacy of grounding systems remain unchanged, which include touch voltage, step voltage and grounding resistance to the remote earth. Once these three parameters satisfy the safety requirements, the grounding system is considered adequate.

There are two methods to compute the grounding systems safety metrics, one is approximated calculation using experienced IEEE standard equations [1] and the other is accurate calculation using numerical computation.

This kind of computations of safety metrics are based on some substation physical parameters, which are 1) the shape and size of the substation, 2) the soil model and characteristics, 3) the magnitude of the fault current. The author will focus on how to model soil structure and calculate soil parameters, because the other two parameters are easier obtained.

Finally, it is necessary to consider the economical savings when designing and constructing a grounding system. Once the grounding systems safety metrics are lower than the safety allowable values, the cost of labor and components of the grounding system would better be reduced to the lower level. Therefore, an optimization problem is proposed and solved using the combination of a traditional method (Newton method) and heuristic methods (pattern search and genetic algorithms).

1.2 Literature Review

A two-layer soil model is accepted in the industry as an adequate representation of nonhomogeneous soil for grounding system design. Parameters of two-layer soil models are obtained from soil resistivity measurements at the proposed site of the grounding system. The measurements are most commonly made using the Wenner four-probe

method. Evaluation of two-layer soil model from the measured data is done either by graphical methods or by the newer computer based methods. Graphical methods require interpolation and judgment, especially when the actual soil is more complex than a real two-layer pattern. Computer based methods, however, give an optimal two-layer soil fit when the actual soil structure is complex.

A. P. Meliopoulos [2] presented a method and a computer program for interpreting soil measurement data. The method employed a statistical estimation of soil parameters from four pin or three pin measurements. The analysis provided (1) the best estimate of soil parameters, (2) the error of the parameters versus confidence level, (3) a pictorial view of how well the estimated soil model fits the measurements, and (4) the specific measurements, which are not consistent (bad measurements). In it, the method of analyzing the error of the parameters versus confidence level is new and helpful for allowing the users to judge if the measurements and results can be used or more measurements are needed to obtain an acceptable soil model.

Hans R. Seedher [3] developed finite-series expressions for the Wenner apparent resistivity for two-layer soil model instead of infinite series expression, which most researchers used. This method is more convenient to implement the least squares algorithm. The author is using this method to calculate soil parameters. However, the weakness of this method is it assumes the probes are point sources, while those used for

making the measurements have length and diameter.

The grounding systems safety metrics, which contain step voltage, touch voltage and grounding resistance, are the most important criterion to check if the grounding system is adequate or not. Hence, the researchers have focused on how to get these metrics for more than half century. In the beginning, the method using approximate expressions were adopted by the industry and IEEE standard. However, this traditional method cannot fulfill the requirement of accuracy. The numerical computing method has been used since the 1970s and related computer programs have been created.

F. Dawalibi [4], [5] first proposed segmenting grounding conductors and rods in ground grid numerical simulations and then using the principle of superposition. In addition, two ways to compute potentials contributed by each segment were proposed. One is taking a segment as a point source leading to a series expression and another is taking a segment as a line source leading to an integral expressions. Dawalibi also was the first to show that multi-step analysis of interconnected grounding electrodes could be used to handle unbalanced current distribution.

Robert J. Heppe [6] did some promising work on computing grounding resistances while considering the effects of variation of leakage current density caused by the proximity of parallel conductors, cross conductors, angled conductors, and end effects. In

addition, this method can also be used to calculate the surface voltages near grounding conductors, which means the touch and step voltages can be obtained.

Y. L. Chow [7] proposed a new concept of complex images, which could be implemented to model grounding electrodes in layered soils. The image locations and amplitudes are determined by the Prony Method [8]. In addition, the author used an example, which proved that one real image, and four complex images are equivalent to one thousand conventional images in a four-layer soil model.

Once the numerical calculation method is applied to calculate the safety metrics, it is not possible to use traditional optimization method, i.e. Newton method, because the numerical calculation procedure cannot form one or several continuous or differentiable equations. However, it is possible to use direct search method, i.e. pattern search method and heuristic search method, i.e. genetic algorithms.

John Holland [9] introduced Genetic algorithms for the formal examination of the mechanisms of natural evolution, such as inheritance, mutation, selection, and crossover.

Joakim Agnarsson [10] compared several optimization solvers from MATLAB Optimization Toolbox [11] and Global Optimization Toolbox [12], which including pattern search method and genetic algorithms. The author gave us not only the theory of these methods, but also the selection strategy among the optimization solvers developed in MATLAB.

Maurício Caldora Costa [13] combined the response surface technique in the application of genetic algorithms in order to improve the speed of implementing genetic algorithms. The object is to minimize the number of conductors of grounding grids, guaranteeing the safety levels defined by the maximum touch potential. The author only considered the influence of the touch potential and involved in the unequally spaced grounding grids.

1.3 Study Objective

The aim of the thesis is to design grounding systems such that, in case of high fault currents, the acceptable levels of step and touch potentials are hedged below their maximum permissible levels and to investigate techniques, which are capable of reducing grounding resistances to the acceptable value (0.5Ω).

Before designing grounding systems, the two-layer soil model parameters (upper layer soil resistivity, lower layer soil resistivity and upper layer thickness) must be calculated. This will be accomplished using a least squares algorithm to do a nonlinear fit of the soil model to the measurement and then an error analysis will be conducted to get the error bound when confidence level is eighty percent.

Finally, the design has to be made in a cost effective way. In other words, with the three grounding systems metrics (step voltage, touch voltage and grounding resistance)

held under the permissible levels, it is important to minimize the cost of material and the labor. Hence, this is an optimization problem.

All of these methods will be merged into one computer application.

1.4 Thesis Organization

In addition to the introduction and conclusion, there are three principal chapters covering, respectively, the analysis of the soil model, numerical calculations of grounding systems metrics and optimization methods.

Chapter 2 presents how to create a two-layer soil model and compute soil parameters.

Chapter 3 presents the procedure of calculating grounding systems metrics (step voltage, touch voltage and grounding resistance).

Chapter 4 presents the optimization methods and the implementation of the computer program developed by the author in designing a specific grounding system.

In Chapter 5, conclusions and the guidelines to conduct future research are provided.

2 SOIL RESISTIVITY MEASUREMENTS AND ANALYSIS

This section presents the methodology by which the soil measurements are interpreted to define the parameters of a mathematical soil model. The soil model is illustrated in Fig. 2.1. The parameters of the model are:

ρ_1 : upper layer soil resistivity ($\Omega \text{ m}$);

ρ_2 : lower layer soil resistivity ($\Omega \text{ m}$);

h : upper layer soil thickness (m).

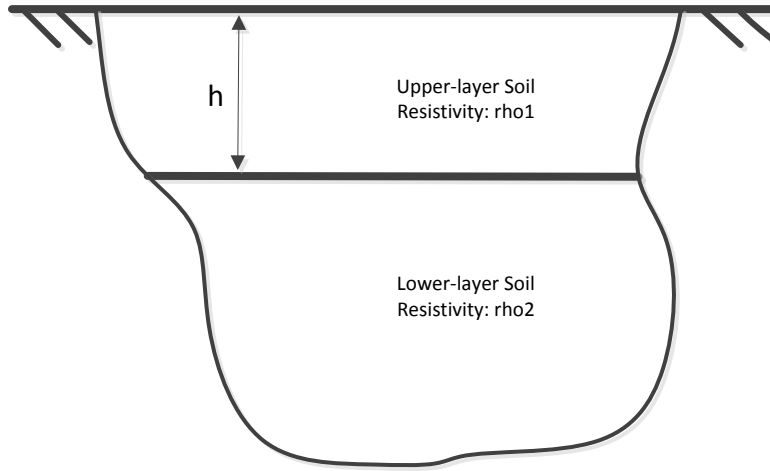


Fig. 2.1 Two-layer soil model

2.1 Soil Resistivity Measurements

Before the design of the grounding system begins, soil resistivity measurements need to be taken at the substation site [2]. The data of soil resistivity is the prerequisite of grounding systems metric calculation. Substations with a uniform soil model throughout

the entire area are rarely found. Usually, the results of measurements are the apparent soil resistivity (ρ_a). If it is available to know the soil geological structure, this is helpful to design the grounding systems. Generally, there are three structures for the soil, which are uniform soil, horizontal layered soil and vertical layered soil. The last two structures are shown as Fig. 2.2.



Fig. 2.2 Two different structures of soil model

Practically, two different measurement ways are used to obtain soil resistivity measurements: (1) three pin arrangement (driven rod method), and (2) four pin arrangement (Wenner and Schlumberger-Palmer method).

(1) Three Pin Measurements (Driven Rod Method)

Three pin measurements are obtained with the arrangement shown in Fig. 2.3. The voltage and current probes (ground electrodes) are driven into earth to a certain depth. The rod is driven to different depths. A measurement of the ratio V/A (resistance) is obtained for a given length of the rod in contact with the soil. Thus, a number of resistance values and rod lengths are generated.

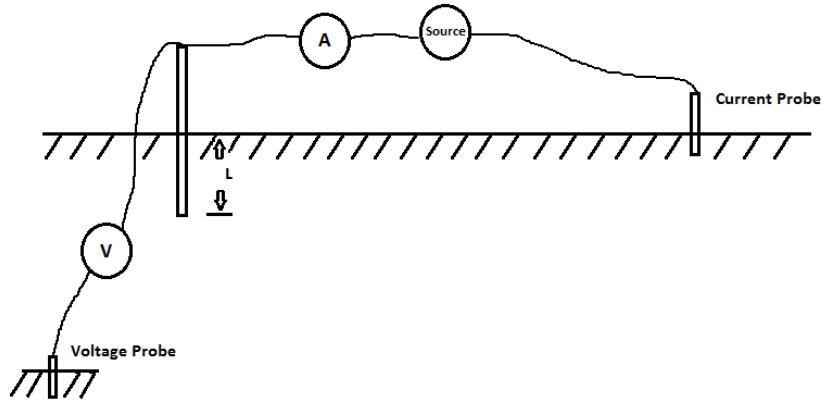


Fig. 2.3 Arrangement for driven rod measurements

The formula used to compute apparent resistivity is:

$$\rho_a = \frac{2\pi l R}{\ln \frac{8l}{d} - 1} \quad (2.1)$$

where,

V = voltage measurement (volts) from the voltmeter shown in Fig. 2.3;

A = current measurement (amps) from the ammeter shown in Fig. 2.3;

$R = V/A$ (Ω);

l = rod driven depth (m);

d = rod diameter (m).

(2) Four Pin Measurements

Four pin measurements are obtained with the arrangement shown in Fig. 2.4. Four identical ground probes are driven into the soil. The probes are located in a straight line and placed at a series of prescribed distance from each other. For the Wenner method, the distances between neighbor probes are equal. Electric current (A) is injected at the two

outer electrodes and the voltage (V) between the other two is measured. A resistance value is obtained with the ratio $R=V/A$. The separation (a) is arbitrarily but, for our work, was taken as prescribed by SRP. For every prescribed separation, a resistance value is computed.

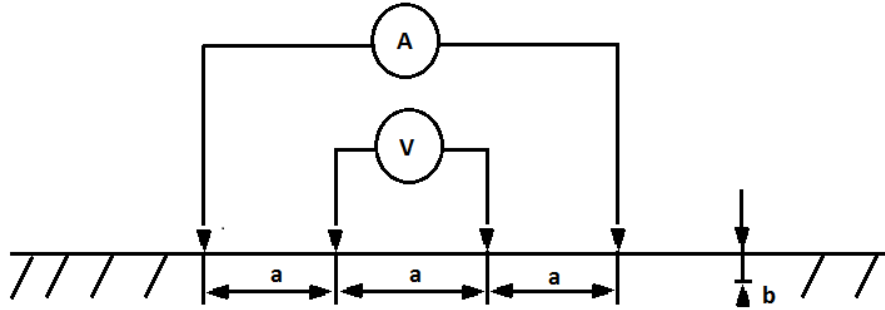


Fig. 2.4 Arrangement for Wenner measurements

The formula used to compute apparent resistivity is:

$$\rho_a = \frac{4\pi a R}{1 + \frac{2a}{\sqrt{a^2 + 4b^2}} - \frac{a}{\sqrt{a^2 + b^2}}} \quad (2.2)$$

where,

V = voltage measurement (volts) from the voltmeter shown in Fig. 2.4;

A = current measurement (amps) from the ammeter shown in Fig. 2.4;

$R = V/A$ (Ω);

a = separation (m);

b = rod length (m).

Commonly, the probes, which are used for the Wenner method, are small enough that

their lengths and diameters can be neglected. Therefore, b is assumed zero and the formula can be simplified as:

$$\rho_a = 2\pi a R \quad (2.3)$$

2.2 Calculation of Apparent Soil Resistivity

The potential distribution of point source in a horizontally layered soil model is developed using Green's functions in Chapter 3. In this chapter, the author omits the derivation of formula (2.3). Therefore, the potential at a point P located at a horizontal distance a away from a point current source S , when both P and S lie on the surface of a two layer earth is [2],

$$V_p = \frac{I\rho_1}{2\pi a} \left[1 + 2 \sum_{n=1}^{\infty} \frac{k^n}{\sqrt{1 + (2nh/a)^2}} \right] \quad (2.4)$$

where,

ρ_1 = upper layer resistivity (Ω m);

ρ_2 = lower layer resistivity (Ω m);

h = upper layer thickness (m);

k = reflection factor $(\rho_2 - \rho_1) / (\rho_2 + \rho_1)$;

I = current flowing from the point source S (A).

For a given soil model, ρ_1 , h and k are fixed. Hence, equation can be written as

$$V_p = IF(a) \quad (2.5)$$

where,

$$F(a) = \frac{\rho_1}{2\pi a} \left[1 + 2 \sum_{n=1}^{\infty} \frac{k^n}{\sqrt{1 + (2nh/a)^2}} \right].$$

Based on Fig. 2.4, there are two current sources, which have the same magnitudes and different directions. When superposition is used, the potential difference between the inner two voltage probes is

$$\begin{aligned} V &= IF(a) - IF(2a) + (-I)F(2a) - (-I)F(a) \\ &= 2IF(a) - 2IF(2a) = 2I[F(a) - F(2a)] \end{aligned} \quad (2.6)$$

Therefore, the formula of apparent resistivity is given as

$$\rho_a = \rho_1 \left[1 + 4 \sum_{n=1}^{\infty} k^n \left(\frac{1}{\sqrt{1 + (2nh/a)^2}} - \frac{1}{\sqrt{4 + (2nh/a)^2}} \right) \right] \quad (2.7)$$

As found before, the equation of apparent resistivity is an infinite series. With the help of [3], this infinite expression can be accurately approximated by a finite-series expression.

When $\rho_2 > \rho_1$, the finite-series expression for ρ_a is:

$$\begin{aligned} \rho_a &= \rho_1 + 4\rho_1 ka \left(\frac{1}{\sqrt{a^2 + 4h^2}} - \frac{1}{\sqrt{4a^2 + 4h^2}} \right) \\ &\quad + 4\pi V_b a \left(\sqrt{\frac{c}{c + (a/h)^\beta}} - \sqrt{\frac{c}{c + (2a/h)^\beta}} \right) \end{aligned} \quad (2.8)$$

where,

$$V_b = \rho_1 [-k - \ln(1 - k)] / (2\pi h);$$

$$c = x_1 (\ln(\rho_2 / \rho_1))^{x_3};$$

$$\beta = 2 - x_2 \ln(\rho_2 / \rho_1);$$

$$x_1 = 16.4133;$$

$$x_2 = 0.136074;$$

$$x_3 = 0.393468.$$

When $\rho_2 < \rho_1$, the finite expression for ρ_a is:

$$\rho_a = \rho_2 + (\rho_1 - \rho_2) \left[2e^{-b(a)a} - e^{-b(2a)2a} \right] \quad (2.9)$$

where,

$$b = \left[b_m - (b_m - x_1)e^{-x_2 a / h} \right] / h;$$

$$b_m = x_3 - x_4 (\rho_2 / \rho_1)^{x_5}.$$

$$x_4 = 0.882645;$$

$$x_5 = 0.673191.$$

Because the measured data is displayed as resistance instead of apparent resistivity based on SRP rules, the computed apparent resistance R is calculated by rearranging (2.3)

$$R = \rho_a / 2\pi a \quad (2.10)$$

2.3 Estimation of Two Layer Soil Parameters

Based on the measured data and the finite expressions, obtaining the two-layer soil model parameters can be seen as a nonlinear regression problem. In other words, the desire is to find the estimated parameters (ρ_1, ρ_2, h) of the above expressions which best fit the measured data points. In theory, either a least squares regression method or least absolute

deviation method can be used. In this work, the least squares regression method is used; therefore, the objective function to be minimized in the search process is formulated as

$$f(\rho_1, \rho_2, h) = w_i \sum_{i=1}^n [R_i - R_{mi}(\rho_1, \rho_2, h)]^2 \quad (2.11)$$

where,

n = number of measurement;

R_i = measured apparent resistance for i th measurement (Ω);

R_{mi} = computed apparent resistance for i th measurement using equations (2.8), (2.9) and (2.10) (Ω);

$w_i = 1/(\alpha R_i)$.

The weights w_i are selected to be inversely proportional to the measurement errors for R_i which is assumed to be proportional to the value R_i . The variable α is the proportionality constant. It is an unconstrained nonlinear minimization problem. The classical state-estimation algorithm, based on estimation theory as suggested in [14] has been found to be quite convenient for the present development. The details of the mathematical basis for the algorithm are neglected, only a simple functional description is outlined here. It has been observed in [14] that rate of convergence increases substantially if measured and computed quantities in (2.11) are replaced by their logarithms. It is further observed that the parameter values should not change by more

than 50%, otherwise convergence can become problematic. These two observations have been applied in this thesis leading to the following iteration scheme.

$$P^{k+1} = P^k + (H_k^T W H_k)^{-1} H_k^T W \eta \quad (2.12)$$

where,

k = iteration index.

$$P = \begin{bmatrix} \rho_1 \\ \rho_2 \\ h \end{bmatrix};$$

$$H_k = \{H(i, j)\} = \left\{ \frac{\partial R_{mi}}{\partial P_j} \right\};$$

$$W = \text{diag}\{R_i^{-2}\};$$

$$\eta = \{\eta_i\} = \{R_i - R_{mi}(\rho_1, \rho_2, h)\};$$

i = number of measurements;

j = number of soil parameters.

In above definitions, p is the parameter vector. The initial values of ρ_1 and ρ_2 are determined by the apparent resistivities calculated using (2.3) when the two probes have their minimum and maximum spacings respectively. Besides, the initial value of h is arbitrarily set equal to 1 [3]. H_k is a $(n \times 3)$ matrix, W is a $(n \times n)$ diagonal matrix, η is the vector of errors, and k presents the iteration count. The algorithm (and the estimate) is independent of the constant α , which is useful in implementing error analysis.

Based on [2], it is necessary to include an acceleration factor, a , into the original

equation (2.12) in order to insure the parameter values do not change by more than 50% in each iteration. Thus, the factor a should be tuned experimentally to obtain convergence. The final equation used for iteration is changed as:

$$P^{k+1} = P^k + a(H_k^T W H_k)^{-1} H_k^T W \eta \quad (2.13)$$

2.4 Rejection of Bad Data

The accuracy of soil resistivity measurements is always affected by: (1) human mistakes, (2) instrument inaccuracies and (3) the longitudinal variation in soil structure. Therefore, it is possible that some measured data with the same measurement conditions are more inconsistent than the others with the rest of the measurements. These measured data are referred to as “bad” data.

Some especially “bad” data are easy to detect by inspection because of obvious differences when compared with other data. However, many bad data points eliminate them by hand. Fortunately, statistical techniques for “bad” data identification and rejection have been developed. The methodology of adaptive weight functions is used here.

This technique is based on the computation of the expected standard deviation of a specific measurement. Specifically, the general model described in Section 2.3 computes for a given measurement R_i the following: (1) the expected value of the measurement \hat{R}_i and (2) the expected standard deviation of the measurement σ_{Ri} . The value of σ_{Ri} is

determined using following equation:

$$\sigma_{R_i} = \frac{R_i}{\sum_{i=1}^n R_i} \cdot n \cdot \sqrt{\frac{\eta^2}{m}} \quad (2.14)$$

where m is the degree of freedom and it equals to $n-3$. Statistically, the measurement R_i is acceptable only when the difference $|R_i - \hat{R}_i|$ is not greater than $3\sigma_{R_i}$. This is based on the assumption of a Gaussian distribution. Thus, if $|R_i - \hat{R}_i| > 3\sigma_{R_i}$ then the measurement R_i is probably a bad datum. In this case, the weight, w , in the optimization problem is assigned a small value. A small value of the weight, w , effectively minimizes the impact of i th measurement in the computation of the parameters.

2.5 Estimation of Soil Parameter Errors

The previous defined objective function is:

$$J = \sum_{i=1}^n w_i^2 \eta_i^2 \quad (2.15)$$

The difference, η , between the measured value and the computed value can be considered a random variable assuming that η is Gaussian distributed with zero mean and standard deviation proportional to the measurement value:

$$\sigma_i = \alpha R_i \quad (2.16)$$

where,

α = scalar factor which is smaller than one.

Based on equation (2.10), the weights w_i are selected to be the inverse of the standard deviation of the random error η_i .

$$w_i = \frac{1}{\sigma_i} \quad (2.17)$$

Since the objective function is the sum of the squares of the normalized Gaussian random variables η_i , the objective function J is also a random variable, which is chi-square distributed. In addition, there are three parameters and n measurements (n random variables) in the model. Hence the variable J is chi-square distributed with $m=n-3$ degrees of freedom.

When parameters are selected as their best estimates $(\hat{\rho}_1, \hat{\rho}_2, \hat{h})$, the corresponding objective value J^* shall be minimized as

$$J^* = \sum_{i=1}^n \frac{1}{\sigma_i^2} (R_i - R_{mi}(\hat{\rho}_1, \hat{\rho}_2, \hat{h}))^2 \quad (2.18)$$

In other words, any other values of ρ_1, ρ_2, h will yield a larger value of J . However, this example is too perfect to be done in reality. Therefore, it is necessary to define a probability P_I when J is bigger than J^* .

Based on equation (2.16), the probability P_I depends on σ_i . Because σ_i is determined by α , the probability P_I is a function of α . If α is increased, the value of J^* is decreased. As a result, the probability P_I will increase. As the selected per unit error α increases, the probability P_I will also increase. Now the error of the measurements can be

transformed into error of the estimates. From the theory of least square estimation [2], the covariance matrix of the estimates is:

$$COV(\hat{P}) = \alpha^2 (H^T W H)^{-1} = \alpha^2 I_0 \quad (2.19)$$

Moreover, the standard deviation of each estimated parameter is the square root of the corresponding diagonal element of the covariance matrix.

$$\sigma_{\rho_1} = \alpha \sqrt{I_0(1,1)} \quad (2.20)$$

$$\sigma_{\rho_2} = \alpha \sqrt{I_0(2,2)} \quad (2.21)$$

$$\sigma_h = \alpha \sqrt{I_0(3,3)} \quad (2.22)$$

According to the equations (2.18), (2.19) and (2.20), the standard deviations of estimated parameters are linearly related to the proportionality factor α . Therefore, the probability P_I is also a function of any of the standard deviations σ_{ρ_1} , σ_{ρ_2} and σ_h . Thus, the probability P_I versus any of the standard deviations σ_{ρ_1} , σ_{ρ_2} and σ_h can be plotted from previous equations. For example, the three curves shown in Fig. 2.5 reflect the three parameters' error (variance) tendencies with respect to the confidence levels. Observe that the error of ρ_I is the smallest, while the error of h is the largest.

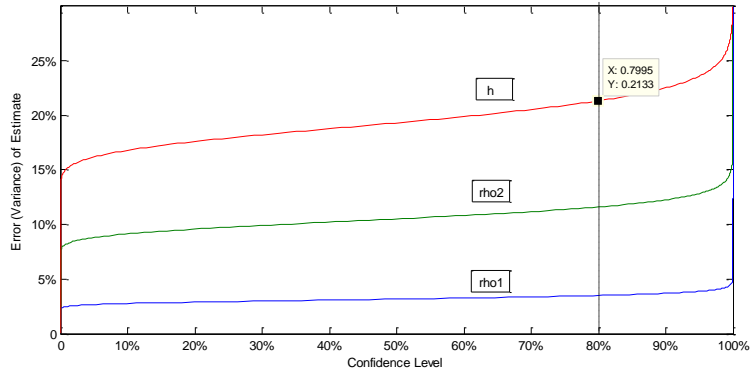


Fig. 2.5 Error of estimate versus confidence level

As found in Fig. 2.5, there is a point cursor, whose coordinate is (0.80, 0.21). It means the error (variance) of h is 21% when the confidence level is 80%. In other words, the confidence interval of h at 80% confidence level is $(\hat{h} - 0.21 \bullet \hat{h} \leq h \leq \hat{h} + 0.21 \bullet \hat{h})$, where h is the true value and \hat{h} is the estimated value. However, for the rule of Salt River Project, the errors of all three parameters at 80% confidence level should be lower than 25%. Hence, the estimated parameters in this example are acceptable. If not, another set of Wenner measurements, must be taken.

2.6 Description of Computer Program Modeling

The methodology of calculating soil parameters and analyzing quality of the estimation is implemented using a computer program, which was created by the author. This program is developed and operated in MATLAB and uses a MATLAB GUI. The flowchart of this program is shown in

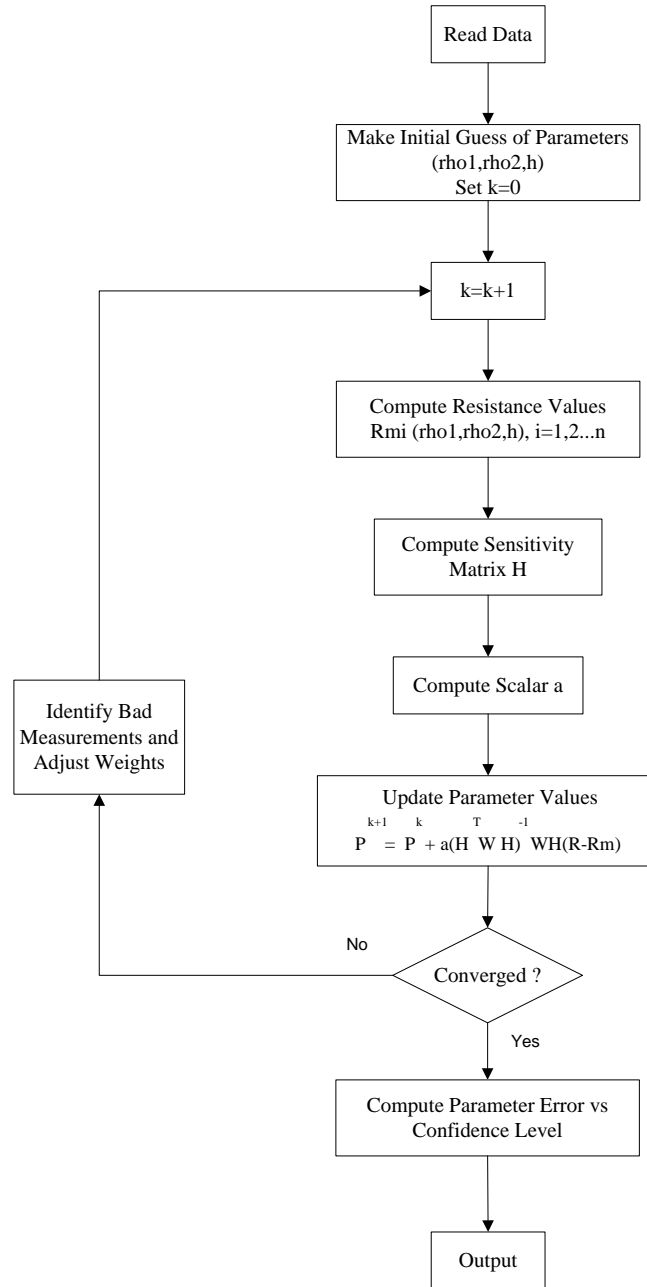


Fig. 2.6 Flowchart of the program analyzing soil model

The input data are the resistance measurements (R_i) and the corresponding separation distances (a). In addition, the output results are the best estimates of parameters, the parameter errors at 80% confidence level and the plots of model fit versus measurements.

All the input, calculations and output procedures were programmed using MATLAB. The graphical user interface (GUI) of this program was similarly developed using MATLAB. The soil model editor window is shown in Fig. 2.7.

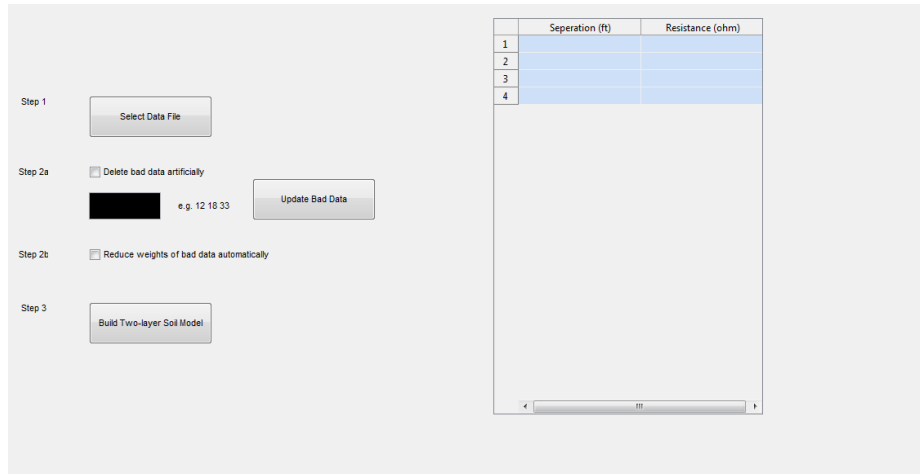


Fig. 2.7 Soil model editor window

Before entering the data into the program, an excel file with a certain format is needed. An example is shown in Fig. 2.8.

	A	B	C	D
1	Field Trip #1			
2	Probe Distance(ft)			
3	Voltage	Current	Seperation	Resistance
4	2.5	7.5	5	7.59
5	3.5	10.5	7	5.15
6	5	15	10	3.51
7	10	30	20	1.72
8	15	45	30	1.5
9	25	75	50	0.92
10	33	99	66	0.72
11	50	150	100	0.68
12	75	225	150	0.36
13	100	300	200	0.24
14	3.5	10.5	7	4.77
15	5	15	10	3.88
16	10	30	20	2.02
17	25	75	50	1.01
18	2.5	7.5	5	6.92
19	3.5	10.5	7	4.6
20	5	15	10	3.13
21	10	30	20	2.15

Fig. 2.8 Soil model excel-formatted input example

After clicking the button of “Select Data File”, the user can see the window like Fig. 2.9 shown below. The excel files must be stored with the program in the same folder. Therefore, the user can select a desired file from this specific folder.

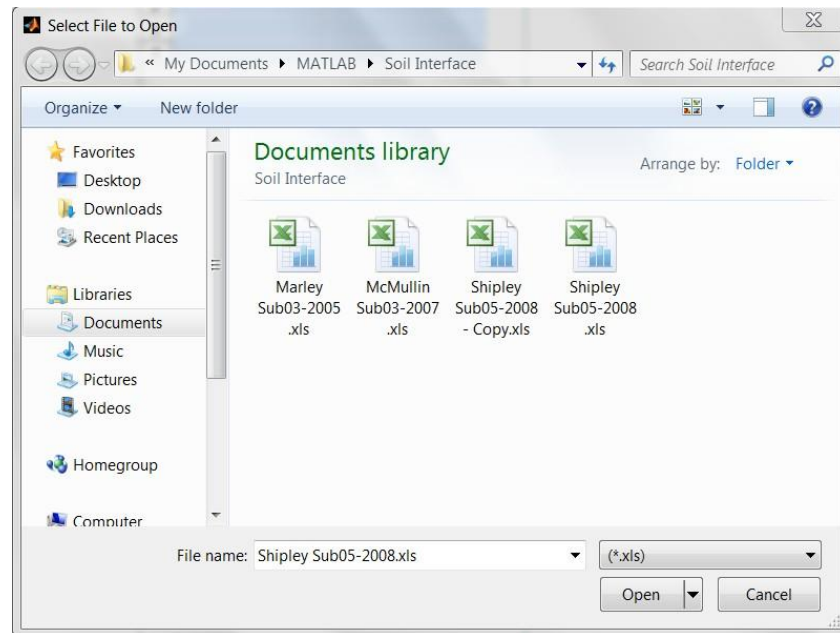


Fig. 2.9 Select file

Once an excel data is selected, the data is read in and the original window is updated as shown in Fig. 2.10.

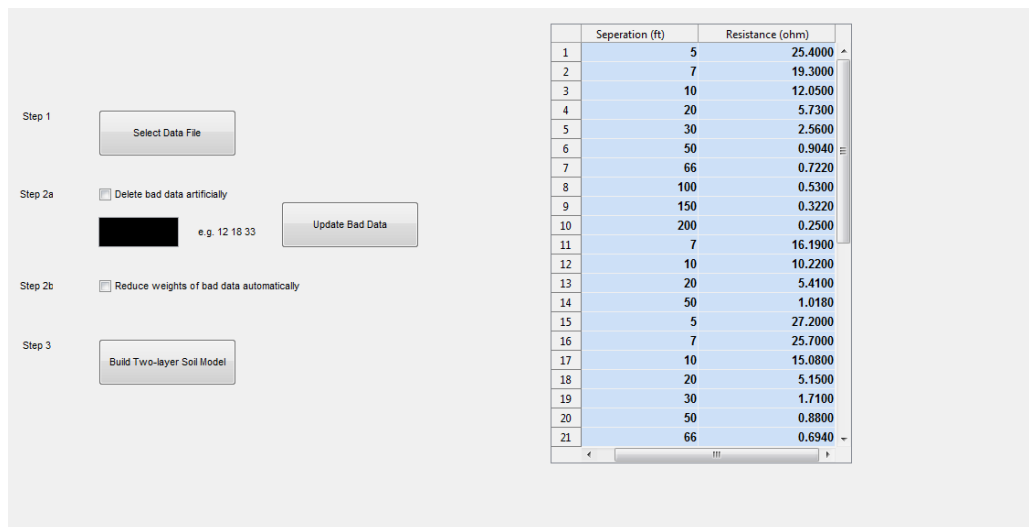


Fig. 2.10 Read data

There are two methods to reduce the affects of bad data. As indicated in steps 2a and 2b in Fig. 2.10, the first method is deleting bad data artificially while the other one is reducing weights of bad data automatically. If the bad data or the outliers are obviously different from the other normal measurements, the user will have a choice to delete the bad data by hand. Unfortunately, most bad data are cannot be identified through a cursory inspection. Consequently, the bad data will be automatically detected and its affect in the regression minimized by multiplying it by a small weight, which was described in Section 2.5.

After clicking the button of “Build Two-layer Soil Model”, this command opens a new interface, which shows all the results and plots as shown in Fig. 2.11.

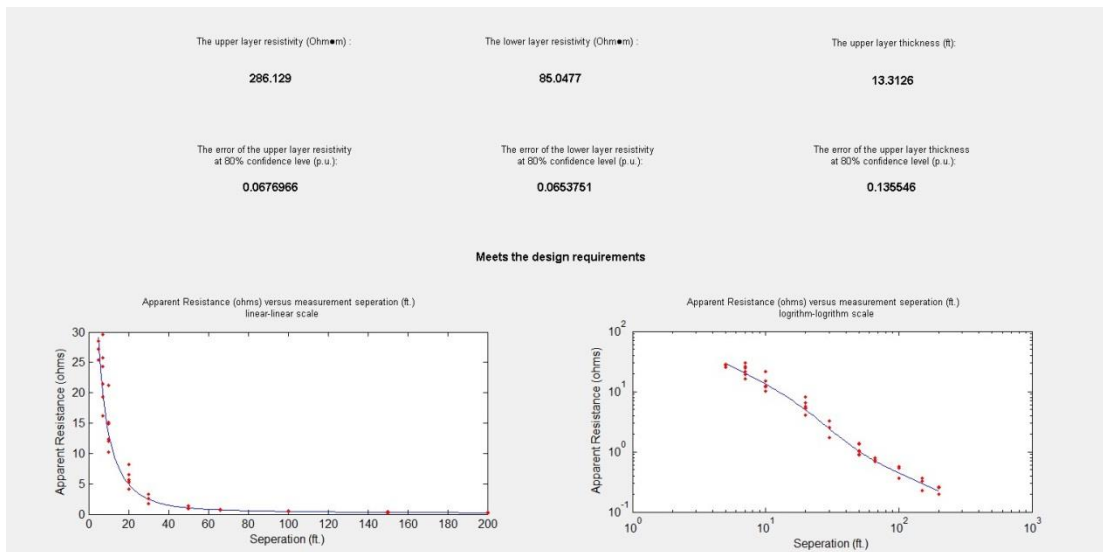


Fig. 2.11 Results and figures

All the calculated results are shown in Fig. 2.12, including:

- The upper layer resistivity ($\Omega\text{ m}$);

- The lower layer resistivity (Ω m);
- The upper layer thickness (ft.);
- The error of the upper layer resistivity at 80% confidence level (p.u.);
- The error of the lower layer resistivity at 80% confidence level (p.u.);
- The error of the upper thickness at 80% confidence level (p.u.).

Where the error (in %) is the absolute difference between the author's result and WINIGS's result divided by the WINIGS's result.

The upper layer resistivity (Ohms*Meters) :	The lower layer resistivity (Ohms*Meters) :	The upper layer thickness (ft):
286.129	85.0477	13.3126
The error of the upper layer resistivity at 80% confidence level (p.u.):	The error of the lower layer resistivity at 80% confidence level (p.u.):	The error of the upper layer thickness at 80% confidence level (p.u.):
0.0676966	0.0653751	0.135546

Fig. 2.12 Soil model results

Depending on the calculated results, the program will warn the user if the results violate the design requirements. For example, a warning is shown as Fig. 2.13.

Warning: The error of the lower layer resistivity and the upper layer thickness at 80% confidence level exceeds 0.25 p.u. This violates the design requirements.

Fig. 2.13 Warning example

There are two figures shown on the bottom of the output window. An example for the plot of apparent resistance (ohms) versus separation (ft.) is shown as Fig. 2.14 . Another plot (Fig. 2.15) shows the logarithmic value of apparent resistance (ohms) versus the logarithmic value of separation (ft.). For most people it is easier to visually identify any bad data measurements from the log-log plot than from the linear-linear plot.

In the figures shown, all the discrete points represent the measured values and blue lines are drawn by using nonlinear least square theory described in previous sections.

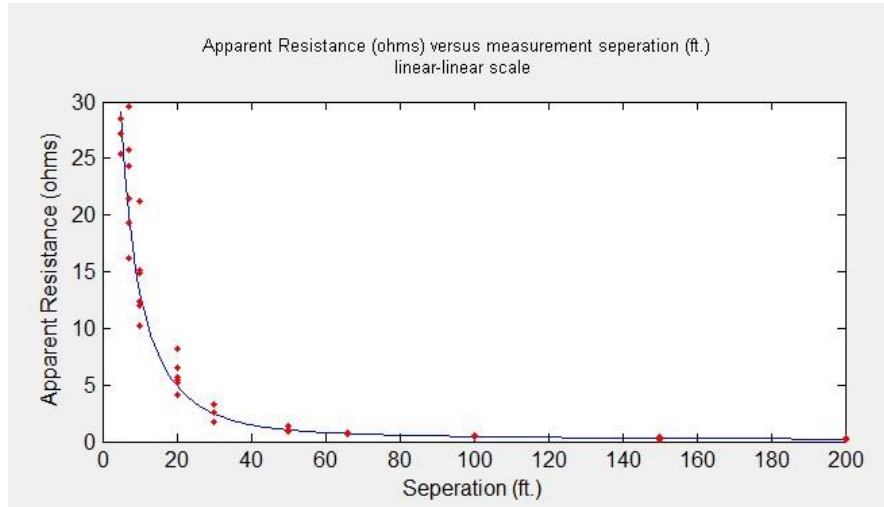


Fig. 2.14 Linear-linear plot for apparent resistance vs. separation

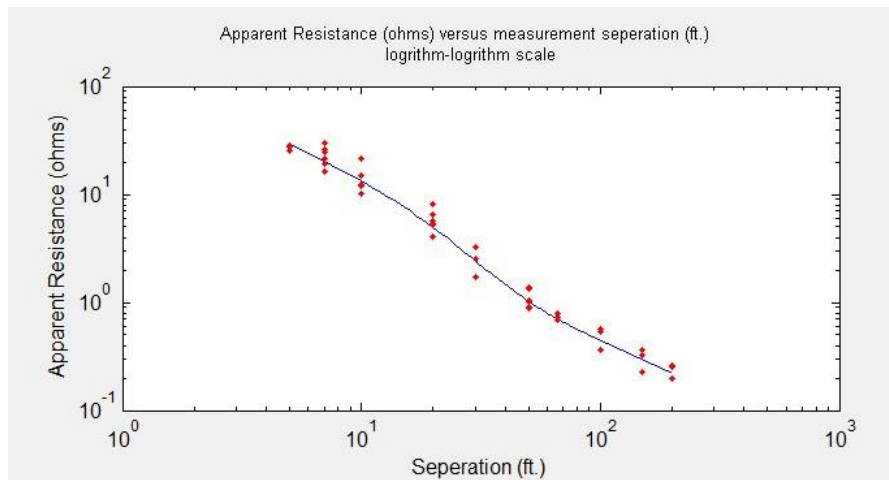


Fig. 2.15 Log-log plot for apparent resistance vs. separation

2.7 Case Study and Comparison with WINIGS Results

WINIGS is an industry-wide accepted software application used to perform analysis and design of grounding systems. One aspect of the software is to build soil models from measured Wenner-method data. In this chapter, a comparison is made

between the results obtained by WINIGS and by our application.

As shown below, Fig. 2.16 is the input window and Fig. 2.17 is the corresponding output window of WINIGS.

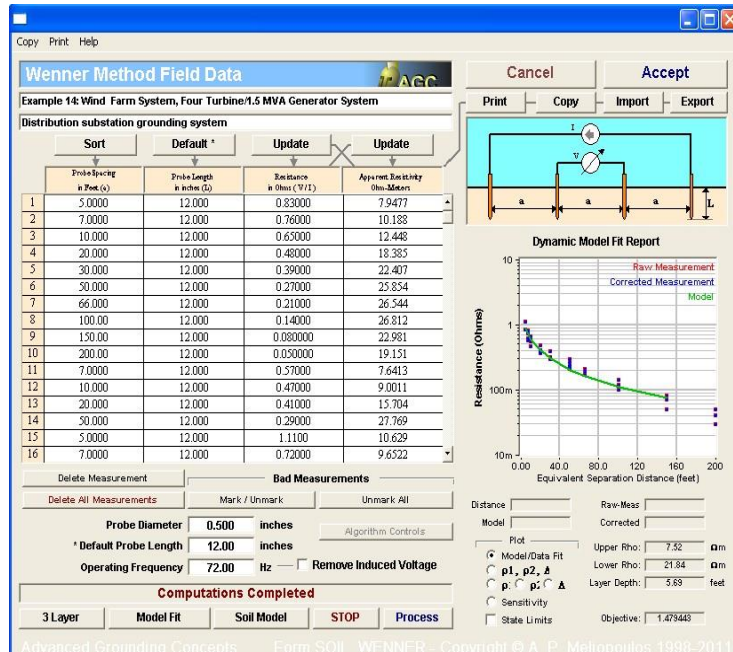


Fig. 2.16 Input window of Wenner method field data

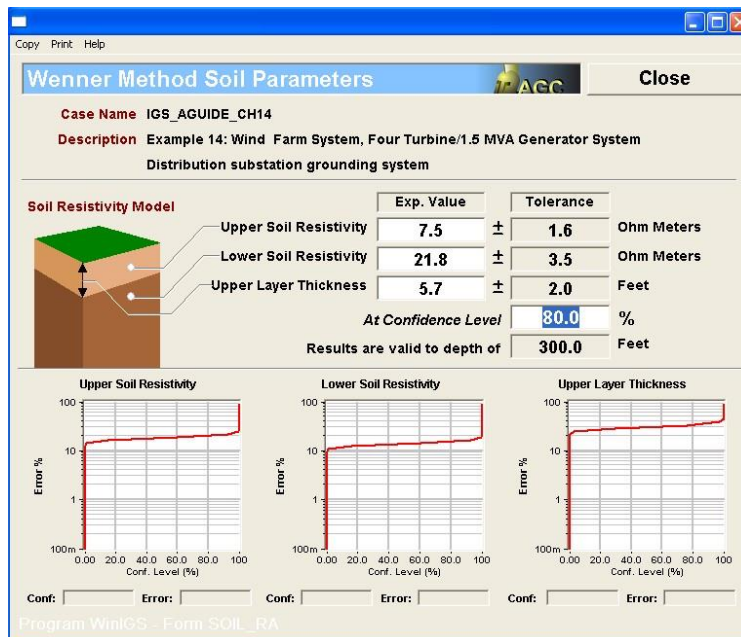


Fig. 2.17 Output window of Wenner method soil parameters

The author used thirteen data cases received from SRP (Salt River Project) and compared the results of our applications with WINIGS. These results are shown below.

Table 2.1 The Comparison of Soil Parameters

	Tenney		Cell Tower		AFGS		Burton		New Hunt	
	1	2	1	2	1	2	1	2	1	2
ρ_1	39.1	37.4	67.9	62.2	61.4	63.3	19.8	19.4	45.6	44.9
ρ_2	8.9	7.1	37.7	35.2	20.3	20.7	54.2	54.8	21.2	20.5
h	80.3	89.7	11.1	17	10.3	9.1	41.1	41.8	44.1	45.4
	Cheatham		McPherson		Shipley		McMullin		Clark	
	1	2	1	2	1	2	1	2	1	2
ρ_1	28	25.6	61.5	60.3	86.2	80.5	291.8	283.5	7.5	7.2
ρ_2	11.4	11.2	39.8	38	31.7	30.7	84.5	84.7	21.9	19.8
h	43.9	45.8	45.5	51.8	14.7	16.1	15.2	13.8	5.8	5.2
	Sinnott		Dinosaur		Marley					
	1	2	1	2	1	2				
ρ_1	52.7	52.4	171.6	150.8	66.1	64.1				
ρ_2	19.8	20.2	114.5	114.7	87.7	85.2				
h	34.5	33.8	5.6	4.4	7.8	8				

In the table shown above, the first row contains the names of each substation for which a soil model was build. The second row is a number indicating which method was used to calculate the soil parameters, where method “1” is indicates WINIGS, and “2” indicates our method. The next three rows list the values of ρ_1 , ρ_2 , and h using these methods. For example, soil parameters of “Sinnott” calculated by author’s method are very close to the WINIGS results and the errors are all lower than 2%. However, there are some larger differences between the results calculated by these two methods for “Tenney” where the largest error is about 20% in ρ_2 . There is no way to know which method is more accurate than another. One value of this method, as communicated to us by SRP

personnel, is that this alternative approach and result allows the substation engineer to have two results from different applications, on providing a check on the other. The engineer can then use both results in an advisory way, creating a design that is conservative for both soil models. The “percent error” in this discussion is defined as the absolute difference between the results of the two methods divided by the WINIGS result multiplied by 100. A detailed comparison between the results of these two methods shows that the number of cases in which each of the parameters differs by less than 10% is seven out of thirteen. Larger errors tend to occur on upper layer thickness (h), particularly where the upper layer thickness is small, a situation where, in many cases, the substation engineer may choose to use a single layer soil model.

Based on section 2.5, it is possible to analyze the quality of the soil parameters estimates with some statistical methods. As described before, the error (confidence interval) at the 80% confidence level for each of soil parameters is used by SRP engineers as a figure of merit. Therefore, all the corresponding errors in percentage (with the base of the WINIGS’s results) for three soil parameters from these thirteen substations are listed in Table 2.2.

Table 2.2 Errors of Estimates at 80% Confidence Level

Substation Name	Error% at 80% CL* for ρ_1	Error% at 80% CL for ρ_2	Error% at 80% CL for h
Tenney	4.17%	100%	34.46%
Cell Town	4.19%	4.75%	20.19%
AFGS	4.61%	2.99%	8.00%
Burton	5.27%	7.21%	34.57%
New Hunt	3.52%	11.62%	21.40%
Cheatham	6.75%	24.00%	41.48%
McPherson	2.60%	12.17%	37.71%
Shipley	5.44%	5.74%	14.20%
McMullin	6.45%	6.42%	13.31%
Sinnott	35.51%	2.88%	66.30%
Clark	1.81%	3.66%	6.51%
Dinosaur	19.00%	4.60%	89.05%
Marley	10.56%	1.04%	76.49%

* “CL” is the abbreviation of “confidence level” shown in this table.

If the error of any soil parameter is greater than 25% at 80% confidence level, both the measurement data and the result estimates for corresponding substation are rejected.

Otherwise, they are accepted. Using this rule, the acceptability of the models built above is indicated in Table 2.3. It can be seen in Table 2.3 that there are three more cases accepted using the author's method than WINIGS.

Table 2.3 The Comparison of Case Acceptance

Substation Name	Acceptance Situation of WINIGS	Acceptance Situation of OPTIMGRID
Tenney	Reject	Reject
Cell Town	Reject	Accept
AFGS	Accept	Accept
Burton	Reject	Reject
New Hunt	Reject	Accept
Cheatham	Reject	Reject
McPherson	Reject	Reject
Shipley	Reject	Accept
McMullin	Reject	Accept
Sinnott	Reject	Reject
Clark	Accept	Accept
Dinosaur	Reject	Reject
Marley	Reject	Reject

As mentioned before, there is no guarantee that one method is more accurate or reliable than another due to the different models used. One important benefit is that OPTIMGRID will bring a second reference value. It is expected that the substation engineer's experience might consider both values when making design decisions.

3 ANALYSIS OF GROUNDING SYSTEM

Presented in this section is the analysis of grounding system, including safety requirements of grounding system, the calculation of step voltage, touch voltage and grounding resistance (to remote earth) based on both a uniform soil model and a two-layer soil model.

3.1 The Equivalent Circuit of Body Shock

Effects of an electric current passing through the vital parts of a human body depend on the duration, magnitude and frequency of this current. Humans are very vulnerable to the effects of electric current at frequencies of 50 Hz and 60 Hz. Currents about 0.1 Amp can be lethal at these frequencies.

In addition to frequency and amplitude, shock duration plays a role in lethality. Many researchers have proposed curve analysis and equations to determine the range of allowable current magnitude versus shock duration. In order to model equivalent circuit of a human body, it is necessary to approximate the human body as a resistance under the assumption of both direct current and 60 Hz current. It is usually the resistance between one hand and two feet like that shown in Fig. 3.1, or the resistance between one foot and another foot like that shown in Fig. 3.2 that is taken as the critical path and hence is modeled.

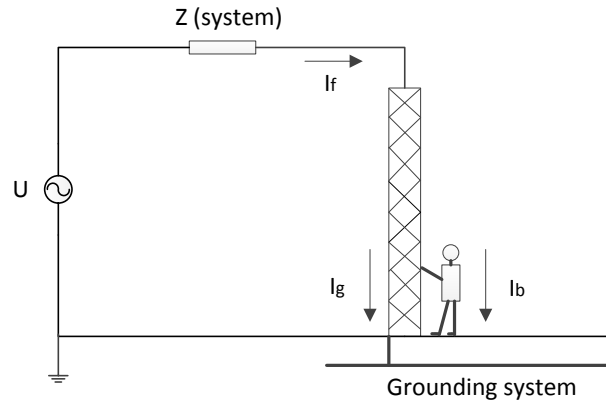


Fig. 3.1 Description of touch voltage

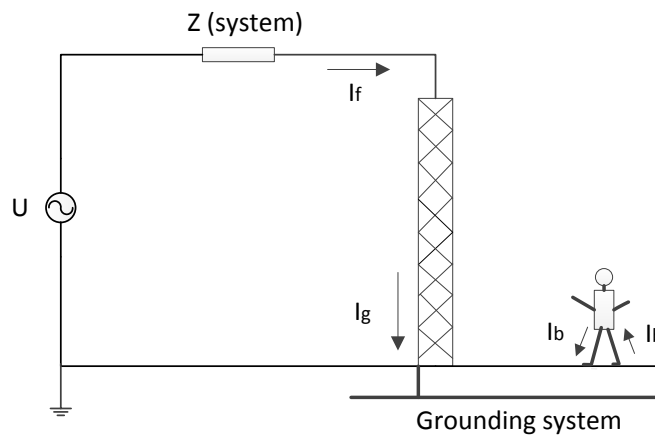


Fig. 3.2 Description of step voltage

However, the value of body resistance is dependent on the many unpredictable factors that follow:

- (1) Skin condition: the human skin with water, sweat, conductive metal dust and skin breakdown.
- (2) Touch voltage (nonlinearity): the resistance decreases as the touch voltage increases.
- (3) Touch condition: the resistance decreases as either the touch area or the touch tightness increases.

(4) Magnitude and duration of shock current: the resistance decreases as either the magnitude or the duration of shock current increases.

According to IEEE Std80-2000 [1], the value of body resistance is usually selected as $1000\ \Omega$.

Once the body resistance (R_b) and the foot resistance (R_f) are determined, the equivalent circuit used to determine the shock current can be drawn as below. Fig. 3.3 represents the equivalent circuit used in calculating both the touch and step voltage by using (3.2) and (3.3) for R_{ft} , respectively. For the touch-voltage-equivalent circuit, the foot resistance is the parallel resistance of two feet and its value is $R_{ft}=R_f/2$. For the step-voltage-equivalent circuit, the foot resistance is the series resistance of two feet and its value is $R_{ft}=2R_f$.



Fig. 3.3 Equivalent circuit of touch voltage

For the purpose of circuit analysis, the human foot is usually represented as a conducting plate touching the surface of the earth. The foot resistance (to remote earth) of the plate of radius b (m) on the surface of a homogeneous earth of resistivity ρ ($\Omega \cdot m$) is given as [1]:

$$R_f = \frac{\rho}{4b} \quad (3.1)$$

Traditionally, the foot is approximated as a circular plate with a radius of 0.08 m. With only slight approximation, equations for R_{ft} can be obtained in numerical form and expressed in terms of ρ as follows [1].

For the touch-voltage-equivalent circuit

$$R_{ft} = \left(\frac{\rho}{4 * 0.08} \right) / 2 \cong 1.5\rho \quad (3.2)$$

And for the step-voltage-equivalent circuit

$$R_{ft} = \left(\frac{\rho}{4 * 0.08} \right) * 2 \cong 6\rho \quad (3.3)$$

Once the touch and step voltage equivalent circuits are modeled, the electric current through the human body is computed as:

$$I_b = \frac{V_{eq}}{R_{eq}} = \frac{V_{eq}}{R_b + R_{ft}} \quad (3.4)$$

3.2 Grounding System Safety Assessment

The electric body current provides the basis for safety assessment of grounding systems. Based on available experimental data, the IEEE Std80-2000 [1] suggests that electric body currents below I_b can be tolerated by average person. Thus according to this standard, the maximum allowable body current is:

$$I_b = \frac{0.116}{\sqrt{t_f}} \text{ amps} \quad (3.5)$$

where,

t =the duration of the electric current in seconds.

Through equivalent circuits and some approximations of R_b and R_{ft} , the allowable touch and step potential can be calculated using equations (3.6), and (3.7), respectively.

$$E_{touch_allowable} = (1000 + 1.5\rho) \frac{0.116}{\sqrt{t_f}} \quad (3.6)$$

$$E_{step_allowable} = (1000 + 6\rho) \frac{0.116}{\sqrt{t_f}} \quad (3.7)$$

where ρ is the earth resistivity, which means it is the surface material resistivity if the high resistivity surface material exists or it is the upper-layer soil resistivity in the two layer soil model or it is the uniform soil resistivity in the uniform soil model, and t is the shock duration.

In order to satisfy with the safety requirements of grounding systems, the maximum touch and step potential should not exceed the allowable values calculated with above equations. Thus, when it is necessary to optimize total cost of grounding systems, the computed values of touch and step potential of each desired grounding grid need to be constrained under the allowable (safe) values. Otherwise, the unqualified design of grounding systems should be abandoned.

3.3 Electromagnetic Analysis and Green's Functions

The key point for analyzing and optimizing grounding systems is how to calculate the grounding systems safety metrics (touch potential, step potential and grounding

resistance) of each specific grounding grid. Once the safety metrics are obtained, it is easy to compare them with allowable values. The author is using two methods, which are called the images method and the complex images method respectively, to do electromagnetic analysis and develop corresponding Green's function, which can be regarded as the potential produced by a point current source with unit current. These two methods are correlated and both combine integrals of Green's function solutions to Laplace's Equation and superposition. For complex images method, the matrix pencil method is used individually. A more detailed description of these methods is provided later.

Generally, the two-layer soil model is accurate enough to simulate the earth. In this chapter, all soil models are modeled as a two-layer conducting medium located below a non-conducting medium of air. The grounding grid is embedded in the conducting medium to help the fault current leak into the deeper earth. Since the fault current flowing into the grounding grid is always at low frequency (60 HZ), the author has neglected the transients such as those associated with lightening surges. Otherwise, the skin effect should be considered.

In order to calculate the grounding system parameters more accurately, it is necessary to break the underground conductors and rods into small horizontal and vertical segments. The segments may be located in either the upper or lower conducting regions.

In addition, it is assumed that the fault current injected into the earth is the direct current without any calculations of inductance or capacitance and the voltage drop from one point of a grounding grid to any other point of same grid is negligible for simplicity of the model.

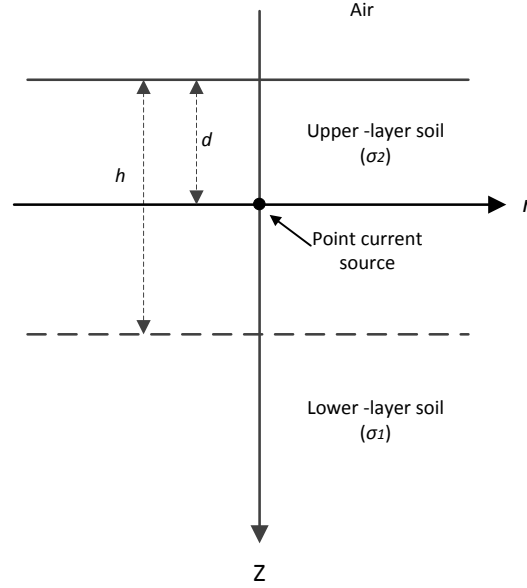


Fig. 3.4 Cylindrical coordinate system for two-layer soil model

The first step in the development of this method is to solve for the potential in the three regions generated by a point current source with unit current in the upper-layer soil shown in Fig. 3.4. This picture depicts the two-layer soil model, where σ_2 , σ_1 , h and d are conductivity of upper layer, lower layer, thickness of upper layer and depth of the point current source respectively. The cylindrical coordinate system should be employed in this problem with three variables, which are radius r , coordinate in z -axis z , and cylindrical angle φ . However, this is a symmetrical system, so the solution is independent of the cylindrical angle. In addition, it is noted that the origin is selected at the location of the

current source point.

In the cylindrical system shown in Fig. 3.4, the general form of Green's function can be expressed by [18]

$$G_{23}(r, z) = \frac{1}{4\pi\sigma_2} \int_0^\infty [A_3(\lambda)e^{-\lambda z} + B_3(\lambda)e^{+\lambda z}] \times J_0(\lambda r) d\lambda \quad (3.8)$$

$$G_{22}(r, z) = \frac{1}{4\pi\sigma_2} \int_0^\infty [e^{-\lambda|z|} + A_2(\lambda)e^{-\lambda z} + B_2(\lambda)e^{+\lambda z}] \times J_0(\lambda r) d\lambda \quad (3.9)$$

$$G_{21}(r, z) = \frac{1}{4\pi\sigma_2} \int_0^\infty [A_1(\lambda)e^{-\lambda z} + B_1(\lambda)e^{+\lambda z}] \times J_0(\lambda r) d\lambda \quad (3.10)$$

where,

J_0 = Bessel function of first kind of order zero;

G_{23} = Green's function for the field point in the air;

G_{22} = Green's function for the field point in the upper-layer soil;

G_{21} = Green's function for the field point in the lower-layer soil;

$A_{1,2,3}, B_{1,2,3}$ = arbitrary functions to be determined by employing the boundary conditions [17].

The derivation process for G_{22} and other Green's functions can be found in [17]. As an example, the expression for G_{22} is given as:

$$G_{22}(r, z) = \frac{1}{4\pi\sigma_2} \int_0^\infty [e^{-\lambda|z|} - k_{32}e^{-\lambda(2d+z)} + f(\lambda)(k_{32}^2 e^{-\lambda(2h+2d+z)} - k_{32}e^{-\lambda(2h+z)} + e^{-\lambda(2h-2d-z)} - k_{32}e^{-\lambda(2h-z)})] J_0(\lambda r) d\lambda \quad (3.11)$$

where,

$$k_{21} = \frac{\sigma_2 - \sigma_1}{\sigma_2 + \sigma_1};$$

$$k_{32} = \frac{\sigma_3 - \sigma_2}{\sigma_3 + \sigma_2};$$

$$f(\lambda) = \frac{k_{21}}{1 + k_{21}k_{32}e^{-2\lambda h}}$$

Based on Taylor Series, it is easy to obtain the equation shown below:

$$\frac{1}{1-x} = \sum_{n=0}^{\infty} x^n \quad (3.12)$$

where, $|x| < 1$.

It is obvious that the absolute values of k_{21} and k_{32} are smaller than 1.0. In addition, $e^{-2\lambda h}$ is smaller than 1.0 as well, since λ and h are positive. When considering the uniform soil model, the value of h should not be zero as well, because it is possible to model uniform soil as two-layer soil with same values of upper and lower resistivity and any positive value of h . Therefore, the function of $f(\lambda)$ can be Taylor decomposed as:

$$f(\lambda) = \sum_{n=0}^{\infty} k_{21} [k_{21}k_{32}e^{-2\lambda h}]^n = \sum_{n=0}^{\infty} k_{21}^{n+1} k_{32}^n e^{-2n\lambda h} \quad (3.13)$$

If the exponential series in (3.13) is substituted into (3.11), then the original exponential terms in (3.13) can be merged with the $f(\lambda)$ in the exponential series (all exponential terms), and then Lipschitz integration [17] is used as shown:

$$\int_0^{\infty} J_0(\lambda r) e^{-\lambda z} d\lambda = \frac{1}{\sqrt{z^2 + r^2}} \quad (\text{Re}(z) > 0) \quad (3.14)$$

It can be used to integrate each exponential term and perform the integral in (3.11)

to have a new form as shown in (3.15) [17].

$$G_{22}(r, z) = \frac{1}{4\pi\sigma_2} \left[\frac{1}{r_0} - \frac{k_{32}}{r_0'} + \sum_{n=0}^{\infty} k_{21}^{n+1} \left(\frac{k_{32}^2}{r_{n1}} - \frac{k_{32}}{r_{n2}} + \frac{1}{r_{n3}} - \frac{k_{32}}{r_{n4}} \right) \right] \quad (3.15)$$

Because k_{32} is always equal to -1.0, the above function can be reduced to:

$$G_{22}(r, z) = \frac{1}{4\pi\sigma_2} \left[\frac{1}{r_0} + \frac{1}{r_0'} + \sum_{n=0}^{\infty} k_{21}^{n+1} \left(\frac{1}{r_{n1}} + \frac{1}{r_{n2}} + \frac{1}{r_{n3}} + \frac{1}{r_{n4}} \right) \right] \quad (3.16)$$

where,

$$r_0 = \sqrt{r^2 + (z-d)^2} ;$$

$$r_0' = \sqrt{r^2 + (z+d)^2} ;$$

$$r_{n1} = \sqrt{r^2 + [2(n+1)h + d + z]^2} ;$$

$$r_{n2} = \sqrt{r^2 + [2(n+1)h - d + z]^2} ;$$

$$r_{n3} = \sqrt{r^2 + [2(n+1)h - d - z]^2} ;$$

$$r_{n4} = \sqrt{r^2 + [2(n+1)h + d - z]^2} .$$

The above Green's function is the result of transferring the origin from the point current source to the interface between the air and the upper-layer soil shown in Fig. 3.5.

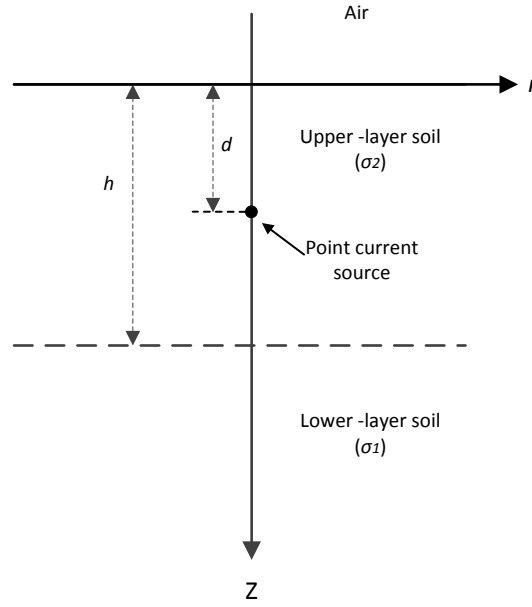


Fig. 3.5 Modified cylindrical coordinate system for two-layer soil model

Based on the images method found in [18], the variable r_n can be looked as the position of one specific image and k_{2l}^{n+l} is correspondingly the image magnitude as shown in Fig. 3.6.

Fig. 3.6 shows an example of images method. In this example, the point current source is located in the upper-layer soil with the cylindrical coordinates of $(r,z)=(0, d)$ and the thickness of upper-layer soil is h . The field point is located at the origin, so its coordinate is $(0, 0)$. Based on equation (3.16), an infinity series of k_{2l}^{n+l}/r_n must be summed. Hence, there should be infinity of images in Fig. 3.6. However, only the zero order (k_{2l}^0) and first order (k_{2l}^1) images are shown.

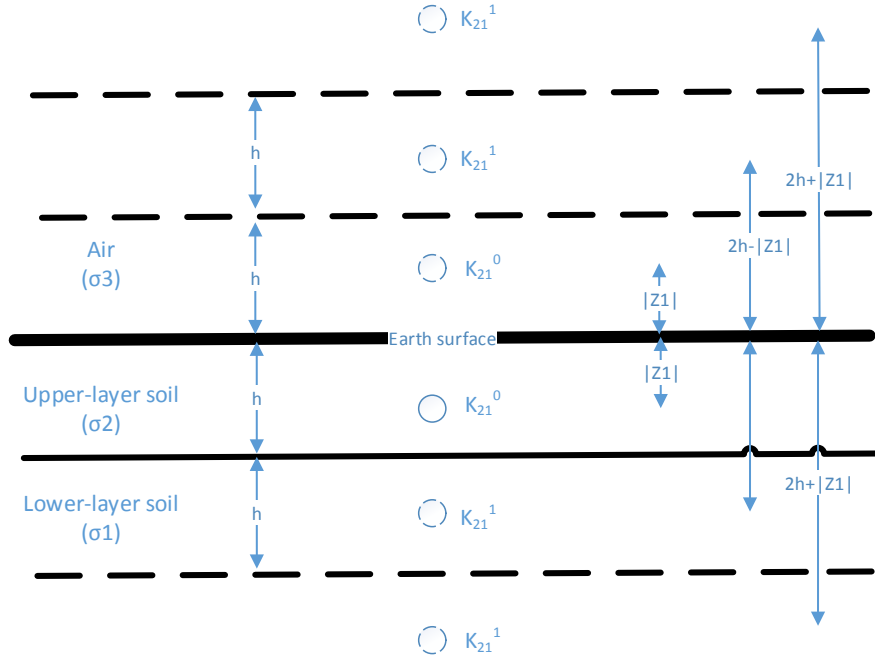


Fig. 3.6 Description of images in image method

As for calculation of $G_{21}(r, z)$, the similar method will be used [17]:

$$G_{21}(r, z) = \frac{1}{4\pi\sigma_2} \left[\frac{1}{r_0} + \frac{1}{r_0'} + \sum_{n=0}^{\infty} k_{21}^{n+1} \left(\frac{1}{r_{n1}} + \frac{1}{r_{n2}} + \frac{1}{r_{n3}} + \frac{1}{r_{n4}} \right) \right] \quad (3.17)$$

where,

$$r_{n3} = \sqrt{r^2 + (2nh + d + z)^2} ;$$

$$r_{n4} = \sqrt{r^2 + (2nh - d + z)^2} .$$

In addition to r_{n3} and r_{n4} , the other r parameters are equal to the corresponding results of the $G_{22}(r, z)$ calculation.

From the analysis shown above, the key point of the images method is the Taylor decomposition of $f(\lambda)$ in order to obtain the specific image magnitude and position. However, the corresponding Green's functions have the form of an infinite series.

Unavoidably, the series-truncation problem should be considered and this will cause difficulty in computing the Green's function accurately. On the other hand, calculating the series requires a longer calculation time when more terms are used.

3.4 Complex Image Method

In order to overcome the shortcomings of the image method and improve the efficiency of Green's functions calculation, the complex images method [15] has been developed to calculate the grounding systems parameters.

The most significant improvement of complex images method is the implementation of finite series of $f(\lambda)$ in place of the infinite Taylor series.

$$f(\lambda) = \frac{k_{21}}{1 - k_{21}e^{-2\lambda h}} \cong \sum_{n=1}^N \alpha_n e^{\beta_n \lambda} \quad (3.18)$$

where,

α_n, β_n = undetermined coefficients, which may be, and are usually, complex numbers;

N = number of series.

The matrix pencil method [16] is used to limit the number of terms and improve the calculation efficiency.

It is necessary to choose M samples of this function (3.18) at intervals of λ_s , in other words, the sampled data y_m are equally spaced. The next step is to find corresponding

coefficients α and β in order to fit the sampled data and thus, fit the function (3.18) as well as possible. Therefore, (3.18) can be written as

$$\begin{aligned} y_m = f(m\lambda_s + \lambda_0) &= \sum_{n=1}^N \alpha_n e^{\beta_n(m\lambda_s + \lambda_0)} = \sum_{n=1}^N \alpha_n e^{\beta_n \lambda_0} (e^{\beta_n \lambda_s})^m \\ &= \sum_{n=1}^N R_n z_n^m \quad m = 0, \dots, M-1 \end{aligned} \quad (3.19)$$

where,

λ_0 = initial point of the sample;

λ_s = selected interval between two adjacent sampled data values;

$R_n = \alpha_n e^{\beta_n \lambda_0} \quad n = 1, \dots, N$;

$z_n = e^{\beta_n \lambda_s} \quad n = 1, \dots, N$;

M = number of data samples.

Based on [15], N is arbitrarily selected as 4. Next, define two matrices Y_1 and Y_2 [16] and in them, the variables of y_1 to y_{M-1} are defined by (3.19)

$$[Y_1] = \begin{bmatrix} y_1 & y_2 & \dots & y_L \\ y_2 & y_3 & \dots & y_{L+1} \\ \vdots & \vdots & \ddots & \vdots \\ y_{M-L} & y_{M-L+1} & \dots & y_{M-1} \end{bmatrix}_{(M-L) \times L} \quad (3.20)$$

$$[Y_2] = \begin{bmatrix} y_0 & y_1 & \dots & y_{L-1} \\ y_1 & y_2 & \dots & y_L \\ \vdots & \vdots & \ddots & \vdots \\ y_{M-L-1} & y_{M-L} & \dots & y_{M-2} \end{bmatrix}_{(M-L) \times L} \quad (3.21)$$

where L is arbitrarily selected to equal to 4 [16], and M is determined from several experiments (mentioned later).

The value of z_n , shown in (3.19), is equal to the generalized eigenvalues of the matrix which is the product of the pseudo-inverse of $[Y_2]$, $[Y_2]^{-1}$, and $[Y_1]$ as shown in [16]. Hence, it is possible to use MATLAB's "eig" function to get the values of z_n shown as:

$$z_n = \text{eig}([Y_2]^{-1}[Y_1]) \quad n=1, \dots, N \quad (3.22)$$

Once M and z_n are determined, the value of R_n is easily obtained through solving the following matrix equation, which is a matrix representation of (3.19).

$$\begin{bmatrix} y_0 \\ y_1 \\ \vdots \\ y_{M-1} \end{bmatrix} = \begin{bmatrix} 1 & 1 & \cdots & 1 \\ z_1 & z_2 & \cdots & z_N \\ \vdots & \vdots & \ddots & \vdots \\ z_1^{M-1} & z_2^{M-1} & \cdots & z_N^{M-1} \end{bmatrix} \begin{bmatrix} R_1 \\ R_2 \\ \vdots \\ R_N \end{bmatrix} \quad (3.23)$$

From (3.19), the values of α_n and β_n can be obtained by solving

$$R_n = \alpha_n e^{\beta_n \lambda_0} \quad n=1, \dots, N \quad (3.24)$$

$$z_n = e^{\beta_n \lambda_s} \quad n=1, \dots, N \quad (3.25)$$

where R_n and z_n are obtained from (3.23) and (3.22).

However, it is still necessary to determine the values of λ_0 , λ_s and M to calculate α_n and β_n from (3.24) and (3.25). In order to capture the behavior of $f(\lambda)$ versus λ curve as much as possible and given that the range of λ is $[0, +\infty]$, the value of λ_0 should be zero while the value of λ_{max} ($\lambda_{max} = M * \lambda_s$) would ideally be positive infinity, which is not possible.

Therefore, it is necessary to find a suitable λ_{max} . Because $-1 < k_{2I} < 1$, the starting and

ending values of $f(\lambda)$ are calculated by substituting the appropriate limiting values of k_{2I} into (3.18) and the results are shown as:

$$f(\lambda)_0 = \frac{k_{2I}}{1-k_{2I}} \quad f(\lambda)_{+\infty} = k_{2I} \quad (3.26)$$

Because $f(\lambda)_0 - f(\lambda)_{+\infty} = k_{2I}^2 / (1-k_{2I})$, which is always greater than zero, it is concluded that $f(\lambda)_0$ is always greater than $f(\lambda)_{+\infty}$. In other words, $f(\lambda)$ should have an exponentially decaying curve from $f(\lambda)_0$ to $f(\lambda)_{+\infty}$ and the degree of damping is determined by h as shown in (3.18). Therefore, the curve of $f(\lambda)$ would have a time-constant, which equals $1/(2h)$. Then, λ_s may be chosen as one tenth of the time-constant, which equals to $1/(20h)$.

In order to capture the behavior of $f(\lambda)$ it is necessary to select the sampling interval, λ_s , (as given above) and the sample range, λ_{max} , appropriately. This means selecting λ_{max} , so that most of the information contained the $f(\lambda)$ is retained. This can be achieved if the sampling range encloses most of the dynamic (not steady state) behavior of $f(\lambda)$. An appropriate range of λ_{max} can be found using the following function, which is used to find an appropriate value of λ_{max} at which $f(\lambda)$ is within $\varepsilon(f(\lambda)_0 - f(\lambda)_{+\infty})$ of $f(\lambda)_{+\infty}$, where ε is chosen as a small number.

$$f(\lambda) = f(\lambda)_{+\infty} + \varepsilon(f(\lambda)_0 - f(\lambda)_{+\infty}) \quad (3.27)$$

Note that $[f(\lambda)_0 - f(\lambda)_{+\infty}]$ is the droop interval of the decaying function $f(\lambda)$ and ε is arbitrarily selected as 0.001.

In order to check the accuracy of the approximation for $f(\lambda)$ versus λ curve, there

are four extreme cases to be considered and compared with the original curve. Based on (3.18), $f(\lambda)$ is only influenced by the value of k_{2I} and h . In addition, due to $5ft \leq h \leq 100ft$ (from SRP rules) and $-0.9 \leq k_{2I} \leq 0.9$ (typically, but expansion of the range is undergoing further study), the four cases are described respectively in the following.

- Case 1:

Fig. 3.7 shows the original curve of $f(\lambda)$ versus λ by (3.18) when $k_{2I}=-0.9$, $h=100ft$.

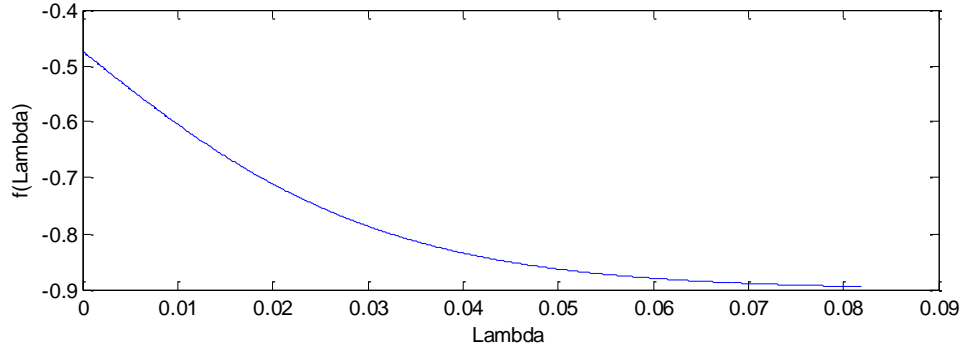


Fig. 3.7 $f(\lambda)$ versus λ curve from the original function ($k_{2I}=-0.9$, $h=100ft$)

Fig. 3.8 is the plot of the normalized absolute value of the error between the approximate and original $f(\lambda)$ -versus- λ curves when $k_{2I}=-0.9$, $h=100ft$. The normalization base is $f(\lambda)_0 - f(\lambda)_{+\infty}=0.4263$. The time-constant is $1/(2*100*0.3048)=0.0164$, hence the test range of λ would be selected as 5 times 0.0164 (time-constant), which is 0.082 as shown in the x-axes in Fig. 3.8.

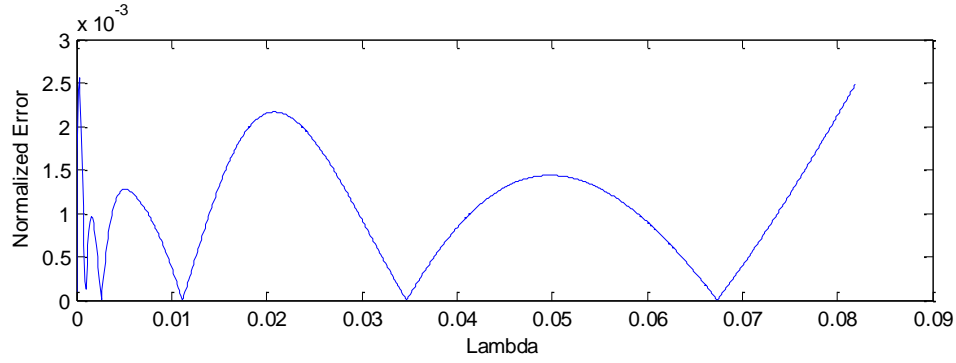


Fig. 3.8 Normalized absolute value of error between approximate and original $f(\lambda)$ versus λ curve ($k_{2I}=-0.9$, $h=100ft$)

As found from Fig. 3.8, the average value of the normalized errors (for case 1) is about $5.82e-4$.

- Case 2:

Fig. 3.9 shows the original curve of $f(\lambda)$ versus λ when $k_{2I}=-0.9$, $h=5ft$.

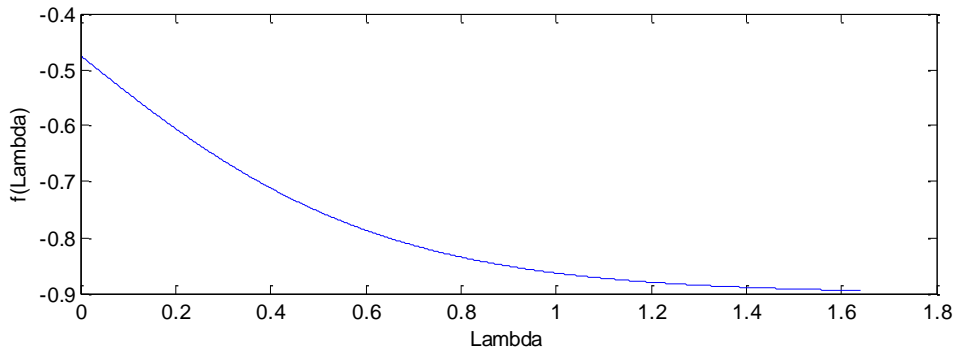


Fig. 3.9 $f(\lambda)$ versus λ curve from the original function ($k_{2I}=-0.9$, $h=5ft$)

Fig. 3.10 is the plot of the normalized absolute value of error between approximate and original $f(\lambda)$ versus λ when $k_{2I}=-0.9$, $h=5ft$. The normalization base is $f(\lambda)_0 - f(\lambda)_{+\infty}=0.4263$. The time-constant is $1/(2*5*0.3048)=0.3281$, hence the test range of λ would be selected as 5 times 0.3281 (time-constant), which is 1.6404 as shown in the

x-axes in Fig. 3.10.

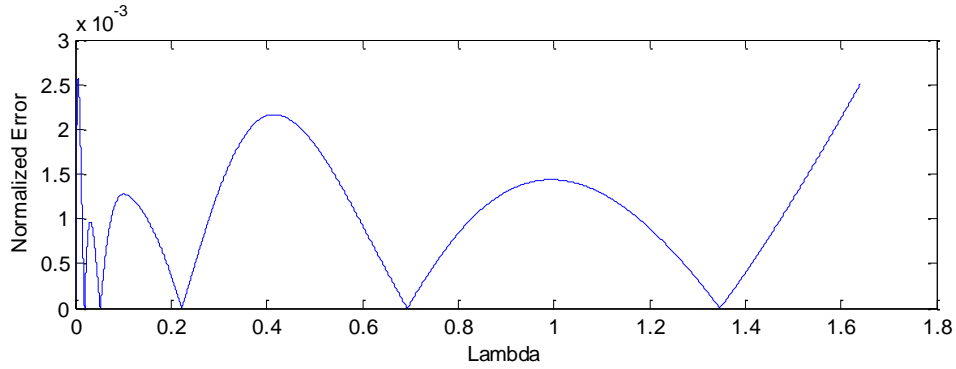


Fig. 3.10 Normalized absolute value of error between approximate and original $f(\lambda)$ versus λ curve ($k_{2I}=-0.9$, $h=5ft$)

As found from Fig. 3.10, the average value of the normalized errors (for case 2) is about $5.81e-4$.

- Case 3:

Fig. 3.11 shows the original curve of $f(\lambda)$ versus λ when $k_{2I}=0.9$, $h=100ft$.

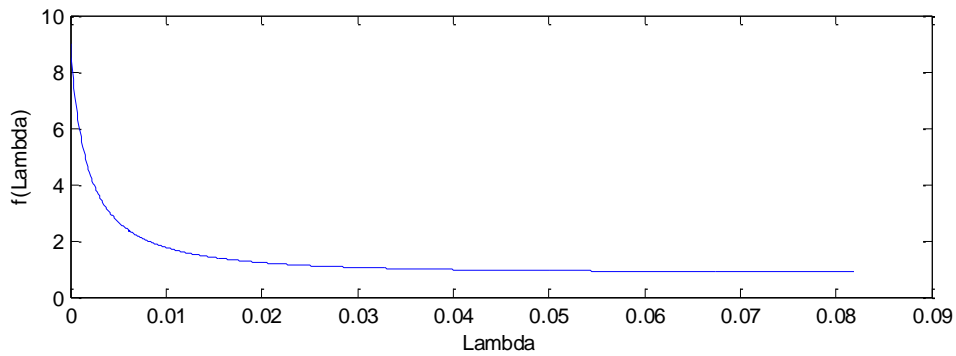


Fig. 3.11 $f(\lambda)$ versus λ curve from the original function ($k_{2I}=0.9$, $h=100ft$)

Fig. 3.12 is the plot of the normalized absolute value of error between approximate and original $f(\lambda)$ versus λ when $k_{2I}=0.9$, $h=100ft$. The normalization base is $f(\lambda)_0 - f(\lambda)_{+\infty}=8.1$. The time-constant is $1/(2*100*0.3048)=0.0164$, hence the test range of λ

would be selected as 5 times 0.0164 (time-constant), which is 0.082 as shown in the x-axes in Fig. 3.12.

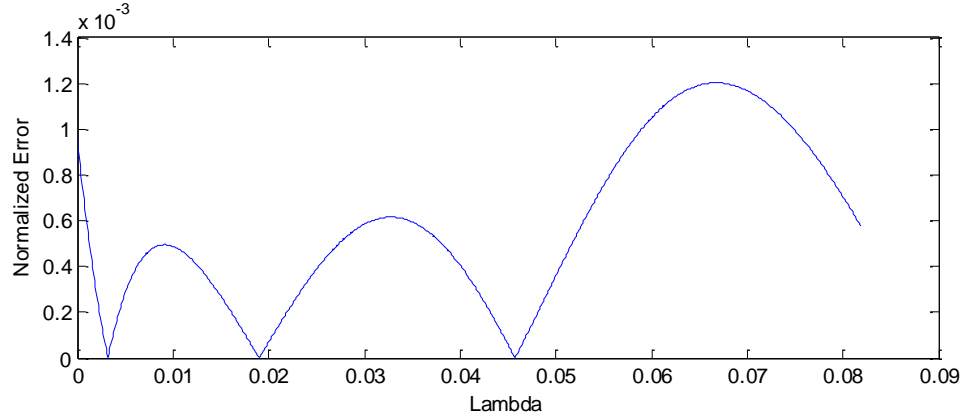


Fig. 3.12 Normalized absolute value of error between approximate and original $f(\lambda)$ versus λ curve ($k_{2I}=0.9$, $h=100ft$)

As found from Fig. 3.12, the average value of the normalized errors (for case 3) is about $1.1e-3$.

- Case 4:

Fig. 3.13 shows the original curve of $f(\lambda)$ versus λ when $k_{2I}=0.9$, $h=5ft$.

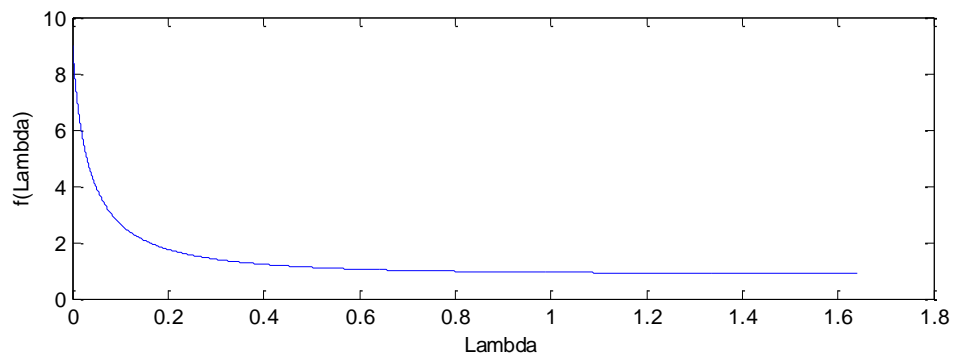


Fig. 3.13 $f(\lambda)$ versus λ curve from the original function ($k_{2I}=0.9$, $h=5ft$)

Fig. 3.14 is the plot of the normalized absolute value of error between approximate and original $f(\lambda)$ versus λ when $k_{2I}=0.9$, $h=5ft$. The normalization base is $f(\lambda)_0$ -

$f(\lambda)_{+\infty}=8.1$. The time-constant is $1/(2*5*0.3048)=0.3281$, hence the test range of λ would be selected as 5 times 0.3281 (time-constant), which is 1.6404 as shown in the x-axes in Fig. 3.14.

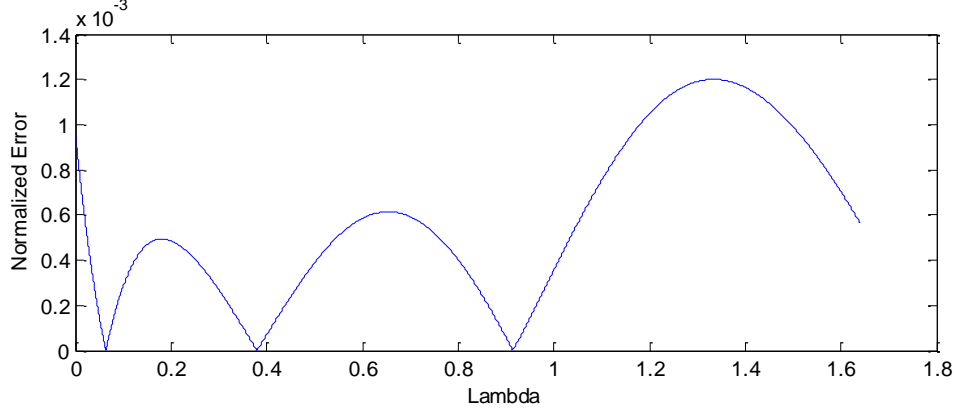


Fig. 3.14 Normalized absolute value of error between approximate and original $f(\lambda)$ versus λ curve ($k_{2I}=0.9$, $h=5ft$)

As found from Fig. 3.14, the average value of the normalized errors (for case 4) is about $1.1e-3$. The results for these four extreme cases show that the errors between the approximate and original $f(\lambda)$ versus λ curve are relatively small. Therefore, it is possible to use $\lambda_s=1/(20h)$ (one tenth of time-constant) and $\lambda_{max}=k_{2I}+0.001*[k_{2I}^2/(1-k_{2I})]$ (based on (3.27)) to do the sampling of the original $f(\lambda)$ versus λ curve.

Finally, $f(\lambda)$ can be decomposed into four exponential series and substituted in (3.11). By employing the Lipschitz integration (3.14), the new Green's function for both source point and field point in the upper-layer is changed as [15]:

$$G_{22}(r, z) = \frac{1}{4\pi\sigma_2} \left[\frac{1}{r_0} + \frac{1}{r_0} + \sum_{n=1}^4 \alpha_n \left(\frac{1}{r_{n1}} + \frac{1}{r_{n2}} + \frac{1}{r_{n3}} + \frac{1}{r_{n4}} \right) \right] \quad (3.28)$$

where,

$$\begin{aligned}
r_0 &= \sqrt{r^2 + (z-d)^2} ; \\
r_0' &= \sqrt{r^2 + (z+d)^2} ; \\
r_{n1} &= \sqrt{r^2 + [2h - \beta_n + d + z]^2} ; \\
r_{n2} &= \sqrt{r^2 + [2h - \beta_n - d + z]^2} ; \\
r_{n3} &= \sqrt{r^2 + [2h - \beta_n - d - z]^2} ; \\
r_{n4} &= \sqrt{r^2 + [2h - \beta_n + d - z]^2} .
\end{aligned}$$

The unified expression using complex images method for Green's functions is written as

$$G(r, z) = \frac{1}{4\pi\sigma_i} \left[\frac{1}{r_0} + \frac{1}{r_0'} + \sum_{n=1}^4 \alpha_n \left(\frac{1}{r_{n1}} + \frac{1}{r_{n2}} + \frac{1}{r_{n3}} + \frac{1}{r_{n4}} \right) \right] \quad (3.29)$$

where,

G = general abbreviation of G_{22} , G_{2I} , G_{I2} and G_{II} ;

$$r_{nk} = \sqrt{r^2 + (z + H_{nk})^2} .$$

The following Table 3.1 indicates different expressions of σ_i and H_{nk} that need to be substituted into (3.29) to get the corresponding equations with Green's function abbreviations shown in the first column of the following table. The values of soil model parameters, σ_1 , σ_2 and h , depth of point current source, d , are parameters that are determined by the site and grid burial depth and the calculated complex coefficients, β_n , are obtained as described above. Equation (3.28) is an example of how to take the information found in the second row of Table 3.1 to form the specific Green's function

G_{22} . Then, all the expressions in the second row, from σ_2 to $-(2h-\beta_n-d)$, are substituted, respectively, for σ_i to H_{n4} in (3.29). As a result, it is possible to obtain the same equation as (3.28).

Table 3.1 Parameters Used In Complex Image Equations

G	σ_i	H_{n1}	H_{n2}	H_{n3}	H_{n4}
G_{22}	σ_2	$2h-\beta_n+d$	$2h-\beta_n-d$	$-(2h-\beta_n+d)$	$-(2h-\beta_n-d)$
G_{21}	σ_2	$2h-\beta_n+d$	$2h-\beta_n-d$	$-\beta_n+d$	$-\beta_n-d$
G_{12}	σ_1	$2h-\beta_n+d$	$-(2h-\beta_n-d)$	$-\beta_n+d$	$-\beta_n-d$
G_{11}	σ_1	$2h-\beta_n+d$	$-2h+\beta_n+d$	Infinity	Infinity

It can be expanded to solve the complex images in multi-layered soil model and the specific steps are written as

- 1) Write the general solutions of each layer's voltage expression such as (3.9).
- 2) Calculate the undetermined arbitrary functions based on boundary conditions to obtain the specific solutions.
- 3) Use the matrix pencil method to decompose the non-exponential function into a finite number of exponential terms.
- 4) Apply Lipschitz integration to the product of exponential function and Bessel's function.

3.5 Comparison between Images Method and Complex Images Method

Table 3.2 Complex Image Amplitudes and Locations

$\sigma_1=0.1\text{S/m}$ $\sigma_2=0.001\text{S/m}$ $h=8\text{m}$		
n	α_n	β_n
1	$0.0228 - j0.0141$	$-12.6497+j21.0365$
2	$0.0228 + j0.0141$	$-12.6497-j21.0365$
3	0.8635	-5.7287
4	-1.4042	-0.7284
$\sigma_1=0.01\text{S/m}$ $\sigma_2=0.001\text{S/m}$ $h=4\text{m}$		
n	α_n	β_n
1	$0.0232 - j0.0136$	$-7.3111 + j10.1381$
2	$0.0232 + j0.0136$	$-7.3111 - j10.1381$
3	0.3927	-3.9844
4	-0.8896	-0.0534

The high accuracy and efficiency of the complex image method is because of the introduction of the imaginary part from image magnitude. In other words, the imaginary part brings some extra degrees of freedom. In order to illustrate the difference between the image method and complex image method, Table 3.2 and Table 3.3 present two examples of unit point current source in the two-layer soil model. The source point is located on the z-axis with cylindrical coordinate (shown in Fig 3.5) $(r, z)=(0, 3 \text{ meters})$ and the field point is located on the surface with $z=0$.

Table 3.3 Potential at (r, 0) Produced by Unit Current Source

$\sigma_1=0.1\text{S/m}$		$\sigma_2=0.001\text{S/m}$		$h=8\text{m}$
$r(\text{m})$	True value(V)	CImage(V)	Image(V)	n
10	4.082994	4.081869	4.083002	681
20	0.490605	0.490556	0.490742	1017
50	0.033472	0.033466	0.033506	1481
$\sigma_1=0.01\text{S/m}$		$\sigma_2=0.001\text{S/m}$		$h=4\text{m}$
$r(\text{m})$	True value(V)	CImage(V)	Image(V)	n
10	2.111362	2.110794	2.111425	129
20	0.828881	0.830276	0.828937	145
50	0.319806	0.318608	0.319861	165

Table 3.2 shows the values of α_n and β_n when $f(\lambda)$ is decomposed into four exponential terms. Table 3.3 shows the voltage results of the images method and the complex images method for different values of r , where r is the horizontal distance from the source point. The voltage results of complex images method are calculated using the coefficients from Table 3.2. The variable n in Table 3.3 is the number of current source images when the images method is employed. As seen from Table 3.3, the value of n is always greater than one hundred, while the number of complex images is four. In general, for our problem, the runtime of the complex images method is much shorter than images method. For reference, the “true” value of voltage is taken as that value calculated with four thousand images using the image method.

3.6 Voltage Produced by Horizontal Lines of Current

In this section, the Green's Function solutions (point current source solutions) are used to determine of the voltages produced in the three regions due to a horizontal one-dimensional-(line) source of current located in the upper-layer or the lower-layer. This problem is solved by using the rectangular components of the cylindrical system shown in Fig. 3.15.

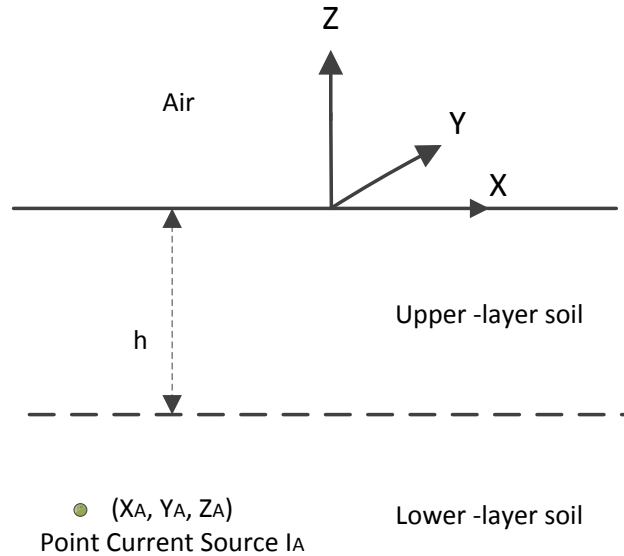


Fig. 3.15 Rectangular coordinate system

First, the superposition theorem is employed to find the voltage in the three regions as a summation of the voltages due to a distribution of point currents, which are located on a horizontal line somewhere in the soil model. The line-source is assumed to be parallel to the x or y -axis with a length $2L_I$ with the center located at the rectangular coordinates (X_I, Y_I, Z_I) . Let the total current (I) be uniformly distributed along the length of the line, resulting in a current density of

$$\rho = \frac{I}{2L_1} \text{ (amps / meter)} \quad (3.30)$$

In other words, the line current source is divided into infinity-many point sources and it is easy to use integration instead of superposition. In addition, the Green's functions derived before are based on cylindrical coordinate system. In this section, the parameter r and d in cylindrical coordinate system should be replaced by $[(x-X_I)^2+(y-Y_I)^2]^{0.5}$ and $-Z_I$ in rectangular coordinate system. For example, the following expression represents the voltage, $VX_{22}(x, y, z)$, at a point in upper-layer soil due to a x-directed line of current in the same region.

$$VX_{22}(x, y, z) = \frac{I}{2L_1} \bullet \frac{1}{4\pi\sigma_2} \int_{x_1-L_1}^{x_1+L_1} \left[\frac{1}{r_0} + \frac{1}{r_0'} + \sum_{n=1}^4 \alpha_n \left(\frac{1}{r_{n1}} + \frac{1}{r_{n2}} + \frac{1}{r_{n3}} + \frac{1}{r_{n4}} \right) \right] dx_s \quad (3.31)$$

where,

$$\begin{aligned} r_0 &= \sqrt{(x-x_s)^2 + (y-Y_1)^2 + (z+Z_1)^2} ; \\ r_0' &= \sqrt{(x-x_s)^2 + (y-Y_1)^2 + (z-Z_1)^2} ; \\ r_{n1} &= \sqrt{(x-x_s)^2 + (y-Y_1)^2 + (z+2h-\beta_n-Z_1)^2} ; \\ r_{n2} &= \sqrt{(x-x_s)^2 + (y-Y_1)^2 + (z+2h-\beta_n+Z_1)^2} ; \\ r_{n3} &= \sqrt{(x-x_s)^2 + (y-Y_1)^2 + (z-2h+\beta_n-Z_1)^2} ; \\ r_{n4} &= \sqrt{(x-x_s)^2 + (y-Y_1)^2 + (z-2h+\beta_n+Z_1)^2} . \end{aligned}$$

Let us separate the long integral in (3.31) into six similar integrals, each associate with the terms $1/r_0$ to $1/r_{n4}$. There is a common form for these six integrals, which is

$$P = \int_{x_1-L_1}^{x_1+L_1} \frac{dx_s}{\sqrt{(x-x_s)^2 + (y-Y_1)^2 + (z+H_{nk})^2}} \quad (3.32)$$

where,

$$H_{nk} = \pm Z_1 \pm 2h - \beta_n$$

The evaluation of this integral is straightforward for all points (x,y,z) not collinear with the line current. For points collinear with the line current but not on the line current, $y-Y_1$ should be zero. The evaluation of this integral for points on the line current will be presented later. In all cases, except for points on the line current, the evaluation of this integral is determined as:

$$P = F(x - X_1, y - Y_1, z + H_{nk}) \quad (3.33)$$

The F function is derived as [17]:

$$F(t, u, v) = \ln \left[\frac{\sqrt{(t+L_1)^2 + u^2 + v^2} + t + L_1}{\sqrt{(t-L_1)^2 + u^2 + v^2} + t - L_1} \right] \quad (3.34)$$

where,

$$t = x - X_1;$$

$$u = y - Y_1;$$

$$v = z + H_{nk}.$$

Substituting (3.33), (3.34) into (3.31), the voltage $VX_{22}(x, y, z)$ becomes:

$$\begin{aligned}
VX_{22}(x, y, z) = & \frac{I}{8\pi L_1 \sigma_2} \{ F(x - X_1, y - Y_1, z + Z_1) + F(x - X_1, y - Y_1, z - Z_1) \\
& + \sum_{n=1}^4 \alpha_n [F(x - X_1, y - Y_1, z + 2h - \beta_n - Z_1) \\
& + F(x - X_1, y - Y_1, z + 2h - \beta_n + Z_1) \\
& + F(x - X_1, y - Y_1, z - 2h + \beta_n - Z_1) \\
& + F(x - X_1, y - Y_1, z - 2h + \beta_n + Z_1)] \}
\end{aligned} \tag{3.35}$$

Similarly, the general voltage function $VX(x, y, z)$ at point (x, y, z) due to a x-directed line current source is given as:

$$\begin{aligned}
VX(x, y, z) = & \frac{I}{8\pi L_1 \sigma_i} \{ F(x - X_1, y - Y_1, z - Z_1) + F(x - X_1, y - Y_1, z + Z_1) \\
& + \sum_{n=1}^4 \alpha_n [F(x - X_1, y - Y_1, z + H_{n1}) + F(x - X_1, y - Y_1, z + H_{n2}) \\
& + F(x - X_1, y - Y_1, z + H_{n3}) + F(x - X_1, y - Y_1, z + H_{n4})] \}
\end{aligned} \tag{3.36}$$

where σ_i and H_{nk} both come from Table 3.1 due to different locations of field point and line current source.

If the current source line is y-directed, the general expression is written as:

$$\begin{aligned}
VY(x, y, z) = & \frac{I}{8\pi L_1 \sigma_i} \{ F(y - Y_1, x - X_1, z - Z_1) + F(y - Y_1, x - X_1, z + Z_1) \\
& + \sum_{n=1}^4 \alpha_n [F(y - Y_1, x - X_1, z + H_{n1}) + F(y - Y_1, x - X_1, z + H_{n2}) \\
& + F(y - Y_1, x - X_1, z + H_{n3}) + F(y - Y_1, x - X_1, z + H_{n4})] \}
\end{aligned} \tag{3.37}$$

Similarly, for the z-directed line current source, the general expression is written as:

$$\begin{aligned}
VZ(x, y, z) = & \frac{I}{8\pi L_1 \sigma_i} \{ F(z - Z_1, x - X_1, y - Y_1) + F(z + Z_1, x - X_1, y - Y_1) \\
& + \sum_{n=1}^4 \alpha_n [F(z + H_{n1}, x - X_1, y - Y_1) + F(z + H_{n2}, x - X_1, y - Y_1) \\
& + F(z + H_{n3}, x - X_1, y - Y_1) + F(z + H_{n4}, x - X_1, y - Y_1)] \}
\end{aligned} \tag{3.38}$$

This section is significant because the expressions presented here need to be implemented to calculate the earth surface potential of any specific position located on the earth surface above the grounding system.

3.7 Calculation of Mutual and Self Resistance

The equations for calculating the ground grid resistance to remote earth and touch/step potential are developed in terms of mutual and self resistance of conductors. In this section, the process for arriving at the equations describing these quantities is developed.

The equations (3.36), (3.37), and (3.38) are used for calculating the voltage at a field point caused by a line current source, which are not directly applicable to the computation of mutual resistance. The definition of mutual resistance is the voltage induced on a second conductor by the current of another (first) conductor, then divided by inducing current on the first conductor. If the conductor whose induced voltage to be calculated is at a different location from the source, the potential on this conductor would vary along its length. However, this conductor is assumed lossless and the potentials along it should be uniform. Then, the voltage along the second conductor is the average of the potentials computed along its length.

There are thirty-six different equations for the average voltage of the second conductor because the source conductor may be x -directed, y -directed or z -directed and

may be in either upper-layer soil or lower-layer soil. Simultaneously, the second conductor can also have different orientations and locations.

The function $F(t,u,v)$ can be taken as an integral of the potentials at a field point with respect to the points lying on the source conductor, while $H(t,u,v)$, which is developed based on $F(t,u,v)$, is the integral of potentials at points lying on the field conductor with respect to the source conductor.

Therefore

$$\begin{aligned} H(t,u,v) &= \int_{t-L}^{t+L} F(t_p, u, v) dt_p \\ &= \int_{t-L}^{t+L} \ln \frac{\sqrt{(t_p + L_1)^2 + u^2 + v^2} + t_p - L_1}{\sqrt{(t_p - L_1)^2 + u^2 + v^2} + t_p - L_1} dt_p \end{aligned} \quad (3.39)$$

where,

L_0 = the half of length of field conductor;

L_1 = the half of length of source conductor.

Since

$$\int \ln(x + \sqrt{x^2 + a^2}) dx = x \ln(x + \sqrt{x^2 + a^2}) - \sqrt{x^2 + a^2} \quad (3.40)$$

Expression (3.39) can be written as

$$\begin{aligned} H(t,u,v) &= \\ &+ \sqrt{(t - L_0 + L_1)^2 + u^2 + v^2} - (t - L_0 + L_1) \ln(t - L_0 + L_1 + \sqrt{(t - L_0 + L_1)^2 + u^2 + v^2}) \\ &- \sqrt{(t + L_0 + L_1)^2 + u^2 + v^2} + (t + L_0 + L_1) \ln(t + L_0 + L_1 + \sqrt{(t + L_0 + L_1)^2 + u^2 + v^2}) \\ &- \sqrt{(t - L_0 - L_1)^2 + u^2 + v^2} + (t - L_0 - L_1) \ln(t - L_0 - L_1 + \sqrt{(t - L_0 - L_1)^2 + u^2 + v^2}) \\ &+ \sqrt{(t + L_0 - L_1)^2 + u^2 + v^2} - (t + L_0 - L_1) \ln(t + L_0 - L_1 + \sqrt{(t + L_0 - L_1)^2 + u^2 + v^2}) \end{aligned} \quad (3.41)$$

Therefore, if there are two conductor segments with the same direction, it is necessary to use $H(t,u,v)$, (3.41), to replace the $F(t,u,v)$ in (3.36), (3.37) and (3.38), to obtain (3.42), (3.43) and (3.44).

Undoubtedly, both $F(t,u,v)$ and $H(t,u,v)$ depend on the Green's functions, which is the fundamental analytical model calculating the potential of the field point with respect to the point source.

As a result, the equations for parallel configurations are similar as (3.36) (3.37) and (3.38). In addition to the change from F functions to H functions, another difference is the additional coefficient of $1/2L_0$ and it is because of the assumption mentioned before that the voltage of the perfect conductor is the average of the potentials calculated by dividing the length of field conductor ($2 L_0$).

Thus, the following equations (3.42), (3.43) and (3.44) illustrate the average potential of field conductor in each direction caused by the parallel source conductor. If there are two conductors with the same orientation (e.g., parallel with the z-axis), this kind of configuration is called parallel configuration. On the other hand, if the two conductors are in oriented at an angle, they must be perpendicular (assuming the traditional ways in which the grounding grid is constructed) and their configuration is called the perpendicular configuration. The notation that will be used here is: if two conductors are both x-directed, they are in the parallel configuration and it is herein

called the X-X configuration. Using this nomenclature, the voltage results for the other configurations are shown below.

For the X-X configuration, the general voltage equation is

$$\begin{aligned}
 V_{XX}(x, y, z) = & \frac{I}{16\pi L_1 L_0 \sigma_i} \{ H(x - X_1, y - Y_1, z - Z_1) + H(x - X_1, y - Y_1, z + Z_1) \\
 & + \sum_{n=1}^4 \alpha_n [H(x - X_1, y - Y_1, z + H_{n1}) + H(x - X_1, y - Y_1, z + H_{n2}) \\
 & + H(x - X_1, y - Y_1, z + H_{n3}) + H(x - X_1, y - Y_1, z + H_{n4})] \}
 \end{aligned} \tag{3.42}$$

For Y-Y configuration, the voltage equation is

$$\begin{aligned}
 V_{YY}(x, y, z) = & \frac{I}{16\pi L_1 L_0 \sigma_i} \{ H(y - Y_1, x - X_1, z - Z_1) + H(y - Y_1, x - X_1, z + Z_1) \\
 & + \sum_{n=1}^4 \alpha_n [H(y - Y_1, x - X_1, z + H_{n1}) + H(y - Y_1, x - X_1, z + H_{n2}) \\
 & + H(y - Y_1, x - X_1, z + H_{n3}) + H(y - Y_1, x - X_1, z + H_{n4})] \}
 \end{aligned} \tag{3.43}$$

For Z-Z configuration, the voltage equation is

$$\begin{aligned}
 V_{ZZ}(x, y, z) = & \frac{I}{16\pi L_1 L_0 \sigma_i} \{ H(z - Z_1, x - X_1, y - Y_1) + H(z + Z_1, x - X_1, y - Y_1) \\
 & + \sum_{n=1}^4 \alpha_n [H(z + H_{n1}, x - X_1, y - Y_1) + H(z + H_{n2}, x - X_1, y - Y_1) \\
 & + H(z + H_{n3}, x - X_1, y - Y_1) + H(z + H_{n4}, x - X_1, y - Y_1)] \}
 \end{aligned} \tag{3.44}$$

where σ_i and H_{nk} both come from Table 3.1 due to different locations of field conductor and line current source, and the value of I is the magnitude of current flowing in the line current source.

When the two conductors are not parallel, the integration is different from the previous forms. Hence, O functions are developed instead of the F functions.

$$\begin{aligned}
O(t, u, v) &= \int_{u-L_0}^{u+L_0} F(t, u_p, v) du_p \\
&= \int_{u-L_0}^{u+L_0} \ln \frac{\sqrt{(t+L_1)^2 + u_p^2 + v^2} + t - L_1}{\sqrt{(t-L_1)^2 + u_p^2 + v^2} + t - L_1} du_p
\end{aligned} \tag{3.45}$$

Based on [17], there is a mathematical transformation shown as:

$$\begin{aligned}
&\int \ln(A + \sqrt{r^2 + B^2}) dr = -r + A \ln(2r + 2\sqrt{r^2 + B^2}) \\
&+ \sqrt{B^2 - A^2} \sin^{-1} \left[\frac{-A\sqrt{r^2 + B^2} - B}{B\sqrt{r^2 + B^2} + A} + r \ln(A + \sqrt{r^2 + B^2}) \right]
\end{aligned} \tag{3.46}$$

Then, (3.46) can be substituted into (3.45) and the resultant function of $O(t, u, v)$ is given as:

$$\begin{aligned}
O(t, u, v) = & \\
& + (u + L_0) \ln \left[\frac{t + L_1 + \sqrt{(t + L_1)^2 + (u + L_0)^2 + v^2}}{t - L_1 + \sqrt{(t - L_1)^2 + (u + L_0)^2 + v^2}} \right] \\
& + (t + L_1) \ln \left[\frac{u + L_0 + \sqrt{(t + L_1)^2 + (u + L_0)^2 + v^2}}{u - L_0 + \sqrt{(t + L_1)^2 + (u - L_0)^2 + v^2}} \right] \\
& + (u - L_0) \ln \left[\frac{t - L_1 + \sqrt{(t - L_1)^2 + (u - L_0)^2 + v^2}}{t + L_1 + \sqrt{(t + L_1)^2 + (u - L_0)^2 + v^2}} \right] \\
& + (t - L_1) \ln \left[\frac{u - L_0 + \sqrt{(t - L_1)^2 + (u - L_0)^2 + v^2}}{u + L_0 + \sqrt{(t - L_1)^2 + (u + L_0)^2 + v^2}} \right] \\
& + |v| \left\{ \sin^{-1} \frac{-(t + L_1) \sqrt{(t + L_1)^2 + (u + L_0)^2 + v^2} - (t + L_1)^2 - v^2}{\sqrt{[(t - L_1)^2 + v^2][(t - L_1)^2 + (u + L_0)^2 + v^2]} + t + L_1} \right. \\
& - \sin^{-1} \frac{-(t - L_1) \sqrt{(t - L_1)^2 + (u + L_0)^2 + v^2} - (t - L_1)^2 - v^2}{\sqrt{[(t - L_1)^2 + v^2][(t - L_1)^2 + (u + L_0)^2 + v^2]} + t + L_1} \\
& - \sin^{-1} \frac{-(t + L_1) \sqrt{(t + L_1)^2 + (u - L_0)^2 + v^2} - (t + L_1)^2 - v^2}{\sqrt{[(t + L_1)^2 + v^2][(t + L_1)^2 + (u - L_0)^2 + v^2]} + t + L_1} \\
& \left. + \sin^{-1} \frac{-(t - L_1) \sqrt{(t - L_1)^2 + (u - L_0)^2 + v^2} - (t - L_1)^2 - v^2}{\sqrt{[(t - L_1)^2 + v^2][(t - L_1)^2 + (u - L_0)^2 + v^2]} + t - L_1} \right\}
\end{aligned} \tag{3.47}$$

As in the parallel configuration, it is desired to express the average voltage equations for the perpendicular configurations in terms of O functions.

The terminology “X-Y configuration” means line current source is x-directed and current field line is y-directed, and this is the same rule for the rest of other configurations. The general equation for X-Y configuration is

$$\begin{aligned}
VXY(x, y, z) = & \frac{I}{16\pi L_1 L_0 \sigma_i} \{O(x - X_1, y - Y_1, z - Z_1) + O(x - X_1, y - Y_1, z + Z_1) \\
& + \sum_{n=1}^4 \alpha_n [O(x - X_1, y - Y_1, z + H_{n1}) + O(x - X_1, y - Y_1, z + H_{n2}) \\
& + O(x - X_1, y - Y_1, z + H_{n3}) + O(x - X_1, y - Y_1, z + H_{n4})]\}
\end{aligned} \tag{3.48}$$

For Y-X configuration, the general equation is

$$\begin{aligned}
VYX(x, y, z) = & \frac{I}{16\pi L_1 L_0 \sigma_i} \{O(y - Y_1, x - X_1, z - Z_1) + O(y - Y_1, x - X_1, z + Z_1) \\
& + \sum_{n=1}^4 \alpha_n [O(y - Y_1, x - X_1, z + H_{n1}) + O(y - Y_1, x - X_1, z + H_{n2}) \\
& + O(y - Y_1, x - X_1, z + H_{n3}) + O(y - Y_1, x - X_1, z + H_{n4})]\}
\end{aligned} \tag{3.49}$$

For X-Z configuration, the general equation is

$$\begin{aligned}
VXZ(x, y, z) = & \frac{I}{16\pi L_1 L_0 \sigma_i} \{O(x - X_1, z - Z_1, y - Y_1) + O(x - X_1, z + Z_1, y - Y_1) \\
& + \sum_{n=1}^4 \alpha_n [O(x - X_1, z + H_{n1}, y - Y_1) + O(x - X_1, z + H_{n2}, y - Y_1) \\
& + O(x - X_1, z + H_{n3}, y - Y_1) + O(x - X_1, z + H_{n4}, y - Y_1)]\}
\end{aligned} \tag{3.50}$$

For Z-X configuration, the general equation is

$$\begin{aligned}
VZX(x, y, z) = & \frac{I}{16\pi L_1 L_0 \sigma_i} \{O(z - Z_1, x - X_1, y - Y_1) + O(z + Z_1, x - X_1, y - Y_1) \\
& + \sum_{n=1}^4 \alpha_n [O(z + H_{n1}, x - X_1, y - Y_1) + O(z + H_{n2}, x - X_1, y - Y_1) \\
& + O(z + H_{n3}, x - X_1, y - Y_1) + O(z + H_{n4}, x - X_1, y - Y_1)]\}
\end{aligned} \tag{3.51}$$

For Y-Z configuration, the general equation is

$$\begin{aligned}
VYZ(x, y, z) = & \frac{I}{16\pi L_1 L_0 \sigma_i} \{O(y - Y_1, z - Z_1, x - X_1) + O(y - Y_1, z + Z_1, x - X_1) \\
& + \sum_{n=1}^4 \alpha_n [O(y - Y_1, z + H_{n1}, x - X_1) + O(y - Y_1, z + H_{n2}, x - X_1) \\
& + O(y - Y_1, z + H_{n3}, x - X_1) + O(y - Y_1, z + H_{n4}, x - X_1)]\}
\end{aligned} \tag{3.52}$$

For Z-Y configuration, the general equation is

$$\begin{aligned}
 VZY(x, y, z) = & \frac{I}{16\pi L_1 L_0 \sigma_i} \{ O(z - Z_1, y - Y_1, x - X_1) + O(z + Z_1, y - Y_1, x - X_1,) \\
 & + \sum_{n=1}^4 \alpha_n [O(z + H_{n1}, y - Y_1, x - X_1) + O(z + H_{n2}, y - Y_1, x - X_1) \\
 & + O(z + H_{n3}, y - Y_1, x - X_1) + O(z + H_{n4}, y - Y_1, x - X_1)] \}
 \end{aligned} \tag{3.53}$$

The mutual resistance and self-resistance should be derived using the voltage equations (3.42) to (3.44) and (3.48) to (3.53) developed earlier. The mutual resistance is the voltage induced in the field conductor by unit current from the source conductor. The process for calculating self-resistance is a special case of the process for calculating mutual resistance. This special case is introduced in the following.

The line of current may be replaced with a conducting cylinder of length $2L$ and diameter $2a$ as shown in Fig 3.16. Assume a total current I is leaving the surface of the cylinder and is uniformly distributed over its surface area. From [17], to evaluate the average self-potential for an x-directed or y-directed conducting cylinder, the voltage equation developed for the two parallel lines located in the same soil layer are used and evaluated at

$$x - X_1 = 0 \quad y - Y_1 = 0 \quad z - Z_1 = a \tag{3.54}$$

where,

(X_1, Y_1, Z_1) = the coordinate of the center of the cylinder;

(x, y, z) = the coordinate of any point on the surface of the cylinder.

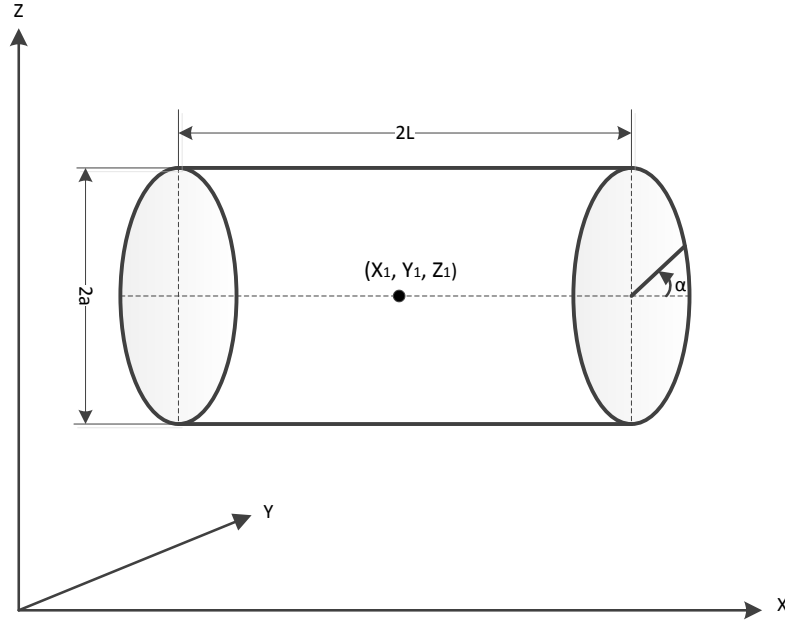


Fig. 3.16 Cylindrical x-directed conductor model for calculation of self-resistance

If the cylinder is z-directed, (3.54) needs to change to

$$x - X_1 = a \quad y - Y_1 = 0 \quad z - Z_1 = 0 \quad (3.55)$$

Or

$$x - X_1 = 0 \quad y - Y_1 = a \quad z - Z_1 = 0 \quad (3.56)$$

In other words, it is possible to model self-resistance of a cylindrical conductor as a mutual resistance between two line conductors, one of which is located at the center of the cylinder and the other of which is located at outer surface of the cylinder respectively.

3.8 Matrix Method

As derived in the previous section, it is possible to obtain the mutual resistance r_{jk} ($j \neq k$) between segment j and segment k , where segment k is the line current source with

source current i_k and segment j is the field segment shown as following.

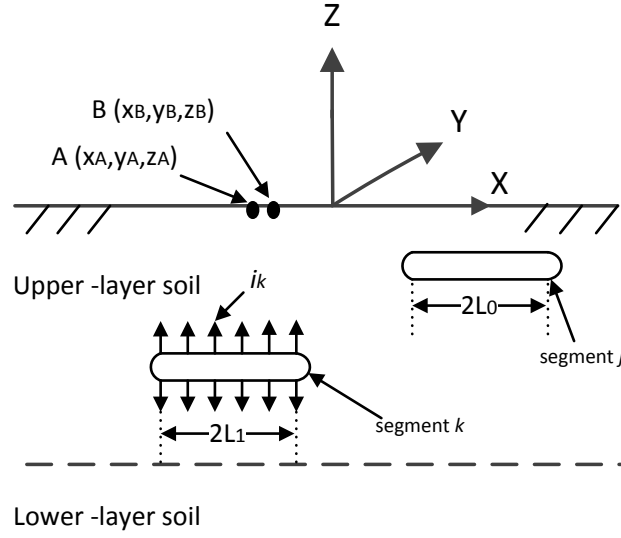


Fig. 3.17 Two earth embedded conductor segments of length $2L_0$ and L_1

If j is equal to k , it is self-resistance r_{jj} , which can be calculated also. The voltage v_j of each segment j could be calculated as:

$$\sum_{k=1}^n r_{jk} i_k = v_j \quad j = 1, 2, 3, \dots, n \quad (3.57)$$

Rewriting the summation (3.57) in matrix format and using name of Voltage Distribution Factor matrix (VDF) to define the matrix containing the mutual and self resistances gives:

$$[VDF][I] = V \quad (3.58)$$

where,

$$VDF = \begin{bmatrix} r_{11} & \cdots & r_{1n} \\ \vdots & \ddots & \vdots \\ r_{n1} & \cdots & r_{nn} \end{bmatrix}_{n \times n} ;$$

$$I = \begin{bmatrix} i_1 \\ \vdots \\ i_n \end{bmatrix}_{n \times 1} ;$$

$$V = \begin{bmatrix} v_1 \\ \vdots \\ v_n \end{bmatrix}_{n \times 1} .$$

It will be assumed herein that all of the segments are at the same voltage, v . This is usually acceptable at 60Hz frequency because the resistance and inductance of the wires are small compared to resistance between the segments and the earth.

In addition, the current source is modeled to simulate the fault current injected into the earth when fault occurs in a substation. Therefore, the sum of source currents from all segments should be equal to the fault current, which is also the current flowing from the current source.

Thus,

$$\sum_{k=1}^n i_k = I_F \quad (3.59)$$

where,

I_F = fault current.

Hence, (3.58) can be written as:

$$AX = b \quad (3.60)$$

where,

$$A = \begin{bmatrix} r_{11} & \cdots & r_{1n} & -1 \\ \vdots & \ddots & \vdots & -1 \\ r_{n1} & \cdots & r_{nn} & -1 \\ 1 & \cdots & 1 & 0 \end{bmatrix}_{(n+1) \times (n+1)} ;$$

$$X = \begin{bmatrix} i_1 \\ \vdots \\ i_n \\ v \end{bmatrix}_{(n+1) \times 1} ;$$

$$b = \begin{bmatrix} 0 \\ \vdots \\ 0 \\ I_F \end{bmatrix}_{(n+1) \times 1} .$$

Since matrix A and vector b are known, the unknown vector X can be found. As a result, one can obtain the values of each segment source current (i) and ground potential rise (v). Taking Fig. 3.17 as an example, it is assumed that this grounding system only has conductor segment j and segment k . The segment source currents (i_j, i_k), segment lengths ($2L_1, 2L_0$) and the surface point A 's coordinate (x_A, y_A, z_A) can be substituted in (3.36), (3.37) and (3.38) to get the values of potential at point A on earth surface, then it is necessary to sum them up to get the total earth potential at A (E_A) induced by both segment j and k . Finally, the touch voltage at point A is

$$E_{touch} = GPR - E_A \quad (3.61)$$

where, GPR is the grounding potential rise, which equals to v in (3.60).

For the step voltage calculation, it is assumed that one person's two feet contact the earth at point A and B . Hence, it is necessary to use the same method discussed above to calculate the earth potential at B (E_B), and then the step voltage is:

$$E_{step} = E_B - E_A \quad (3.62)$$

3.9 Results Compared with WINIGS

With the equations derived before, it is possible to calculate the self-resistance, mutual resistance and the earth surface potential caused by each conducting segment.

The scenario depicted in Fig. 3.18 is used to verify the self-resistance of a horizontal conductor with length l and verify the surface potential at the field point (shown) with perpendicular projected distance w from middle of the horizontal conductor.

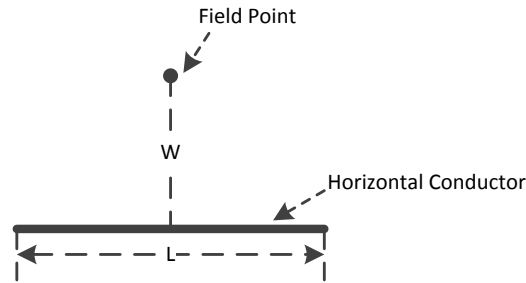


Fig. 3.18 Horizontal conductor and field point

The application developed based on the above equations was given the name OPTIMGRID.

Table 3.4 and Table 3.5 shown below contain metrics that can be used to compare both the OPTIMGRID and WINIGS results.

The soil parameters ρ_1 , ρ_2 and h are upper layer resistivity, lower layer and upper

layer thickness respectively. The variable d is the depth of the conductor under the surface. In this example, the horizontal conductor is selected as copper with diameter of 0.528 ft.

Table 3.4 Comparison of Self-resistance and Surface Potential

$\rho_1=\rho_2=100 \Omega \text{ m}, d=0.5 \text{ m}, l=8 \text{ m}, \text{dia}=0.528 \text{ ft}$		
	WINIGS	OPTIMGRID
Self resistance (Ω)	17.09	17.12
Surface potential at $w=4\text{m}$ (V)	3446	3456
Surface potential at $w=8\text{m}$ (V)	1904	1906
$\rho_1=100 \Omega \text{ m}, \rho_2=10 \Omega \text{ m}, h=5 \text{ m}, d=0.5 \text{ m}, l=8 \text{ m}, \text{dia}=0.528 \text{ ft}$		
	WINIGS	OPTIMGRID
Self resistance (Ω)	15.59	15.62
Surface potential at $w=4\text{m}$ (V)	2012	2021
Surface potential at $w=8\text{m}$ (V)	678	679

The scenario depicted in Fig. 3.19 is used to verify the mutual resistance of two parallel conductors with length l from the square grid and the surface potential at the field point with perpendicular projected distance w from the bottom horizontal conductor.

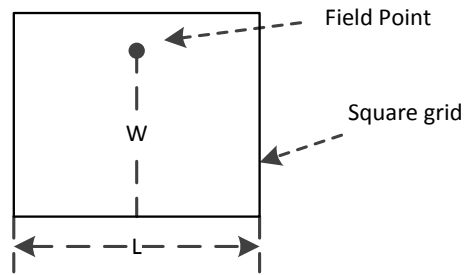


Fig. 3.19 Square grid and field point

Table 3.5 shown below is similar to the previous table of used to validate self-resistance with the same interpretation.

Table 3.5 Comparison of Mutual Resistance and Surface Potential

$\rho_1=\rho_2=100 \Omega \text{ m}$, $d=1.5 \text{ ft}$, $l=8 \text{ ft}$, $\text{dia}=0.528 \text{ ft}$		
	WINIGS	OPTIMGRID
Mutual resistance (Ω)	5.95	5.93
Surface potential at $w=2\text{m}$ (V)	11244	11261
Surface potential at $w=4\text{m}$ (V)	10893	10908
$\rho_1=100 \Omega \text{ m}$, $\rho_2=10 \Omega \text{ m}$, $h=5 \text{ m}$, $d=1.5 \text{ ft}$, $l=8 \text{ ft}$, $\text{dia}=0.528 \text{ ft}$		
	WINIGS	OPTIMGRID
Mutual resistance (Ω)	4.11	4.09
Surface potential at $w=2 \text{ ft}$. (V)	9366	9381
Surface potential at $w=4 \text{ ft}$. (V)	9010	9023

In order to verify the accuracy of the author's model applied to calculating the grounding systems safety metrics (touch voltage, step voltage, grounding resistance), the

author has run 54 cases using different two-layer soil models. There are four influential factors, which are the combination of resistivity, thickness of upper layer soil, size of the substation and mesh size in the grounding grid. For the combination of soil resistivity, there are two choices: (1) $\rho_1=100 \Omega \text{ m}$, $\rho_2=10\Omega \text{ m}$ and (2) $\rho_1=10\Omega \text{ m}$, $\rho_2=100\Omega \text{ m}$. For the thickness of upper layer soil, there are three choices: (1) $h=5 \text{ ft}$, (2) $h=20 \text{ ft}$ and (3) $h=100 \text{ ft}$. For the substation size, there are three choices: (1) 50ft by 50ft, (2) 200ft by 200ft and (3) 600ft by 600ft. For the mesh size, there are also three choices: (1) 50ft by 50ft, (2) 25ft by 25ft and (3) 10ft by 10ft. The author has simulated every combination of these parameters as laid out here.

It is possible to model the fault current injected into one specific grounding grid in WINIGS as shown in Fig. 3.20. The source is the single-phase current source with magnitude of 1kA and phase angle of 0 degree. Hence, there is 1kA fault current injected into the grounding system.

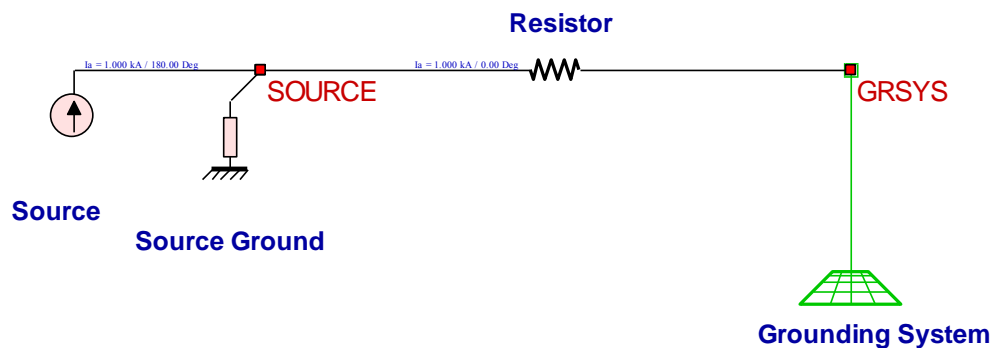


Fig. 3.20 WINIGS single line fault diagram

Fig. 3.21 is the grounding system diagram seen from z -direction. The red-arrow line is the path along which it is desired to know the touch voltage and step voltage.

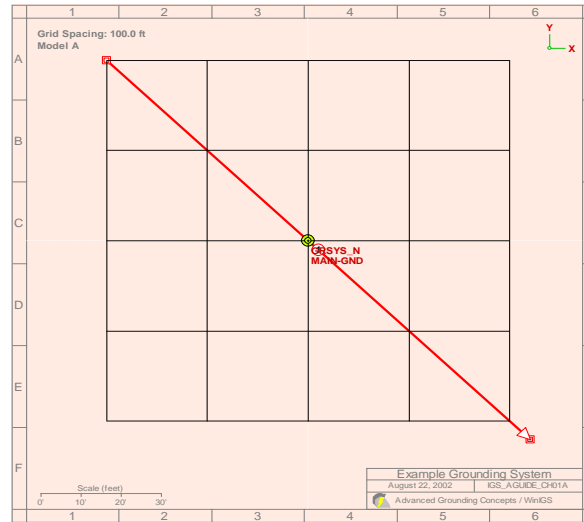


Fig. 3.21 WINIGS grounding system diagram

Fig. 3.22 shows the touch voltage plot along the red arrow line shown in Fig. 3.21. The worst (largest) touch voltage typically occurs near the center of the corner mesh. Therefore, the touch potential at the center of the corner mesh is arbitrarily chosen as the worst touch potential to be compared with the allowable value in OPTIMGRID.

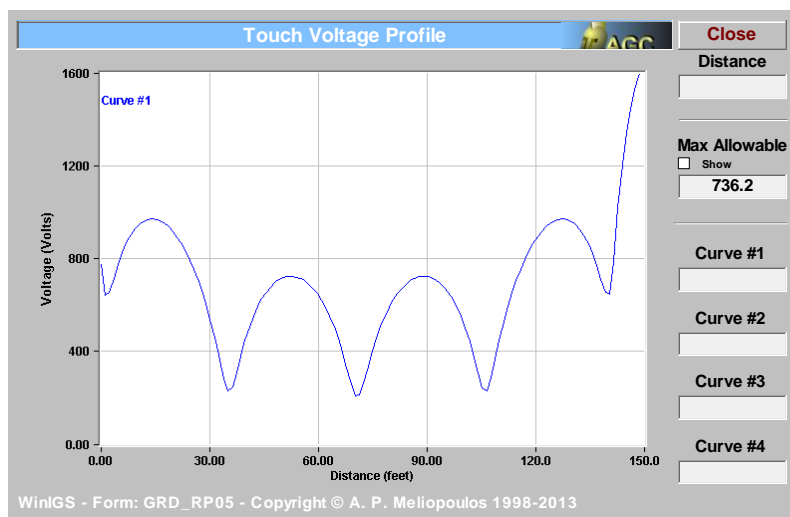


Fig. 3.22 WINIGS touch voltage profile

Fig. 3.23 shows the step voltage plot along the red arrow line shown in Fig. 3.21. The worst (largest) step voltage typically occurs off the corner in a direction parallel to a line, which bisects the corner angle.

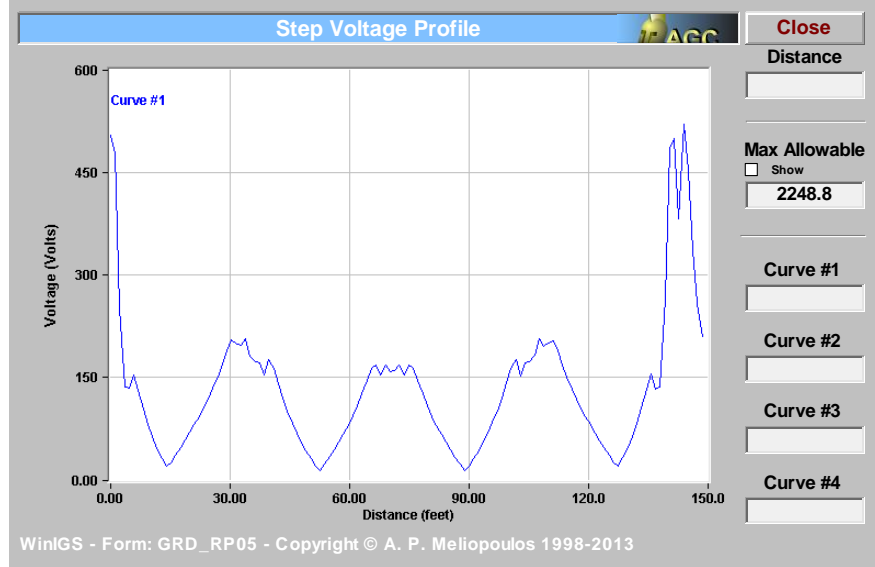


Fig. 3.23 WINIGS step voltage profile

In order to compare the results from the author's method and from WINIGS method explicitly, this thesis applies following equation (3.63) for detecting the deviations between these two methods.

$$error_{E_{mesh}} = \frac{E_{mesh_WINIGS} - E_{mesh_OPTIMGRID}}{E_{mesh_WINIGS}} \times 100\% \quad (3.63)$$

where WINIGS and OPTIMGRID represent the value of worst touch potential (E_{mesh}) coming from WINIGS method and OPTIMGRID method respectively for the scenario depicted in Fig. 3.24.

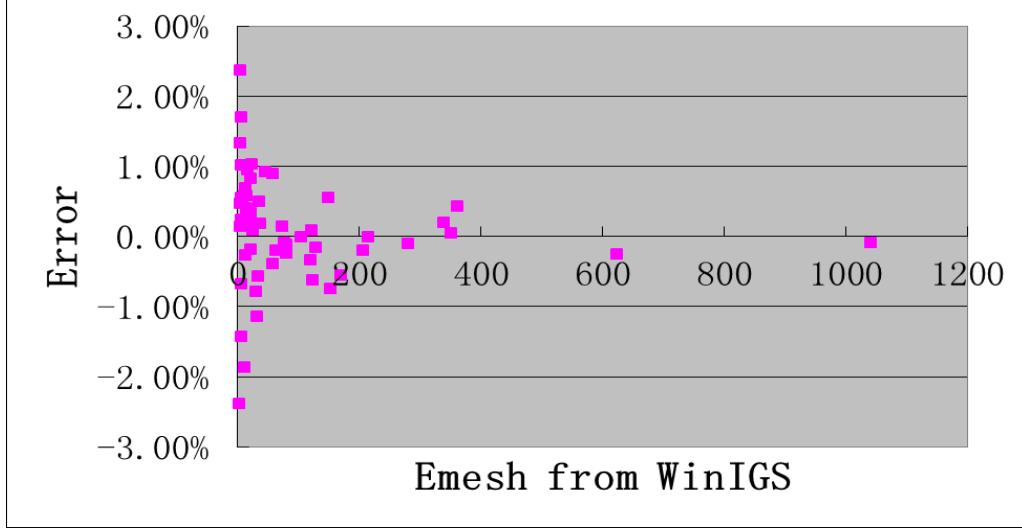


Fig. 3.24 Error of Emesh between two methods

Based on (3.64), WINIGS and OPTIMGRID represent the value of worst step potential (E_{step}) coming from WINIGS method and OPTIMGRID method respectively for

Fig. 3.25.

$$error_{E_{step}} = \frac{E_{step_WINIGS} - E_{step_OPTIMGRID}}{E_{step_WINIGS}} \times 100\% \quad (3.64)$$

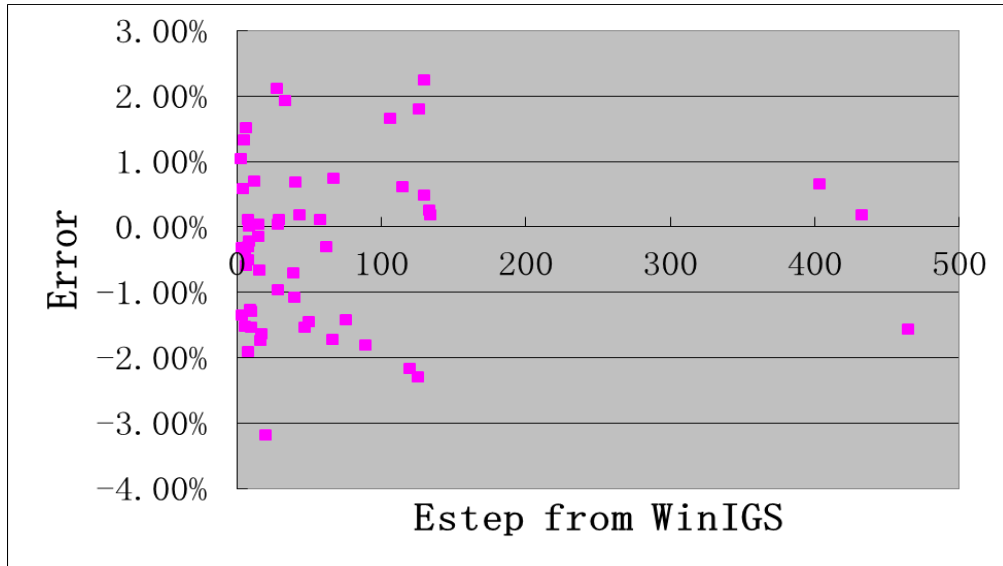


Fig. 3.25 Error of Estep between two methods

Based on (3.65), WINIGS and OPTIMGRID represent the value of grounding resistance (R_g) coming from WINIGS method and OPTIMGRID method respectively for Fig. 3.25.

$$error_{R_g} = \frac{R_{g_WINIGS} - R_{g_OPTIMGRID}}{R_{g_WINIGS}} \times 100\% \quad (3.65)$$

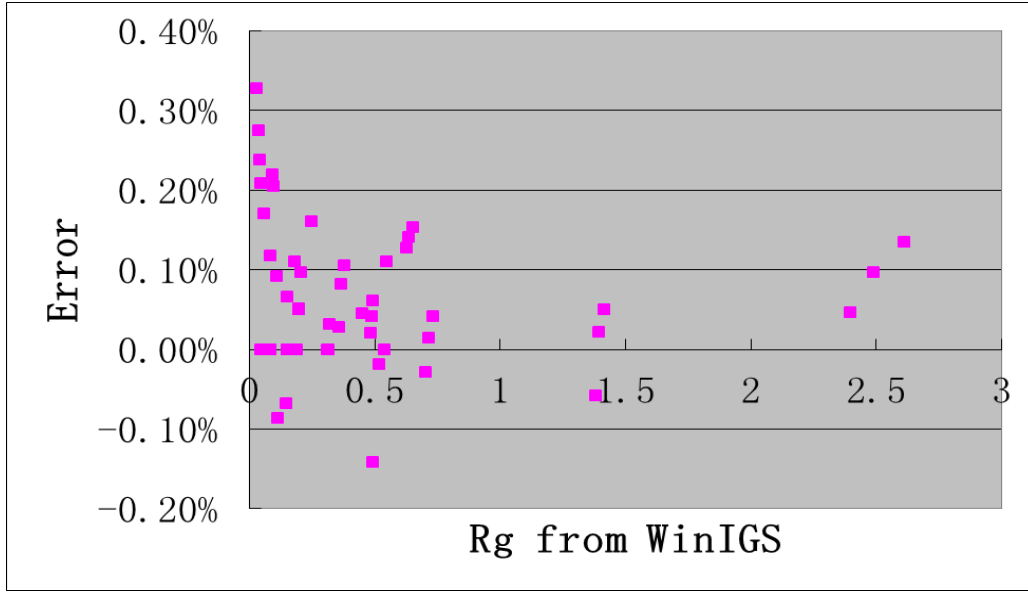


Fig. 3.26 Error of R_g between two methods

The three figures, Fig. 3.24 to Fig. 3.26, show that the difference of the calculated grounding resistance between OPTIMGRID and WINIGS is very small and the differences are lower than 0.4% for the example chosen. The differences of worst touch voltage and worst step voltage are less than 3%, which means the OPTIMGRID results are close to the WINIGS results for this example.

4 GROUNDING SYSTEM OPTIMIZATION

Presented in this chapter is a novel optimization strategy used in minimizing labor and material cost for substations with rectangular geometries. The key requirement for an optimization method capable of grounding-system optimization is that it must be able to deal with the discontinuous and non-differentiable constraints. The author will apply a new three-step optimization process combining a traditional optimization method with a heuristic probabilistic optimization method, comprised of a pattern search method and genetic algorithms.

While the equations of Chapter 3 are used to determine acceptability of the ground grid design, the optimization procedure that uses these equations is enhanced if it has a good starting point. A convenient way of getting a good starting point is to begin with (approximate) IEEE equations [1] for ground grid design. Since these equations are continuous and differentiable, efficient and robust optimization methods can be used to find an approximate optimum, which can then be used as a starting point for the second-step optimization procedure (describe below) which uses the equation of Chapter 3. In all, the optimization process is a three-step procedure. A description of the first step follows immediately.

4.1 Step 1: Use of IEEE Standard Equations for Optimization

The first step in the three-step procedure for designing an optimal ground grid is to use approximate relationships, given by the IEEE standards, that are continuous and differentiable, relationships to which traditional robust optimization techniques can be applied. The result of this optimization procedure will be the initial estimate to be used in the second step of the optimization process.

In ground grid design, the mesh voltage is traditionally treated as the worst-case touch voltage on the earth surface above a grounding system and its value is obtained from following equation (4.1):

$$E_m = \frac{\rho K_m K_i I_g}{L_M} \quad (4.1)$$

where,

ρ = equivalent uniform soil resistivity (Ω m);

K_m = geometrical factor [1];

K_i = corrective factor [1];

I_g = maximum fault current through the grounding system (A) [1];

L_M = effective grounding systems conductors and rods length (m) [1].

The detailed expressions and calculation process of ρ , K_m , K_i , I_g and L_M are described and explained in [1]. While some of these parameters are exogenous parameters, i.e., I_g and ρ , the other parameters are functions of conductor spacing (D) in

meters, depth of grounding grid (Dep) in meters, conductor diameter (dia_c) in meters, length (a) and width (b) of the substation in meters, number of rods (n_r), rod length (l_r) in meters, rod diameter (dia_r), fault current (I_f) in amps, and fault current division factor (D_f). Among them, only D and n_r are the variables needed to minimize the objective as all other parameters either are determined by these variables or are either cite specific and endogenous or are specified by the sponsor of this research as company requirements.

Similarly, the predicted step voltage values for any given grid design are obtained from following equation [1]:

$$E_s = \frac{\rho K_s K_i I_g}{L_s} \quad (4.2)$$

where,

K_s = geometrical factor in calculating step voltage [1];

L_s = effective grounding systems conductors and rods length (m) in calculating step voltage [1].

The final grounding systems parameter to be considered is the grounding resistance to remote earth (R_g), which is given as:

$$R_g = \rho \left[\frac{1}{L_T} + \frac{1}{\sqrt{20A}} \left(1 + \frac{1}{1 + h\sqrt{20/A}} \right) \right] \quad (4.3)$$

where,

L_T = total length (m) of all the grounding conductors and rods [1];

Dep = depth (m) of the grounding system under the earth surface;

A = area (m^2) of the substation.

The purpose of above development is to present the differentiable constraint equations, i.e., (4.1), (4.2) and (4.3). Enforcing these constraints and using the approximate safety metrics provided by the IEEE equations, a traditional optimization procedure can be used so that minimization of value of the objective function, defined in section 4.4, can be achieved.

Traditional optimization of this problem is achieved by using the “fmincon” solver in the MATLAB Optimization Toolbox [11] as well as “GlobalSearch” function in MATLAB Global Optimization Toolbox [12] to model this constrained nonlinear minimization problem. With the help of the “GlobalSearch” function, the “fmincon” solver can be made more efficient and made be less dependent on the initial values. The details about the combination of “GlobalSearch” and “fmincon” can be found in [12].

4.2 Step 2: Use of Pattern Search Method for Optimization

With the initial values obtained from the first step, the MATLAB solver called “patternsearch (PS)” has been used for the second-step of the optimization process. PS is a member of the family of direct search methods. A direct search algorithm searches a set of points around the current point, looking for one where the value of the objective function is lower than the value at the current point. The most significant advantage of

the direct search methods is that they do not require that the objective function and constraint functions be differentiable or continuous. Therefore, the more accurate non-differentiable and discontinuous constraints described in Chapter 3 can be applied in this second step. The objective function to be used in this step is referenced in section 4.4.

However, the disadvantage of direct search method and heuristic method (like genetic algorithms discussed later) is the computation time expense. These methods are unlike gradient-based methods, which the user can implement without knowing a direction to search for lower objective values. Instead, PS needs to test multiple points near the current point, just like a “mesh” around this point. The MATLAB “patternsearch” solver forms the “mesh” by:

- Generating a set of vectors $\{d_i\}$ by multiplying each pattern vector v_i by a scalar Δ^m , which is called the mesh size. Content and generation of these vectors will be introduced with a numerical example presented later.
- Adding the $\{d_i\}$ to the present point, which is the point with the best objective function value found at the previous step [11].

In OPTIMGRID, the variables (described in detail in section 4.4) to be optimized are spacing between two conductors (D) and the method of rod placement (m_r). Hence, it is necessary to generate two-dimension-coordinate oriented pattern search algorithm. For

example, assume the present point has coordinates [2.6, 3.2] and its present mesh size (Δ^m) equals 4.0. In addition, the pattern vectors are set as:

$$v_1 = [1, 0]; v_2 = [0, 1]; v_3 = [-1, 0]; v_4 = [0, -1].$$

The vectors $\{d_i\}$ are obtained as:

$$d_1 = 4.0 * [1, 0] = [4.0, 0];$$

$$d_2 = 4.0 * [0, 1] = [0, 4.0];$$

$$d_3 = 4.0 * [-1, 0] = [-4.0, 0];$$

$$d_4 = 4.0 * [0, -1] = [0, -4.0];$$

The algorithm adds $\{d_i\}$ to the present point to obtain the following mesh.

$$[2.6, 3.2] + [4.0, 0] = [6.6, 3.2]$$

$$[2.6, 3.2] + [0, 4.0] = [2.6, 7.2]$$

$$[2.6, 3.2] + [-4.0, 0] = [-1.4, 3.2]$$

$$[2.6, 3.2] + [0, -4.0] = [2.6, -0.8]$$

If one of the four new points has the smallest objective among these five points, the new point will be set as the present point at the next iteration with a new mesh. However, if none of the new points has an objective function with a smallest value, the mesh size (Δ^m) will be reduced. This mesh size reduction is continued until either a smaller value is found or the minimum size of Δ^m is reached. In OPTIMGRID, the initial mesh size (Δ^m) is set as 8.0. In addition, MATLAB's implementation of the pattern search algorithm

gives users the option of changing the mesh size scaling parameters, which is used to reduce the mesh size or expand the mesh size automatically. A large initial mesh size (Δ^m) increases the range of m_r options, however, as the mesh size is reduced, the range of m_r options consider may decrease; this is a limitation that may or may not effect the outcome of the optimization procedure. Removing this uncertainty is a task of the student following up with this research. The variable m_r is an integer but once Δ^m is applied, the m_r value, in general will be a real number; therefore, a real-to-integer conversion is used to round off the number to an integer. It is important in the process that m_r varies so that the rounding off process does not constrain Δ^m to always remain unchanged. A larger mesh size decreases the probability that m_r would remain unchanged. For example, if $m_r = 3$ and $\Delta^m = 1.2$, then after application of the mesh operator and real-to-integer conversion, two new points with $m_r = 2$ and $m_r = 3$ are generated.

PS selects its direction (i.e., pattern vector that produces the “present point”) based on a user-specified polling method, which means the user is “questioning” and “picking” the right points and “mesh” based on a chosen method. For OPTIMGRID, the polling method selected is the MATLAB default selection, which is called “GPS Positive Basis 2N”. In the method’s name, “GPS” is the abbreviation of general patterns search method and “2N” means there are $2N$ pattern vectors, where N is the number of the independent variables. The details of how to choose the polling method are described in [12]. The

previous example with the present point [2.6, 3.2] uses this default polling method. In this example, there are two independent variables, so the points are presented in two-dimension coordinates. In addition, the number of pattern vectors is accordingly four. A conceptual description of the PS algorithm is presented in the flowchart shown in Fig. 4.1.

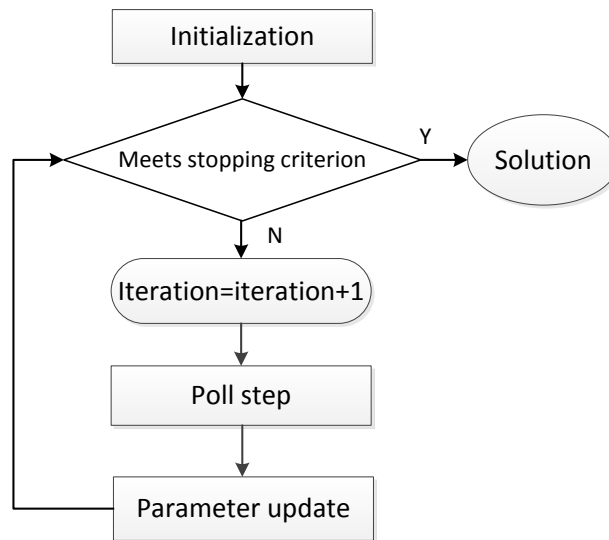


Fig. 4.1 Flowchart of pattern search method

In this figure, the stopping criteria in OPTIMGRID include:

- Reaches the maximum number of iteration (200)
- Reaches the minimum mesh size (1e-6)
- Meets the minimum objective change (1e-6)

4.3 Step 3: Use of Genetic Algorithms for Optimization

The genetic algorithm is the third (optional) step in the optimization procedure as well as the backup step. This step is used if the pattern search approach does not yield the optimal design. The constraints (voltage equations) in Chapter 3 are used in this step, the same as those used in the pattern search method. Genetic algorithms have improved robustness when compared with pattern search methods, but they also are computationally expensive.

The genetic algorithm was first introduced by John Holland for the formal examination of the mechanisms of natural adaptation [9], but since then, it has become a search technique used in computing to find globally optimum or approximate solutions to optimization problems. As a global search heuristic technique, it is used in problems where techniques using traditional algorithms are incapable of obtaining satisfactory solutions.

The genetic algorithm is a particular class of evolutionary algorithms that use techniques inspired by evolutionary biology such as inheritance, evaluation, selection and reproduction.

Conceptually, this technique may be described as follow. As a first step, an individual is produced randomly. The process is repeated until the number of the individuals in the population equals the desired population size, which is selected based

on experience and is limited by computation resources. Each individual is presented by a set of binary numbers (i.e., 1's and 0's), each analogous to a biological “chromosome”. In the following example, there are three variables in the optimization problem, each corresponding to a different artificial chromosome. Therefore, the initial individual “*s*” is made up of a three-elements set with each element, which is an artificial chromosome with binary number chosen randomly. Each member of the set represents one variable with ten “binary genes” one-bit long:

$$s = 1110110101—0110111101—1010101101.$$

It is convenient in the genetic algorithm, to represent “*s*” using the equivalent decimal where each binary sequence is treated as a positive binary integer.

The next step is the evaluation step. In this step, a fitness function is defined and it is calculated (evaluated) every individual. According to the value of fitness function (objective function,) all the individuals will be ranked based on their fitness values. The larger the fitness value is, the more likely the corresponding individual will be selected. These selected individuals will be considered as “Parents”.

The “Parents” reproduction using a two-step process: crossover and mutation. Crossover combines two individuals, or parents, to form two new individuals, or children, for the next generation. In the following “one-point” crossover example, the first set of

individuals is “ s_1 ” and “ s_2 ”. After the crossover process, offspring are created, which are “ s_3 ” and “ s_4 ”. The symbol “|” is the crossover separation point.

Before applying crossover,

$$s_1=1001010001, s_2=11|10110101.$$

After applying crossover,

$$s_3=10|10110101, s_4=11|01010001.$$

In this example, s_1 and s_2 are chosen randomly from a larger set of individuals. The probability of crossover in application of OPTIMGRID is 0.8.

Mutation is the phenomena, where a random "0" becomes "1" or a "1" becomes "0" in an individual "chromosome". The mutation is applied to all bits (genes) with a very low probability of mutation, set to 0.05 in OPTIMGRID. After the above steps are carried out a new generation with a new population has been generated. In the following “one-point” mutation example, the original set of individual is “ s_1 ” and “ s_2 ”. After crossover and mutation, another new set of individuals “ s_3 ” and “ s_4 ” has been produced. The number between the two symbols “|” (presented in the next example) is the one “gene” which is assume to be the only one selected to be mutated from “1” to “0” or from “0” to “1”. In this example, only one bit was selected, but each bit has the same probability of being selected and the number of bits selected cannot be known a priori.

Before applying mutation,

$$s_1=11101|1|0101, s_2=1111|0|10101.$$

After applying mutation,

$$s_1=11101|0|0101, s_2=1111|1|10101.$$

After repeated reproduction, a global or "near-global" optimum can be reached. The termination criterion is achieved if either the mean value of fitness function F_g calculated using all individuals in the population is no longer improved by the process of reproduction or the iteration index, N_g , is equal to the defined maximum number of iteration N_{max} . The general flowchart of the genetic algorithm is shown below in Fig. 4.2.

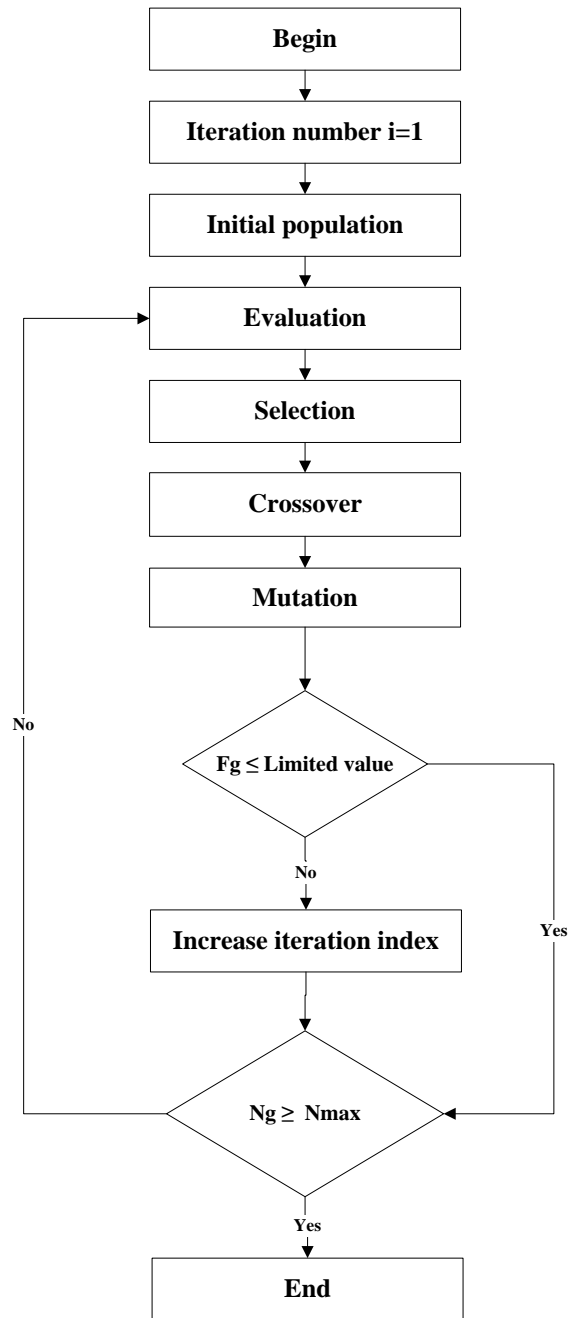


Fig. 4.2 General Flowchart of Genetic Algorithms

4.4 Optimization Problem Based on SRP Design Rules

Formulation of the optimization problem is informed by the grounding systems design rules of Salt River Project (SRP). These rules are incorporated as assumptions in the grounding systems optimization process. There are five design rules described below:

(1) Grounding grid size and mesh resolution requirements:

- The maximum substation dimensions are 1000 ft. by 1000 ft.
- The shape of meshes making up a grounding grid should be square.
- The maximum acceptable mesh size is 50 ft. by 50 ft.
- The minimum acceptable mesh size is 8.2 ft. by 8.2 ft.

(2) Tolerable voltage calculation rules

- The standard body weight in calculating step and touch tolerable voltage should be 50 kg (110 lb) [1]. This body weight leads to the coefficient “0.116” in (3.6) and (3.7) [1].
- The separation distance between feet for step potential calculation should be 1 meter, which is used in calculating the maximum voltage difference.
- The standard radius of a foot should be 0.08 meter. This value is used to calculate the resistance of the human body model, which, in turn is used to calculate the amount of current flowing through the body for any give voltage between feet and hand or between foot and foot.

- The fault duration (t_f) is used to calculate the tolerable voltages in (3.6) and (3.7)

and is determined by the voltage class of a substation. The values are given as:

Table 4.1 Relationship between Voltage Class and Fault duration

Voltage class (kV)	Time (s)
>250	0.25
200 to 250	0.50
22 to 200	0.58
<22	1.10

(3) Grounding grid design rules:

- Grid conductor size should be 4/0 AWG, 7 strand copper (0.522" diameter) for all new installations.
- The standard depth of the grounding system should be 1.5 ft. below finished grade. It does not include any surface material used to obtain a decreased touch and step potential.
- The grounding grid should be designed for the maximum fault level expected for the life of the station.
- In this model, uniform potential distribution (no potential difference along grounding conductors) and uniform mesh size are applied.
- It also ignores the influence of mutual inductance and capacitance.

(4) Grounding rod design rules

- Grounding rods are always placed at each outside corner of the grounding grid.
- When additional grounding rods are used, they should be evenly spaced along the outer grid perimeter, not less than one-rod length apart.
- In this model, interior rods and surge arrestor loops are not considered.
- When a uniform soil model is used, the rod length should be 10 ft. long.
- When a two-layer soil model is used, if the top layer's thickness is less than 10 ft., the rod length shall be 20 ft. long.
- When a two-layer soil model is used, if the top layer's thickness is larger than 10 ft. and smaller than 30 ft., the rod length shall be 30 ft.
- When a two-layer soil model is used, if the top layer's thickness is larger than 30 ft., the rod length should be 10 ft.

(5) Cost data

- The cost of mesh conductor (4/0 copper, 7 strand, soft drawn) and ground rod (cop_clad, 1 strand) is \$3.77/ft. (C_{cond}).
- The cost of exothermic welds is \$19.25 each (C_{exoth}).
- The cost of labor to trench, install cable, and backfill is \$4.00/ft including equipment (C_{trench}).
- The cost of labor to drive rods up to 10 ft. is \$10/ft. (C_{drive}).

- The cost of labor to drill, insert, and backfill rods 11 ft. to 40 ft. is \$32/ft.
- The cost of labor to make exothermic connections from cable to cable or cable to rod is \$40 each ($C_{connect}$).

From the equation and rules shown above, it is possible to specify the optimization problem completely. In addition, it is noted that the units of all lengths, depths and diameters is change from feet to meters in calculation process.

Generally, the optimization variables would be conductor spacing (D) in meters, depth of grounding grid (Dep) in meters, conductor diameter (dia_c) in meters, number of rods (n_r), each rod length (l_r) in meters and rod diameter (dia_r) in meters. However, the parameters Dep , dia_c and dia_r are required to be 0.4572 meters (1.5 ft), 0.0134 meters (0.528 ft) and 0.016 meters (0.628 ft) respectively, and the rod length is fixed as one of three discrete values of 3.048 meters (10 ft), 6.096 meters (20 ft) and 9.144 meters (30 ft) based on the thickness of the upper-layer soil. As a result, only D and n_r are the free variables in the objective function, which is the total cost of the grounding systems.

Using the cost variable defined above, the objective function should be:

$$\begin{aligned}
 \min f(D, n_r) \\
 &= (C_{cond} + C_{trench}) \bullet L_{cond} + (C_{rod} + C_{drive}) \bullet L_{rod} \\
 &+ (C_{connect} + C_{exoth}) \bullet (n_r + n_{exoth})
 \end{aligned} \tag{4.4}$$

where,

$$L_{cond} = \left(\frac{a}{D} + 1 \right) \bullet b + \left(\frac{b}{D} + 1 \right) \bullet a \quad (\text{m});$$

$$L_{rod} = l_r \bullet n_r \text{ (m);}$$

$$n_{exoth} = \left(\frac{a}{D} + 1 \right) \bullet \left(\frac{b}{D} + 1 \right);$$

a = substation length (m);

b = substation width (m).

The constraints are derived from above rules shown as:

$$8.2 \text{ ft.} \leq D \leq 50 \text{ ft.} \quad (4.5)$$

$$E_m \leq E_{touch_allowable} \quad (4.6)$$

$$E_s \leq E_{step_allowable} \quad (4.7)$$

$$R_g \leq 0.5\Omega \quad (4.8)$$

At first, it is necessary to divide each horizontal conductors and vertical rods into suitable number of segments. The word “suitable” means the segmentation must lead to accurate results while the program execution time (efficiency) must be less than 40 mins for most applications. In theory, the more refined the model, i.e., smaller segments, the more accurate the results. However, the more refined the model, the longer the runtime. Runtime increases with finer segmentation because the size of the matrix in equation (3.60) is proportional to number of segments. Hence, some compromises must be made between these two aspects. In OPTIMGRID, the number of segments is decided based on the value of D and number of meshes. Segment length is selected by trading off accuracy

and runtime. The runtime will get longer as the number of meshes is increased. In other words, if the number of meshes is relatively small, it is necessary to make the segment length smaller in order to achieve more accuracy, however, if the number of meshes is larger, to keep the runtime shorter, segment length is increased, sacrificing accuracy. (This may be a flaw in the present approach, because it is necessary to make the accuracy acceptable, even if there is a larger model of grounding system; hence testing is being conducted to determine if the segment-size rules used by the program are acceptable.).

The following table shows the rule for selecting segment length of horizontal grounding grid based on both the spacing D and the number of meshes N_m :

Table 4.2 Rules for Selecting Segment Length

	$D \leq 10$	$10 < D \leq 20$	$20 < D \leq 50$	$D > 50$
$N_m \leq 30$	D	$D/3$	$D/5$	$D/7$
$30 < N_m \leq 40$	D	$D/3$	$D/5$	$D/5$
$40 < N_m \leq 50$	D	$D/3$	$D/3$	$D/3$
$N_m > 50$	D	D	D	D

For the grounding rods, the rule of subdividing them is:

- If the rod does not penetrate to the lower-layer soil, the rod will be subdivided into five segments with equal length.
- If the rod does penetrate to the lower-layer soil, the rod will be subdivided into five segments with two equal-length segments in the upper layer and three equal-length segments in the lower layer.

Once the segment strategy is set, the midpoint coordinate of each segment in the coordinate system must be determined, where the origin is arbitrarily set at the left bottom corner point as shown in Fig. 4.3.

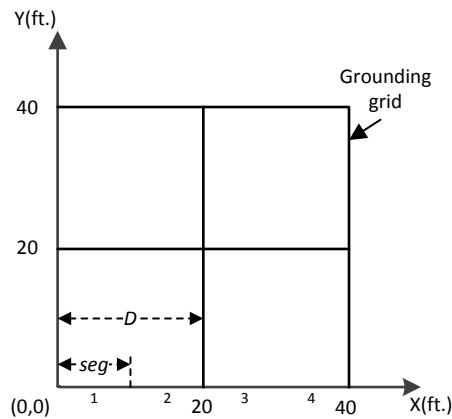


Fig. 4.3 2-by-2 Grounding Grid with X-Y Coordinate System

Fig. 4.3 depicts a 2-by-2 grounding grid without any grounding rods. The distance between two parallel conductors (D) is 20 ft. The segment length is arbitrarily selected as 10 ft. (used in the continuing example) shown in Fig. 4.3. In other words, each conductor with length of D would be separated into two equal-length parts. In order to store all segment midpoint coordinates, segment lengths and segment orientations, it is necessary for OPTIMGRID to number all the segments such as the conductor on the X-axis shown

in Fig. 4.3, where the segment number is from “1” to “4”. For segment “1”, its midpoint coordinate on the X-Y plane is $(X,Y)=(5, 0)$. If the grounding grid is located under the earth surface with depth of 1.5 ft., the completed coordinate of segment “1” should be $(X,Y,Z)=(5, 0, -1.5)$, because the X-Y plane is coplanar with the earth’s surface.


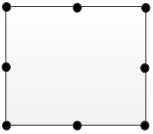
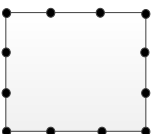
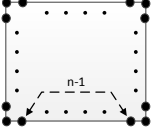
Finally, the method in Chapter 3 is used with such process:

- Calculate all the self and mutual resistances like r_{11} and r_{12} , etc.;
- Implement matrix method to get the values of all the segment leakage currents, which are i_1 and i_2 for the first two segments;
- Substitute the current value, segment midpoint coordinate and the field point coordinate into variables I , (X_I, Y_I, Z_I) and (x, y, z) respectively in equations (3.38), (3.39) and (3.40) in order to obtain the field point potential due to each segment;
- Sum up all the potentials produced by every segment to get the earth potential of specific field point, and calculate worst touch and step voltages.

As mentioned before, it is only possible to get the values of worst touch and step voltage when each segment coordinate is determined including segments of grounding rods, which means it is necessary to know not only the number of rods, but also the coordinates of the rods. As a result, the coordinates of the rods should be variables as well. It is difficult to model the coordinates of rods in this optimization problem using the approach described above; hence the number of ground rods is characterized in this

method by scenario number, which is defined by grounding rod placement number, m_r , that becomes the second variable (the first variable is D) instead of the number of rods n_r . The variable m_r is the combination of n_r and the variable coordinate of each rod. In other words, if m_r is determined, both the number of rods and the coordinate of each rod are determined. However, the variable m_r despite being an integer is a real number in the optimization procedure. Before using m_r to calculate the constraints and the objective it is necessary to perform real-number-to-integer conversion, by rounding all numbers up (down) that are greater than or equal to (less than) $X.5$ to $X+1$ (X .) For example, if the “patternsearch” solver generates $m_r = 1.8$, it will be treated as an integer of 2 for selecting the ground rod placement pattern. In the algorithm, the next step could generate a value of $m_r = 1.6$ and while D remains unchanged, which would not be the same point in the design space. Part of the work going forward will be to determine whether this can occur and how to mitigate this situation if it is indeed a problem with selecting an appropriate value of Δ^m . The detailed relationship between the placement scenario, m_r , n_r and ground rod placement is shown in Table 4.3.

Table 4.3 Description of m_r

scenario (m_r)	Num. of rods (n_r)	Top view description (One black solid point is one rod)
scenario 1 ($m_r=1$)	4	
scenario 2 ($m_r=2$)	8	
scenario 3 ($m_r=3$)	12	
\vdots	\vdots	\vdots
scenario n ($m_r=n$)	$4*n$	

The general rule is that scenario n means $(n-1)$ rods are distributed uniformly on each side length of the area (rectangular). Because the minimum length of a rod should be 10 ft. and the maximum size of a substation should be 1000 ft. by 1000 ft., the value of m_r will be in the range 1 to 100.

Therefore, the new objective function should be changed to:

$$\begin{aligned}
 \min f(D, m_r) &= (C_{cond} + C_{trench}) \bullet L_{cond} + (C_{rod} + C_{drive}) \bullet L_{rod} \\
 &+ (C_{connect} + C_{exoth}) \bullet (n_r + n_{exoth})
 \end{aligned} \tag{4.9}$$

where,

$$n_r = 4m_r;$$

$$L_{cond} = \left(\frac{a}{D} + 1\right) \bullet b + \left(\frac{b}{D} + 1\right) \bullet a \quad (\text{m});$$

$$L_{rod} = l_r \bullet n_r \quad (\text{m});$$

$$n_{exoth} = \left(\frac{a}{D} + 1\right) \bullet \left(\frac{b}{D} + 1\right);$$

a = substation length (m);

b = substation width (m).

4.5 Program Structure

The flowchart of the OPTIMGRID program is shown in Fig. 4.4. First, it is necessary to obtain the substation initial design data used as input data into this program.

The initial data should include:

- Substation shape and dimensions (If the shape of a substation is rectangular, the dimensions contain length and width.)
- Maximum fault current and division factor. The division factor is the ratio of the current flowing into the grounding system divided by the maximum fault current.
- Fault duration time. The fault duration time is related to the voltage class of a substation and the detail relationship is shown in section 4.4.
- Soil model and parameters which are obtained from the Wenner method described in details in Chapter 2

- Resistivity and depth of the surface material. (If there is no high resistivity surface material, the depth of surface material is treated as zero.)

With the initial data, it is necessary to calculate the tolerable (allowable) touch and step voltages from (3.6) and (3.7) respectively, which are used as the upper bounds for the computed touch and step voltages like shown in (4.6) and (4.7).

As stated earlier, the optimization process is a three-step procedure, in the first step, an approximate optimum is reached using the IEEE standard equations introduced in section 4.1. This IEEE standard provides substation engineers with 3 expressions, (4.1), (4.2) and (4.3), which are the approximate formulas to calculate the grounding systems parameters. However, the biggest advantage of these equations is they are continuous and differentiable. In other words, it is possible to use the conventional continuous optimization method like gradient descent methods. Although the optimization result is likely not as accurate as possible (though likely conservative) due to the approximations used in the derivations of equations of [1], the result should not be too far the globally optimal solution. Therefore, optimization using these equations with traditional and robust optimization techniques provides a good initial estimate of the optimal solution for the next stage in the optimization. For this first step, the objective function (4.9) remains unchanged and the E_m , E_s and R_g inequality constraints, (4.6), (4.7) and (4.8) are imposed using the IEEE equations, (4.1), (4.2) and (4.3), to calculate the values of E_m , E_s , and R_g ,

instead of the methods described in Chapter 3., For this first step in the three step optimization process, the MATLAB tool functions “fmincon” and “GlobalSearch” need be used to find this initial estimate of the optimal solution.

In the second step of the optimization procedure, the optimal solution from IEEE equations (first step) is used as an initial estimate for MATLAB’s “patternsearch” solver. This will not only improve the efficiency of pattern search procedure, but also reduce the probability of ending with the local optimal solution if which is more likely to happen if a poor initial estimate is used.

After the pattern search procedure is exhausted, it is necessary to perform the perturbation test to determine whether the point obtained is a local optimum or an optimum at all. For example, Fig. 4.3 shows a 2-by-2 grounding grid with no ground rods. It is assumed that this grid resolution is obtained after running pattern search. If this is the globally optimal solution, the constraints (4.6), (4.7) and (4.8) will not be satisfied when making the grid resolution coarser. In other words, if it is possible to increase D until the grid resolution gets coarser (changed from 2-by-2 to 1-by-1 in this example) and the objective function is reduced while the constraints are still satisfied, the optimal solution at $(D, m_r)=(20, 0)$ is not a global optimal solution and the result is suboptimal. Conversely, if the constraints are violated by making such a change, it is at least plausible that the result is locally (and possibly globally) optimal.

If the optimal result after running pattern search is $(D, m_r) = (20, 1)$ in the example cited, it is necessary not only to verify the plausibility of the solution being optimal by changing $(D, m_r) = (20, 1)$ to $(40, 1)$, which means making the grid resolution coarser. In addition, one must also verify the plausibility of the solution being optimal by changing $(20, 1)$ to $(20, 0)$, which means deleting four rods. In addition to making the grid coarser, deleting rods is another way of making the objective function smaller, a change that would violate the constraints if the solution were optimal.

After completing the perturbation test and finding that the solution is not optimal, as the third step in the optimization procedure is implemented the genetic algorithm. The genetic algorithm used here takes more execution time than the pattern search; that is why the pattern search is the second step in the optimization procedure. Use of the genetic algorithm is the final step in the optimization process.

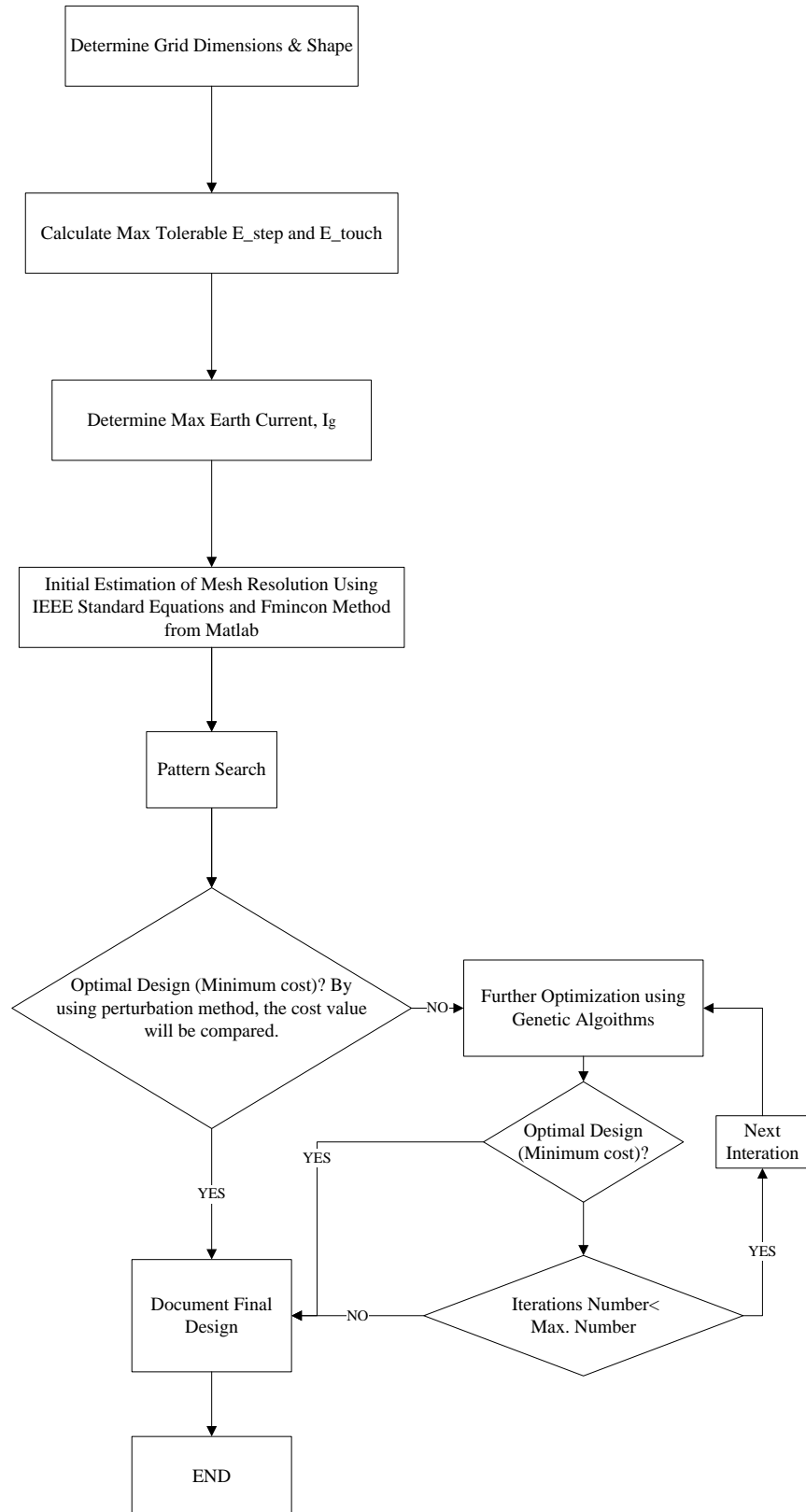


Fig. 4.4 Flowchart of the new grounding systems optimization strategy

4.6 Case Study

Fig. 4.5, shows the top view of the Ealy Substation, which is SRP's 69KV distribution substation.

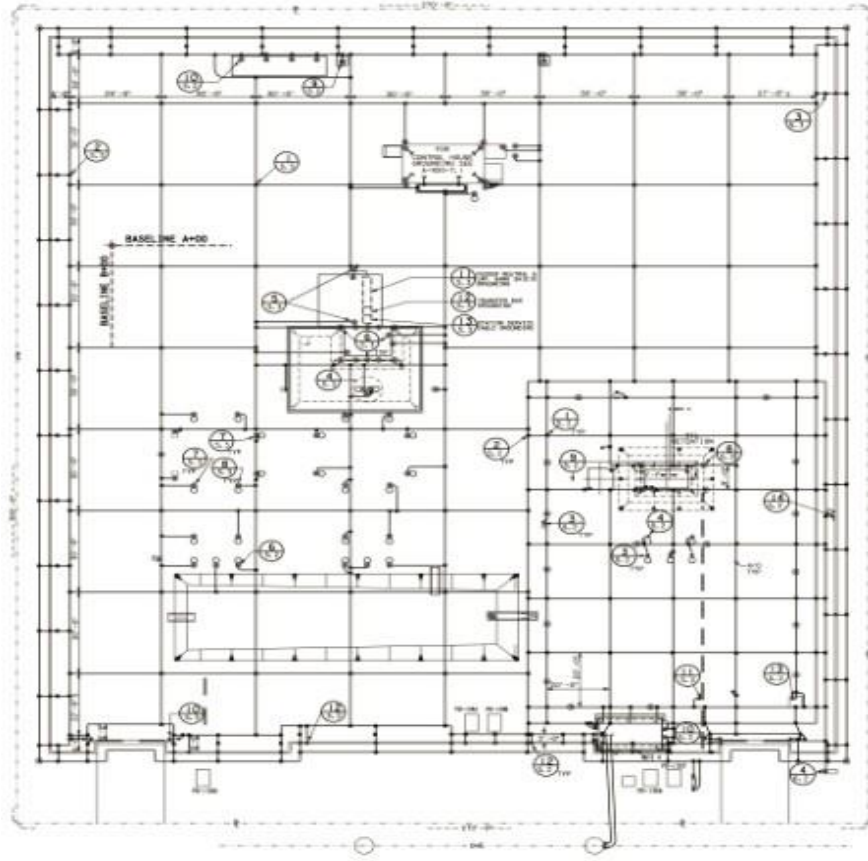


Fig. 4.5 Top view of Ealy substation with the old SRP design

This substation has been in existence for twenty years. Fig. 4.5 is the original design drawing of this substation, including grounding systems and surface equipment. In the following example, we compare the safety metric calculated using OPTIMGRID with those calculated for the same design using WINIGS.

As a test of OPTIMGRID, a redesign of the Ealy ground grid is investigated. The necessary input data for this redesign includes:

- Maximum fault current in 69KV System (I_f) = 7100 A;
- Current division factor for flow path of the fault (D_f) = 0.53;
- Maximum fault current through the grounding system ($I_g = I_f * D_f$) = 3780 A;
- System voltage where highest ground potential rise occurs (V_s) = 69 KV;
- Fault duration (t_f) = 0.58 s;
- Resistivity of upper-layer soil (ρ_1) = 87.7 Ω m;
- Resistivity of lower-layer soil (ρ_2) = 57.6 Ω m;
- Thickness of upper-layer soil (h) = 34.8 ft;
- Resistivity of High Resistivity Surface Material (ρ_s) = 500 Ω m;
- Depth of High Resistivity Surface Material (d_s) = 6 inches;
- Diameter of grounding rod (dia_r) = 0.628 inches;
- Length of grounding rod (l_r) = 10 ft;
- Diameter of horizontal conductor (dia_c) = 0.528 inches;
- Grounding grid length = (a) 270 ft;
- Grounding grid width = (b) 300 ft;
- Depth of the grounding grid below the earth surface (Dep) = 1.5 ft.

While most of this data is preprogrammed in OPTIMGRID based on SRP's current practices, the data listed here is required in commercial applications, such as WINIGS.

The OPTIMGRID application is limited in capability in comparison with WINIGS and assumes the use of SRP's current practices.

Recall that, among all these input data, some are specific to each substation, like grounding grid length and width, while some are fixed based on SRP rules like diameter of the grounding conductor and rods.

Table 4.4 presents the result running the OPTIMGRID program, breaking down the runtime required for each step in the optimization procedure separately. However, the part of program, which executes the genetic algorithm, was taken out and run independently with the same input data, because the third step is a backup step and it was not needed for this case.

Table 4.4 Comparison of the Results Among All Optimization Methods

Method	D (m)	m_r	Cost (\$)	E_{mesh} (V)	E_{step} (V)	R_g (Ω)	Runtime
OPTIMGRID	6.76	1	\$73,962	243	183.3	0.353	72 mins
FMINCON	8.47	1	\$58,637	245.3	175.5	0.396	2.04 s
PS	6.76	1	\$73,962	243	183.3	0.353	71.3 min
GA (run independently)	6.71	1	\$73,962	244.3	186.2	0.355	646 mins
$E_{touch_allowable} = 247$ V, $E_{step_allowable} = 532$ V							

In Table 4.4, the row FMINCON gives results for the conventional optimization method using the MATLAB “GlobalSearch” function and the MATLAB “fmincon” solver. PS is the pattern search method using MATLAB “patternsearch” solver and its initial values are obtained from FMINCON. GA is the genetic algorithm using the MATLAB “ga” solver, which for this example has stopped because the objectives change (function-change tolerance) is smaller than the stopping criteria ($1e-6$).

It can be concluded from Table 4.4 that:

- When the grid is rectangular, the meshes cannot be made exactly square since the length and the width of the grid, in general, cannot both be evenly divided by the same number. Therefore, it is necessary to make some approximations. In the case of Ealy, the mesh dimensions are taken as 6.76 m (22 ft.) on a side for D . For the actual geometry of Ealy, when the length (270 ft.) and the width (300 ft.) are divided by D and the answers are 12.27 and 13.64 increments respectively. To be conservative, the program proposes and does its calculation of a grid with number of meshes on a side equal to 12 by 13 with D equaling to 22 ft. It is this model that is used when evaluating the constraint equations and when comparing these results with allowable values. In the end, it is necessary to make another approximation that makes the grid resolution finer, thus the final report will recommend that the grid resolution should be 13 by 14 meshes and each mesh length and width are $270/13$, $300/14$ respectively.

While this resolution is fortuitously acceptable for the Ealy design (discussed below), such cannot be guaranteed for all design. Presently, there is no way to guarantee that the grid designed by the program is safe. This real-to-integer conversion problem is one that was discovered too late in this phase of the work to be corrected, but is being corrected by another student who is continuing this effort.

- OPTIMGRID did not execute the third step in the optimization procedure, the genetic algorithms solver in MATLAB, because the result after running PS passed the perturbation tests. As evidence that the GA was not run is that the difference in the runtime between OPTIMGRID (total execution time) and PS is less than one minute; this extra execution time was used for finding the initial guess using FMINCON and the perturbation tests and preparation of the final output results.
- Although the cost after running the first optimization step is the minimum, it is with a result of using the approximate equations of [1] when calculating grounding systems safety metrics (E_{mesh} , E_{step} , R_g). Once more accurate calculations are performed, those involving the equation of Chapter 3, the safety constraints are not satisfied. However, the values $(D, m_r) = (8.47, 1)$ obtained from FMINCON are useful as initial estimates for the PS algorithm. The results from FMINCON are not far from the results obtained after executing the second optimization step, PS, which is $(D, m_r) = (6.76, 1)$. Finally, a comment about runtime: Obviously, the conventional optimization method

using the IEEE equations is much faster than the other methods (second and third optimization steps.) In addition, the pattern search method is also much faster than genetic algorithm and the optimal designs determined by both of these are almost equal. In our experience, the pattern search step often obtains the same results as the GA. However, the genetic algorithm is included as a backup method in the event that the pattern search method fails to yield an optimum.

In order to check the accuracy of the OPTIMGRID's solution, the author also applied WINIGS to see whether the safety requirements are satisfied or not for this particular case.

Fig. 4.6 shows the top view of the grounding systems design obtained from OPTIMGRID for the Ealy Substation. The arrow line presents the measuring path and its direction.

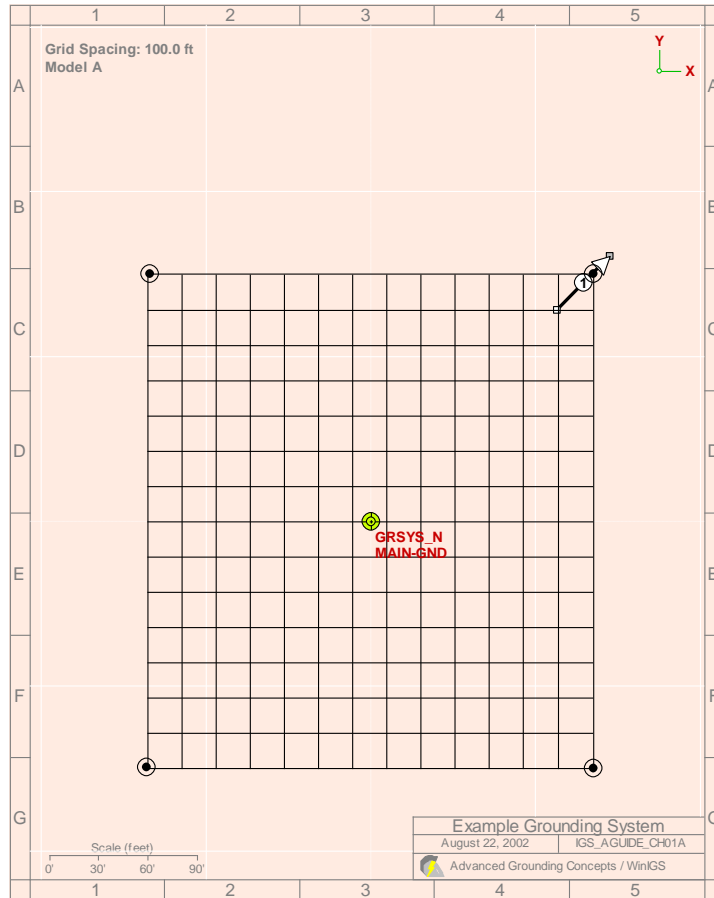


Fig. 4.6 WINIGS grounding system diagram of the designed case

Fig. 4.7 is obtained using WINIGS with the touch-voltage curve corresponding to the arrow line shown in the previous figure. The horizontal line in Fig. 4.7 is the allowable touch voltage. From this figure, the worst touch voltage is very close to the allowable value without exceeding it, which means this design satisfies all safety metrics.

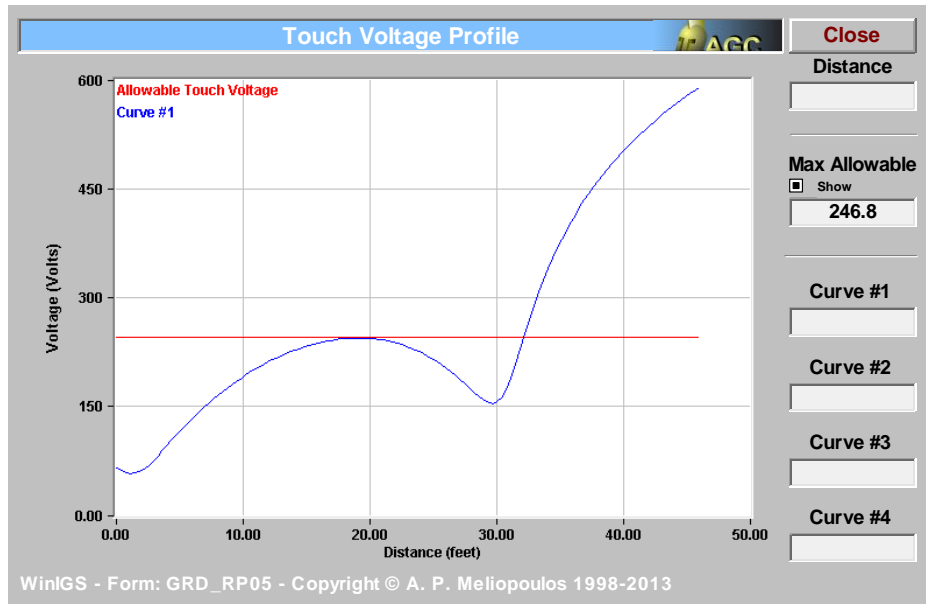


Fig. 4.7 Touch voltage plot of the design case

Similarly, Fig. 4.8 is the corresponding step voltage plot obtained using WINIGS with the allowable step voltage line. Obviously, the worst step voltage calculated with WINIGS is far lower the allowable value. This means that the binding constraint is the touch potential, as it is in most designs.

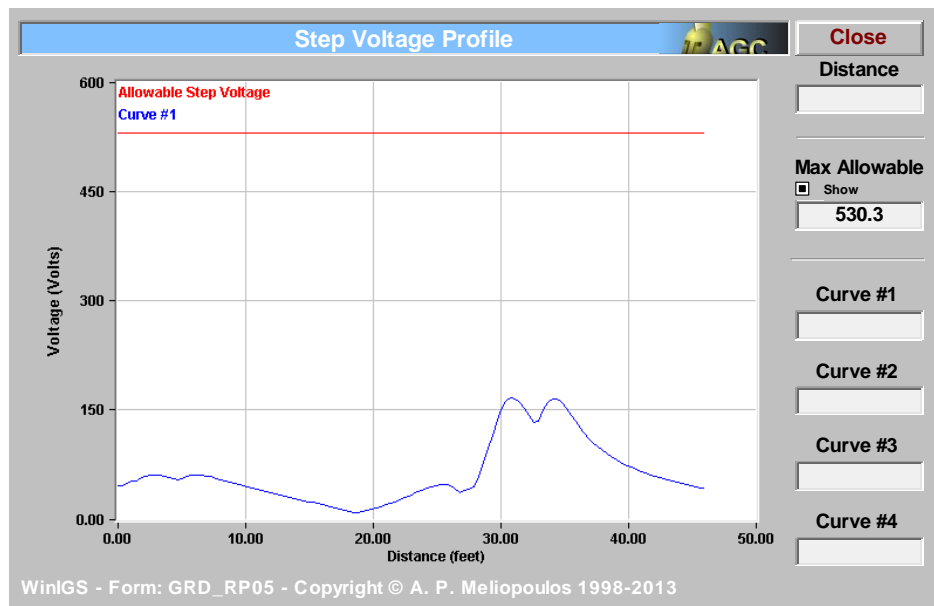


Fig. 4.8 Step voltage plot of the design case

Finally, Fig. 4.9 is the report of the grounding resistance with respect to remote earth. The WINIGS reported grounding resistance, 0.3553 Ω , is essentially the same as the OPTIMGRID's result (0.353 Ω) shown below.

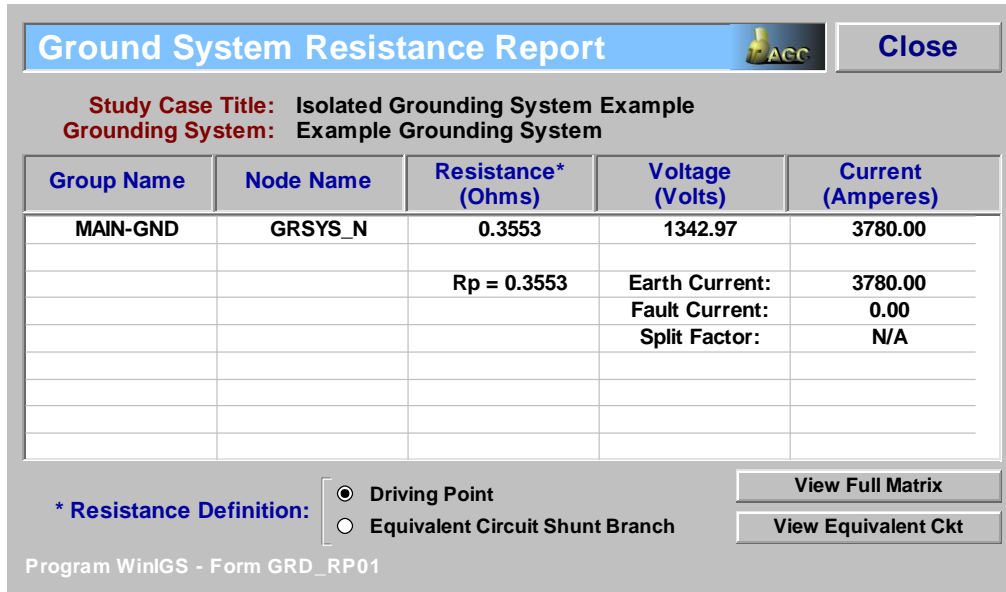


Fig. 4.9 Grounding system resistance report

In conclusion, the OPTIMGRID-recommended design of the Ealy Substation matches closely that obtained from WINIGS and it is believed that it is a reliable application for ensuring the safety of personnel in substations due to ground faults. The total cost for constructing this new grounding system recommended by OPTIMGRID is \$ 74k, based on the cost numbers provide by SRP.

5 CONCLUSIONS AND FUTRUE WORKS

5.1 Conclusions

In this thesis, there are three main parts, including analysis and development of a soil model application, calculation of grounding system safety metrics and optimization of grounding systems. These three parts are not separated from each other. They are all parts of a process need to design a grounding system for a substation. The general flowchart describing the completed substation grounding systems design is shown in Fig.

5.1.

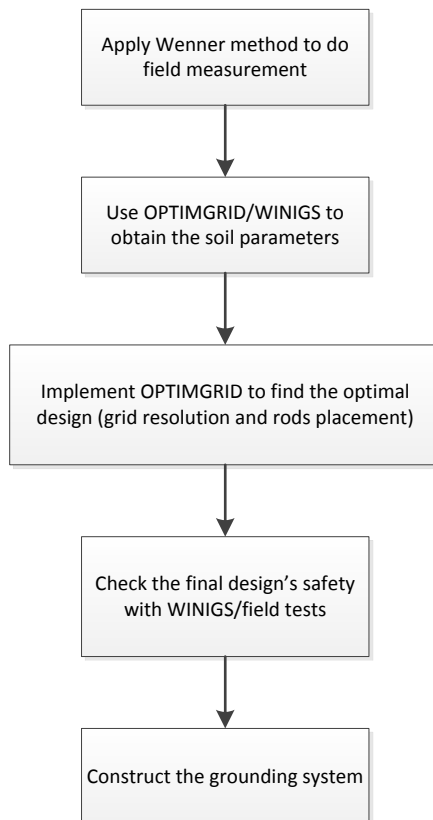


Fig. 5.1 Flowchart of the grounding system design

A summary of this work and major conclusions are drawn follow.

- The four-probe measurement method (Wenner method) is applied in this thesis.

An application to distill a two-layer soil model from Wenner-method measurements was develop and tested against the only existing industry package that builds such models. The tests show reasonable correspondence between the two methods. While there is no way to know which method is more accurate, though every effort has been mad to ensure that the application developed here is accurate, at minimum this package gives the substation engineer both a sanity check on the results from the WINIGS results and allows mutual verification. The two series of data, apparent resistances as well as corresponding separations, are compiled in an Excel document, which is the input data to the OPTIMGRID's Soil Model Application. Using a finite-series approximation to the traditional infinity series apparent resistivity equation allows the three-parameter soil model (ρ_1, ρ_2, h) to be calculated efficiently. These parameters are calculated using Newton's method applied to a nonlinear least square regression, whose objective is to find the best (three) soil parameters that best fit the measure data to a theoretical curve based on those parameters. Finally, an improved Chi-square test is proposed to obtain the confidence interval (error) at 80% confidence level for each soil parameter. It is a practical way to check the quality of the parameters

estimation.

- In order to make persons in the substation safe, the grounding systems safety metrics (E_{mesh} , E_{step} , R_g) need be lower than the allowable values. Due to different grounding systems, it is necessary to calculate the safety metrics for each case. In other words, the safety metrics vary as the design of grounding system is changing. As a result, it is very important to calculate these metrics accurately and they are the left-hand-side of the constraint equations in optimizations.
- To obtain accurate electric field calculations, it was found necessary to subdivide the ground-grid conductors and ground-rods into smaller segments and calculate the self-resistance of each segment and mutual resistance between every pair of these smaller segments. Using this approach, it was found to be possible to find accurate self- and mutual-resistances from the Voltage Distribution Factor (VDF) matrix. With the matrix method, the segment leakage currents and the grounding resistance can be calculated accurately. In this approach, the Green's functions are improved to calculate the field point potential due to any line current source, allowing the earth potential at any point can be computed as well as the touch voltage and the step voltage accurately.
- The complex images method was employed instead of the conventional images method. The author developed all the complex-images equations for calculating

self- and mutual-resistances in all traditional conductor orientations. With the help of complex images method, the computation efficiency has been improved significantly.

- Three optimization methods are used to optimize (minimize cost of) the grounding system and they are all included in the OPTIMGRID. The first one using “fmincon” and “GlobalSearch” is applied to provide the valuable initial guess to the second method “patternsearch”. The “patternsearch” solver is the main solver for optimization process, while the third method, the genetic algorithm, is a backup method with the largest “runtime cost” among these three methods but has a higher degree of reliability than the pattern search algorithm. The application of optimization to ground grid design and, in particular, these three optimization methods and their combination, is the first known approach to ground-grid optimization.
- For simplicity and practicality, the author makes some assumptions based on SRP rules. Therefore, the variables only contain the spacing between two adjacent conductors (D) and the mode of grounding rods placement (m_r). From the actual cost data by SRP, the objective function, which is the total cost, is developed with the two variables.
- The author has used SRP’s Ealy Substation as an example to run OPTIMGRID in

designing an economical grounding system of this substation. With the input data from SRP, it is possible to get the result through the new software. The results from the three-optimization approaches are compared. The comparison for these examples supports the conjecture that the pattern search approach is the best choice as a compromise between another two methods based on the need of accuracy and efficiency.

5.2 Future Works

- The optimization function for OPTIMGRID is limited to square and rectangular shape of substation. However, triangular, L-shape and T-shape substations do occur. Hence, the program will need to be further developed to include these geometries.
- The unequally spaced grounding grid would be more economical. However, it will bring more complexity to the optimization problem, because it is necessary to define more variables in the objective function and constraints.
- The study of how to place grounding rods is meaningful. In the existing model, the rods are only placed around the outside perimeter of a substation. There is no evidence that the interior rods are not economical or useful. As a result, several experiments might be done with different rod locations in order to draw some general conclusions.

- It is always helpful to learn more about optimization theory to determine whether better optimization methods exist that fit this problem and test more optimization solvers could yield improvement in reliability and execution time. In this way, methods more efficient than pattern search and genetic algorithms may be found. The long runtime is the biggest challenge for it.
- There has already been a developed user interface for Soil Model Application. It is necessary to create a completed user interface for the total OPTIMGRID software and a user's manual.

REFERENCE

- [1]. "IEEE Guide for Safety in AC Substation Grounding", IEEE Std. 80, USA, 2000
- [2]. A. P. Meliopoulos, A. D. Papalexopoulos, R. P. Webb, C. Blattner, "Interpretation of Soil Resistivity Measurements: Experiments with the Model SOMIP," IEEE Trans. Power Delivery, vol. PWRD-1, no. 4, Oct. 1986.
- [3]. Hans R. Seedher, J. K. Arora, "Estimation of Two Layer Soil Parameters Using Finite Wenner Resistivity Expressions," IEEE Trans. Power Delivery, vol. 7, no. 3, July 1992.
- [4]. F. Dawalibi, D. Mukhedkar, "Optimum Design of Substation Grounding in Two Layer Earth Structure," part I, IEEE Transactions, vol. PAS-94, no. 2, March/April 1975, pp. 252-272.
- [5]. F. Dawalibi, D. Mukhedkar, "Multi-Step Analysis of Interconnected Grounding Electrodes," IEEE Transactions, vol. PAS-95, no. 1, Jan./Feb. 1976, pp. 113-119.
- [6]. Robert J. Heppe, "Computation of Potential at Surface Above An Energized Grid or Other Electrode, Allowing for Non-Uniform Current Distribution," IEEE Trans. Power Apparatus and Systems, vol. PAS-98, no. 6, Nov./Dec. 1979.
- [7]. Y. L. Chow, J. J. Yang, K. D. Srivastava, "Complex Images of a Ground Electrode in Layered Soils," Journal of Applied Physics, vol. 71, issue 2, 1992, pp. 560-574.
- [8]. R.W. Hamming, Numerical Methods for Scientists and Engineers. New York: Dover, 1973.
- [9]. H. Holland, Adaption in Natural and Artificial Systems. Ann Arbor, MI: Univ. Michigan Press. Reprinted in MIT press, 1992.
- [10]. Joakim Agnarsson, Mikael Sunde, Inna Ermilova, "Parallel Optimization in Matlab," Project to Computational Science: Report, Jan. 2013.
- [11]. MathWorks Optimization Toolbox User's Guide (2013). MATLAB Optimization Toolbox User's Guide, R2013b.

- [12]. MathWorks Global Optimization Toolbox User's Guide (2013). MATLAB Optimization Toolbox User's Guide, R2013b.
- [13]. Maurício Caldora Costa, "Optimization of Grounding Grids by Response Surfaces and Genetic Algorithms," IEEE Trans. Magnetics, vol. 39, no. 3, May 2003.
- [14]. F. C. Schweppe, "Uncertain Dynamic Systems," Prentice Hall, Inc., 1973.
- [15]. Zhongxin Li, Wenjiang Chen, Jianbin Fan, and Jiayu Lu, "A Novel Mathematical Modeling of Grounding System Buried in Multilayer Earth," IEEE Trans. Power Delivery, vol. 21, no. 3, July 2006.
- [16]. Raviraj S. Adve, Tapan Kumar Sarkar, Odilon Maroja C. Pereira-Filho, and Sadasiva M. Rao, "Extrapolation of Time-Domain Responses from Three-Dimensional Conducting Objects Utilizing the Matrix Pencil Technique," IEEE Trans. Antennas and Propagation, vol. 45, no. 1, Jan. 1997.
- [17]. E. B. Joy, A. P. Meliopoulos, R. P. Webb, "Graphical and Tabular Results of Computer Simulation of Faulted URD Cable, " Final Report to EPRI, Georgia Institute of Technology, Atlanta, GA, July 1979.
- [18]. E. D. Sunde, Earth Conduction Effects in Transmission Systems. New York: Dover, 1968.